

**RECYCLING OF WASTE COTTON FABRICS INTO  
BIODEGRADABLE ANTIMICROBIAL PACKAGING  
MATERIALS**

Chufan Zhou

Department of Food Science and Agricultural Chemistry, McGill University, Montreal

May 2021

A thesis submitted to McGill University in partial fulfillment of the requirements of  
the degree of Master of Science in Food Science and Agricultural Chemistry

© Chufan Zhou 2021

# TABLE OF CONTENTS

<b>TABLE OF CONTENTS</b> .....	<b>I</b>
<b>LIST OF FIGURES</b> .....	<b>VI</b>
<b>LIST OF TABLES</b> .....	<b>VIII</b>
<b>ABSTRACT</b> .....	<b>IX</b>
<b>RÉSUMÉ</b> .....	<b>XI</b>
<b>ACKNOWLEDGEMENTS</b> .....	<b>XIII</b>
<b>CONTRIBUTION OF AUTHORS</b> .....	<b>XIV</b>
<b>PUBLICATIONS</b> .....	<b>XV</b>
<b>CONFERENCE PRESENTATION</b> .....	<b>XVI</b>
<b>LIST OF ABBREVIATIONS</b> .....	<b>XVII</b>
<b>CHAPTER 1. INTRODUCTION</b> .....	<b>1</b>
<b>CHAPTER 2. LITERATURE REVIEW 1</b> .....	<b>4</b>
<b>2.1 ABSTRACT</b> .....	<b>4</b>
<b>2.2 INTRODUCTION</b> .....	<b>5</b>
<b>2.3 BIOMASS WASTES FOR FUNCTIONAL MATERIAL SYNTHESIS</b> .....	<b>6</b>
<b>2.3.1 Agricultural and forestry wastes</b> .....	<b>6</b>
2.3.1.1 <i>Crop straw</i> .....	7
2.3.1.2 <i>Rice husk</i> .....	7
2.3.1.3 <i>Peanut shells</i> .....	8
2.3.1.4 <i>Corn cob</i> .....	8
2.3.1.5 <i>Others</i> .....	9
<b>2.3.2 Animal wastes</b> .....	<b>9</b>
<b>2.3.3 Industrial wastes</b> .....	<b>10</b>
<b>2.3.4 Municipal solid wastes</b> .....	<b>11</b>
<b>2.4 EXTRACTION OF NATURAL POLYMERS</b> .....	<b>12</b>
<b>2.4.1 Cellulose</b> .....	<b>15</b>

2.4.2 Lignin .....	17
2.4.3 Collagen .....	19
2.4.4 Gelatin.....	19
2.4.5 Keratin .....	20
2.4.6 Chitin/Chitosan .....	21
<b>2.5 FUNCTIONAL MATERIALS DERIVED FROM BIOMASS WASTES.....</b>	<b>22</b>
2.5.1 Adsorbent materials.....	25
2.5.2 Catalytic materials .....	28
2.5.3 Electrode materials .....	29
2.5.4 Composite materials .....	32
<b>2.6 CONCLUSION AND FUTURE PERSPECTIVES.....</b>	<b>35</b>
<b>2.7 REFERENCES .....</b>	<b>38</b>
<b>CONNECTING STATEMENT I .....</b>	<b>55</b>
<b>CHAPTER 3 LITERATURE REVIEW 2.....</b>	<b>56</b>
3.1 ABSTRACT .....	56
3.2 INTRODUCTION .....	57
3.3 BACTERICIDAL MECHANISM OF NANOSTRUCTURED SURFACES .....	58
3.3.1 Biophysical model .....	60
3.3.2 Thermodynamic model.....	61
3.3.3 Oxidative stress model.....	61
3.3.4 Other models .....	62
3.4 NATURALLY OCCURRING NANOTOPOGRAPHY .....	62
3.4.1 Insect wings .....	64
3.4.2 Gecko skin .....	65
3.5 SYNTHETIC BACTERICIDAL SURFACES .....	65
3.5.1 Black silicon and silicon materials .....	66
3.5.2 Graphene and graphene-derived materials.....	67
3.5.3 Titanium surfaces.....	67

<b>3.5.4 Other bioinspired nanostructured surfaces</b> .....	<b>68</b>
<b>3.6 FACTORS INFLUENCING BACTERICIDAL ACTIVITY</b> .....	<b>69</b>
<b>3.6.1 Bacterial cell properties</b> .....	<b>69</b>
<b>3.6.2 Surface features</b> .....	<b>70</b>
3.6.2.1 <i>Nanostructured surface shape</i> .....	70
3.6.2.2 <i>Other features</i> .....	71
<b>3.7 CONCLUSIONS AND OUTLOOK</b> .....	<b>72</b>
<b>3.8 REFERENCES</b> .....	<b>74</b>
<b>CONNECTING STATEMENT II</b> .....	<b>81</b>
<b>CHAPTER 4. RECYCLING OF WASTE COTTON FABRICS INTO REGENERATED CELLULOSE FILMS THROUGH THREE SOLVENT SYSTEMS: A COMPARISON STUDY</b> .....	<b>82</b>
<b>4.1 ABSTRACT</b> .....	<b>82</b>
<b>4.2 INTRODUCTION</b> .....	<b>83</b>
<b>4.3 MATERIALS AND METHODS</b> .....	<b>84</b>
<b>4.3.1 Materials</b> .....	<b>84</b>
<b>4.3.2 Cotton fabric dissolution and regeneration</b> .....	<b>85</b>
4.3.2.1 <i>H<sub>2</sub>SO<sub>4</sub> aqueous solvent</i> .....	85
4.3.2.2 <i>NaOH/urea aqueous solvent</i> .....	85
4.3.2.3 <i>LiCl/DMAc solvent</i> .....	86
<b>4.3.3 Regenerated cellulose film characterization</b> .....	<b>86</b>
4.3.3.1 <i>Fourier transform infrared spectroscopy</i> .....	86
4.3.3.2 <i>X-ray diffraction</i> .....	86
4.3.3.3 <i>Scanning electron microscopy</i> .....	86
4.3.3.4 <i>Optical transmittance</i> .....	87
4.3.3.5 <i>Mechanical property</i> .....	87
4.3.3.6 <i>Thermogravimetric analysis</i> .....	87
4.3.3.7 <i>Water vapor permeability</i> .....	87

4.3.4 Statistical analysis .....	88
4.4 RESULTS AND DISCUSSION .....	88
4.4.1 Dissolution of cotton fabrics in three solvent systems .....	88
4.4.2 Structure of regenerated films .....	90
4.4.3 Properties of regenerated films.....	92
4.5 CONCLUSION.....	96
4.6 REFERENCES.....	98
CONNECTING STATEMENT III .....	102
<b>CHAPTER 5. ALL-CELLULOSE FILMS WITH MECHANO- BACTERICIDAL ACTIVITY DERIVED FROM WASTE COTTON FABRICS</b> .....	<b>103</b>
5.1 ABSTRACT .....	103
5.2 INTRODUCTION .....	104
5.3 MATERIALS AND METHODS.....	105
5.3.1 Materials .....	105
5.3.2 Preparation of regenerated cellulose films .....	106
5.3.3 Extraction of CNCs.....	106
5.3.4 Fabrication of CNC/RC films .....	106
5.3.5 Characterization .....	107
5.3.5.1 <i>Fourier transform infrared spectroscopy</i> .....	107
5.3.5.2 <i>X-ray diffraction</i> .....	107
5.3.5.3 <i>Scanning electron microscopy</i> .....	107
5.3.5.4 <i>Bactericidal activity</i> .....	107
5.3.5.5 <i>Mechanical properties</i> .....	108
5.3.6 Statistical analysis .....	108
5.4 RESULTS AND DISCUSSION .....	108
5.4.1 Structure of CNC/RC films.....	108
5.4.2 Mechano-bactericidal activity of CNC/RC films .....	110

5.4.3 Mechanical properties of CNC/RC films .....	112
5.5 CONCLUSION.....	113
5.6 REFERENCES.....	115
<b>CHAPTER 6 GENERAL SUMMARY AND CONCLUSION .....</b>	<b>119</b>
6.1 GENERAL SUMMARY .....	119
6.2 SUGGESTIONS FOR FUTURE WORK .....	120
<b>REFERENCES.....</b>	<b>122</b>

## LIST OF FIGURES

### CHAPTER 2

<b>Figure 2.1</b> Films and hydrogels derived from different biomass wastes .....	15
<b>Figure 2.2</b> SEM images of carbon-based materials derived from biomass wastes.....	24
<b>Figure 2.3</b> Schematic diagram of Fe <sub>3</sub> C/C composite for methylene blue removal and NOR degradation.....	29
<b>Figure 2.4</b> SEM images and elemental mapping of composite materials derived from biomass wastes.....	34

### CHAPTER 3

<b>Figure 3.1</b> Schematic diagram of mechano-bactericidal activity on nanopillar surface .....	59
<b>Figure 3.2</b> SEM images of natural bactericidal nanotopographies (top) and bacteria on surfaces (bottom) .....	63
<b>Figure 3.3</b> SEM images of synthetic bactericidal nanotopographies (top) and bacteria on surfaces (bottom) .....	66

### CHAPTER 4

<b>Figure 4.1</b> FT-IR spectra of cotton fabrics and regenerated cellulose films prepared in three solvent systems .....	91
<b>Figure 4.2</b> XRD patterns of cotton fabrics and regenerated cellulose films prepared in three solvent systems .....	91
<b>Figure 4.3</b> SEM images of regenerated cellulose films prepared in three solvent systems: (a) T-H, (b) T-N, (c) T-D, (d) B-H, (e) B-N, (f) B-D, (g) J-H, (h) J-N, and (i) J-D.....	92

<b>Figure 4.4</b> (a) Tr of regenerated cellulose films prepared in three solvent systems at the wavelength of 800 nm; and (b) transparencies of B-H, T-H, and J-H (from top to bottom) .....	93
<b>Figure 4.5</b> Mechanical properties of regenerated cellulose films prepared in three solvent systems (different letters on the tops of columns represented the significant difference ( $p<0.05$ )) .....	94
<b>Figure 4.6</b> TGA and DTG curves of regenerated cellulose films prepared in three solvent systems .....	95
<b>Figure 4.7</b> WVP of regenerated cellulose films prepared in three solvent systems (different letters on the tops of columns represented the significant difference ( $p<0.05$ )) .....	96

## CHAPTER 5

<b>Figure 5.1</b> FT-IR spectra of CNC, RC, and CNC/RC films.....	109
<b>Figure 5.2</b> XRD patterns of CNC, RC, and CNC/RC films.....	110
<b>Figure 5.3</b> Logarithmic reduction of (a) <i>E. coli</i> and (b) <i>L. monocytogenes</i> when incubated with CNC/RC films and controls for 3 min (different letters on the tops of columns represented the significant difference ( $p<0.05$ )) .....	111
<b>Figure 5.4</b> Effect of various contact times on logarithmic reduction of (a) <i>E. coli</i> and (b) <i>L. monocytogenes</i> when incubated with 10%CNC/RC films and controls (different letters on the tops of columns represented the significant difference ( $p<0.05$ )).....	112
<b>Figure 5.5</b> (a) SEM micrograph showing morphology of <i>E. coli</i> on the CNC/RC film; and (b) SEM micrograph showing morphology of <i>L. monocytogenes</i> on the CNC/RC film.....	112
<b>Figure 5.6</b> Mechanical properties of RC and CNC/RC films (different letters on the tops of columns represented the significant difference ( $p<0.05$ )) .....	113

## LIST OF TABLES

### CHAPTER 2

**Table 2.1** Extraction of natural polymers from biomass wastes ..... 12

**Table 2.2** Electrode porous carbons derived from biomass wastes .....29

### CHAPTER 3

**Table 3.1** Bactericidal activities of various natural and synthetic nanostructured surfaces .....63

### CHAPTER 4

**Table 4.1** Optimized dissolution conditions of cotton fabrics in three solvent systems .....88

## ABSTRACT

Today, there is a concern about the rapid increase in waste textile. Traditional treatments (such as landfill and incineration) have resulted in numerous disposal, utilization and management issues. Cotton is one of the most utilized fibers in textile industry, which consists of over 90% of cellulose. Thus, waste cotton fabrics could be a useful resource of cellulosic materials. In this study, the recycling of waste cotton fabrics into biodegradable packaging materials by dissolution and regeneration was investigated, and mechano-bactericidal packaging was developed from the regenerated cellulose films and cellulose nanocrystals (CNCs). In Chapter 2, the recent research on biomass waste utilization and biomass wastes derived functional materials was reviewed, which mainly focused on the following three aspects: (1) extraction of natural polymers from biomass wastes, (2) reuse of biomass wastes, and (3) preparation of carbon-based materials as novel adsorbents, catalyst carriers, electrode materials, and functional composites. In Chapter 3, the formation of natural and synthetic nanopillared surfaces was summarized, and the mechanism of action and the factors that influence their mechano-bactericidal activities were highlighted. In Chapter 4, the dissolution of three typical waste cotton fabrics (t-shirts, bed sheets and jeans) in NaOH/urea aqueous solution, H<sub>2</sub>SO<sub>4</sub> aqueous solution, and LiCl/DMAc solution was investigated. Compared to different types of cotton fabrics, the effects of three solvents on the dissolution of fabrics were more obvious, leading to the significant changes in the structure and properties of regenerated cellulose films. Cotton fabrics (about 2-5%) were rapidly dissolved (8 min) in H<sub>2</sub>SO<sub>4</sub> and NaOH/urea solvents after acid pretreatment, while the dissolution in LiCl/DMAc solvent did not need any pretreatment, but a lower cellulose concentration (1%), higher dissolution temperature (80 °C), and longer dissolution time (24 h) were required. The films produced from bed sheets in NaOH/urea solution exhibited the highest tensile strength, thermal stability, and water vapor barrier property. It was because of the stronger cellulose chain

entanglement and hydrogen bonds induced by the higher cellulose concentration in NaOH/urea solution. In Chapter 5, a new strategy namely mechano-bactericidal effect inspired by the naturally occurring surfaces was applied to construct antibacterial films from waste cotton fabrics. Various amounts of CNCs were deposited on the surface of regenerated cellulose films. The results revealed that the all-cellulose films displayed an obvious and fast bactericidal activity against both Gram-negative (*Escherichia coli*) and Gram-positive (*Listeria monocytogenes*) bacteria within 3 min contact. The increase of CNC contents from 3% to 10% slightly improved the bactericidal activity, but the extension of contacting time (up to 2 h) did not affect the log reduction of bacteria. In addition, the surface coating with CNCs significantly enhanced the tensile strength and Young's modulus of regenerated cellulose films from  $71.31\pm 6.10$  to  $131.44\pm 3.83$  MPa and from  $3051.39\pm 87.81$  to  $5704.33\pm 392.32$  MPa, respectively. Overall, this research proves the feasibility to recycle waste cotton fabrics into biodegradable cellulose films, which can be potentially used in various food and agricultural applications. It also provides great prospects for the development of new generation of antibacterial packaging films.

## RÉSUMÉ

Aujourd'hui, on s'inquiète de l'augmentation rapide des déchets textiles. Les traitements traditionnels (comme l'enfouissement et l'incinération) ont donné lieu à de nombreux problèmes d'élimination, d'utilisation et de gestion. Le coton est l'une des fibres les plus utilisées dans l'industrie textile, qui se compose de plus de 90% de cellulose. Ainsi, les tissus de coton de déchets pourraient être une ressource utile de matériaux cellulosiques. Dans cette étude, le recyclage des tissus de coton de déchets en matériaux d'emballage biodégradables par dissolution et régénération a été étudié, et l'emballage mécano-bactéricide a été développé à partir des films de cellulose régénérés et des nanocristaux de cellulose (NCC). Au chapitre 2, les recherches récentes sur l'utilisation des déchets de biomasse et les déchets de biomasse dérivés des matériaux fonctionnels ont été examinées, qui se sont principalement concentrées sur les trois aspects suivants: (1) extraction de polymères naturels à partir de déchets de biomasse, (2) réutilisation des déchets de biomasse et (3) préparation de matériaux à base de carbone sous forme de nouveaux adsorbants, porteurs de catalyseurs, matériaux électrodes et composites fonctionnels. Au chapitre 3, la formation de surfaces nanopilier naturelles et synthétiques a été résumée, et le mécanisme d'action et les facteurs qui influencent leurs activités mécano-bactériennes ont été mis en évidence. Au chapitre 4, la dissolution de trois tissus de coton de déchets typiques (t-shirts, draps de lit et jeans) dans la solution aqueuse NaOH/urée, la solution aqueuse H<sub>2</sub>SO<sub>4</sub> et la solution LiCl/DMAc a été étudiée. Comparé aux différents types de tissus de coton, les effets de trois solvants sur la dissolution des tissus étaient plus évidents, conduisant à des changements significatifs dans la structure et les propriétés des films de cellulose régénérés. Tissus en coton (environ 2-5%) ont été rapidement dissous (8 min) dans les solvants H<sub>2</sub>SO<sub>4</sub> et NaOH/urée après un prétraitement acide, tandis que la dissolution du solvant LiCl/DMAc n'a pas eu besoin de prétraitement, mais une concentration plus faible de cellulose (1 %), une température de dissolution plus élevée (80 °C) et un temps

de dissolution plus long (24 h) ont été nécessaires. Les films produits à partir de draps de lit dans la solution NaOH/urée présentaient la plus haute résistance en traction, la stabilité thermique et la propriété de barrière de vapeur d'eau. C'était en raison de l'enchevêtrement plus fort de chaîne de cellulose et des liaisons d'hydrogène induites par la concentration plus élevée de cellulose dans la solution de NaOH/urée. Au chapitre 5, une nouvelle stratégie, à savoir l'effet mécano-bactérien inspiré des surfaces naturelles, a été appliquée pour construire des films antibactériens à partir de tissus de coton déchets. Diverses quantités de NCC ont été déposées à la surface des films de cellulose régénérés. Les résultats ont révélé que les films de toute cellulose présentaient une activité bactéricide évidente et rapide contre les bactéries Gram-négatives (*E. coli*) et gram-positives (*L. monocytogenes*) dans un délai de 3 minutes de contact. L'augmentation du contenu du NCC de 3 % à 10 % a légèrement amélioré l'activité bactéricide, mais l'allongement du temps de contact (jusqu'à 2 h) n'a pas eu d'incidence sur la réduction logarithmique des bactéries. En outre, le revêtement de surface avec les NCC a considérablement augmenté la résistance en traction et le module de Young de films de cellulose régénérés de  $71.31 \pm 6.10$  à  $131.44 \pm 3.83$  MPa et de  $3051.39 \pm 87.81$  à  $5704.33 \pm 392.32$  MPa, respectivement. En résumé, cette recherche prouve la faisabilité de recycler les tissus de coton usés en films biodégradables de cellulose, qui peuvent être potentiellement utilisés dans diverses applications alimentaires et agricoles. Il offre également de grandes perspectives pour le développement de nouvelles générations de films d'emballage antibactériens.

## ACKNOWLEDGEMENTS

I would like to thank my supervisor, Dr. Wang for his patient guidance and professional advice throughout my whole master study. His valuable suggestions and support influence me a lot throughout the master study. I would also like to thank Dr. Ronholm for her advice for the literature review and help in the experimental steps.

Thank you to François Girouard for assisting me to do antibacterial test for many times and always being willing to process data and discuss results with me.

Thank you to my lab members, Dr. Roya Koshani, Shuting Huang, Yirong Zhang, Kehao Huang, Camelia Oliva, Jiayu (Millie) Xie, Luxuan (Hannah) Wang and visiting scholar Dr. Fen Wang. All of you are friendly and willing to help me during my research. Especially Millie and Hannah, both of you assisted me to prepare samples voluntarily in the first year of my program. A big thank to Shuting and Yirong, both of you are my best friends in Montreal, giving me a lot of fun and happiness when we are working together in the lab. It is a definitely wonderful journey to be with you in two years.

A big thank to my parents and my boyfriend. When I feel frustrated and want to give up, you are always supporting me and encouraging me to keep going. I would not achieve the degree without your help.

## CONTRIBUTION OF AUTHORS

This thesis is presented in a manuscript format and consists of six chapters. Chapter 1 is a general introduction that includes a brief overview of the recent related work in the literature and states the objectives of the research presented in the thesis. Chapter 2 highlights the research on the utilization of biomass wastes and biomass wastes derived functional materials in last five years, and has been published in the journal *Science and Technology of Advanced Materials*. Chapter 3 summarizes the formation of natural and synthetic nanopillar surfaces, discusses their mechanism of action, and presents the factors that influence their mechano-bactericidal activities, and has been published in the journal *Current Opinion in Food Science*. Chapter 4 discusses the dissolution behavior of waste cotton fabrics in three solvent systems and the properties of regenerated cellulose films, and has been submitted for publication in the *Journal of Applied Polymer Science*. Chapter 5 investigates the structure, mechanical property and mechano-bactericidal activity of regenerated cellulose films coated with cellulose nanocrystals. Finally, Chapter 6 presents a general conclusion of the thesis as well as some recommendations for future research.

The present author, Chufan Zhou, was responsible for the experimental work, data acquisition and analysis, and writing of the thesis. Dr. Yixiang Wang, the thesis supervisor, guided the research and revised the thesis prior to the submission. Dr. Roya Koshani, Bridget O'Brien, Dr. Xudong Cao, and Dr. Jennifer Ronholm were responsible for editing and reviewing Chapter 3. Dr. Ronholm also provided help in the research of Chapter 5. François Girouard was responsible for the antibacterial test and cell fixation for scanning electron microscope.

## PUBLICATIONS

Chufan Zhou, Yixiang Wang. Recent progress in the conversion of biomass wastes into functional materials for value-added applications, *Science and Technology of Advanced Materials*, 2020, 21, 787-804.

Chufan Zhou, Roya Koshani, Bridget O'Brien, Jennifer Ronholm, Xudong Cao, Yixiang Wang. Bio-inspired mechano-bactericidal nanostructures: a promising strategy for eliminating surface foodborne bacteria, *Current Opinion in Food Science*, 2021, 39, 110-119.

Chufan Zhou, Yixiang Wang. Recycling of waste cotton fabrics into regenerated cellulose films through three solvent systems: a comparison study, *Journal of Applied Polymer Science*, 2021, submitted.

Chufan Zhou, François Girouard, Jennifer Ronholm, Yixiang Wang. All-cellulose films with mechano-bactericidal activity derived from waste cotton fabrics, 2021, to be submitted.

## **CONFERENCE PRESENTATION**

Chufan Zhou, Yixiang Wang. Recycling of waste cotton fabrics into regenerated cellulose films through three solvent systems: a comparison study. ACS Spring 2021 (virtual).

## LIST OF ABBREVIATIONS

<b>AC:</b>	Activated carbon
<b>AES:</b>	Acid-enzyme solubilization
<b>ANOVA:</b>	Analysis of variance
<b>ATR:</b>	attenuated total reflectance
<b>BDD:</b>	Boron-doped diamond
<b>BHI:</b>	Brain Heart Infusion
<b>[BMIM][Cl]:</b>	1-butyl-3-methyl-imidazolium chloride
<b>bSi:</b>	Black silicon
<b>CFCP:</b>	Phosphoric acid-modified biochar
<b>CNC:</b>	Cellulose nanocrystal
<b>CNF:</b>	Cellulose nanofibril
<b>CO<sub>2</sub>:</b>	Carbon dioxide
<b>COD:</b>	Chemical oxygen demand
<b>CS<sub>2</sub>:</b>	Carbon disulfide
<b>DMAc:</b>	N, N-dimethylacetamide
<b>DPL:</b>	Dried persimmon leaves
<b>DTG:</b>	The first derivatives of thermograms
<b>Eb:</b>	Elongation at break
<b>EDLC:</b>	Electrochemical double-layer capacitors
<b>ESM:</b>	Eggshell membrane
<b>FT-IR:</b>	Fourier transform infrared spectroscopy
<b>GO:</b>	Graphene oxide
<b>H<sub>2</sub>S:</b>	Hydrogen sulfide
<b>H<sub>2</sub>SO<sub>4</sub>:</b>	Sulfuric acid
<b>HCl:</b>	Hydrogen chloride
<b>KOH:</b>	Potassium hydroxide

<b>LiCl:</b>	Lithium chloride
<b>[MEIM]OAc:</b>	1-ethyl-3-methylimidazolium acetate
<b>MOF:</b>	Metal organic framework
<b>MSW:</b>	Municipal solid wastes
<b>Mt:</b>	Million tons
<b>MWL:</b>	Milled wood lignin
<b>MW-P:</b>	Microwave irradiation-pyrolysis
<b>NaClO:</b>	Sodium hypochlorite
<b>NaOH:</b>	Sodium hydroxide
<b>NB-PPCA:</b>	Nitrogen and boron dual-doped aerogel
<b>nHAP:</b>	Nano-hydroxyapatite
<b>NMMO:</b>	N-methylmorpholine N-oxide
<b>NOR:</b>	Antibiotic norfloxacin
<b>OPF:</b>	Oil palm frond
<b>PBS:</b>	Phosphate-buffered saline
<b>PSB:</b>	Peanut shell biochar
<b>PVA:</b>	Polyvinyl alcohol
<b>RC:</b>	Regenerated cellulose films
<b>rGO:</b>	Reduced graphene oxide
<b>RH:</b>	Relative humidity
<b>ROS:</b>	Reactive oxygen species
<b>RPL:</b>	Raw persimmon leaves
<b>SD:</b>	Standard deviation
<b>SEM:</b>	Scanning electron microscopy
<b>SEM:</b>	Scanning electron microscopy
<b>SMBS:</b>	Sodium dodecyl sulfate
<b>SMBS:</b>	Sodium metabisulfite
<b>SSA:</b>	Specific surface area

<b>TEA-BF<sub>4</sub>:</b>	Tetraethylammonium tetrafluoroborate
<b>TGA:</b>	Thermogravimetric analysis
<b>T<sub>max</sub>:</b>	The maximum decomposition temperature
<b>Tr:</b>	Optical transmittance
<b>TSA:</b>	Tryptic Soy Agar
<b>TSB:</b>	Tryptic Soy Broth
<b>WCFs:</b>	Waste cotton fabrics
<b>WVP:</b>	Water vapor permeability
<b>XRD:</b>	X-ray diffraction

## CHAPTER 1. INTRODUCTION

The generation of biomass wastes increases rapidly every year, leading to the disposal, utilization and management issues. It is estimated that the worldwide biomass waste production is approximately up to 140 Gt per year [1]. Biomass wastes are biomass feedstock from the waste stream, including agricultural residues, animal wastes, forestry residues, industrial wastes, MSW and so on [2]. Among various MSW, global consumption of textile increases quickly because of the living standard improvement, increasing world population and fast-changing trends [3]. Due to the lack of proper waste management strategies, most waste textile are incinerated, landfilled, or discarded, causing environmental and social issues such as ground water contamination, greenhouse gases generation and limited landfilling space. It was reported that in Europe, only 18% of waste textile were recycled and reused in 2014, while the rest were landfilled or incinerated. Thus, developing recycling approaches for waste textile has gained much attention in recent years, including the reuse in building construction, production of composites and nanoparticles, cotton fibers and polyester recovery, and so on [4,5].

Cotton is one of the most utilized fibers in the textile industry, consisting of over 90% of cellulose, so WCFs could be a useful resource of cellulosic materials [6]. Cellulose is found in many forms and applications. Among them, the dissolution and regeneration of cellulose are the key aspects, because cellulose is insoluble in water or other common organic solvents due to the presence of a strong intra- and inter-molecular hydrogen-bonding network in cellulose. The traditional approach to dissolve cellulose is to produce viscose rayon by using NaOH and CS<sub>2</sub>, but the solvent in this process is highly toxic to human health and environment. Therefore, research efforts have been made to explore novel, efficient and eco-friendly solvent systems such as LiCl/DMAc, NMMO, ionic liquid, NaOH/urea, H<sub>2</sub>SO<sub>4</sub> aqueous solution, and so on [7-10]. It was reported that

H<sub>2</sub>SO<sub>4</sub> and pre-cooled NaOH/urea aqueous solvents were capable of dissolving cellulose within only 10 min under a low temperature [11]. The dissolution in LiCl/DMAc solvent was also confirmed, and transparent cellulose solution can be obtained without severe degradation [10]. However, the utilization of these solvents to recycle waste cotton fabrics has been seldom reported.

Contamination of food by bacterial pathogens has gained much attention since it can cause food safety issues, leading to infectious disease and human death [12]. Thus, antimicrobial food packaging and processing materials have been developed to eliminate bacteria from outer surfaces of food products. Traditionally, various organic and inorganic additives have been incorporated as antibacterial agents in polymeric materials to reduce the presence of bacteria. However, such approach is problematic since the overuse of antibiotics can lead to the increased resistance, and the release of antibacterial agents may introduce toxic substances into food products [13]. In nature, it has been reported that insect wings and gecko skin can eliminate bacterial pathogens by nanopillars existed on their surfaces in a physical way [14]. Inspired by these naturally occurring surfaces, synthetic nanostructures have been developed (e.g. graphene, titanium, black silicon, and copper) to mimic this mechano-bactericidal mechanism [15-17]. As bacteria contact hierarchical nanotopographies such as pillars, needles and hairs, they locate on the surfaces, leading to the increased stretching of cell membranes. Once beyond the maximum stretchable potential, cell membranes rupture, finally causing cell death [18]. Compared to the traditional chemical-based approach, this mechano-bactericidal strategy is non-diffusive, non-toxic and sustainable. CNCs possess a narrow, rigid, and rod-like structure with diameter of 2-20 nm and length of 100-500 nm [19]. They can be extracted from plants, animals, microorganisms, and waste materials through acid hydrolysis and oxidation methods [8]. The rod-like shape of CNCs is similar to nanopillars on the natural surfaces, so they may be able to physically eliminate bacteria as well.

The overall aim of this research is to recycle WCFs into biodegradable antimicrobial packaging in an eco-friendly way. Specifically, the objectives of this thesis are: (1) to investigate the dissolution behavior of three typical WCFs, t-shirts, bedsheets, and jeans, in three solvent systems namely H<sub>2</sub>SO<sub>4</sub> aqueous solution, NaOH/urea aqueous solution, and LiCl/DMAc solution; (2) to use CNCs and regenerated cellulose films both derived from WCFs to develop packaging materials with mechano-bactericidal activity.

## CHAPTER 2. LITERATURE REVIEW 1

### 2.1 Abstract

The amount of biomass wastes is rapidly increasing, which leads to numerous disposal problems and governance issues. Thus, the recycling and reuse of biomass wastes into value-added applications have attracted more and more attention. This paper reviews the research on biomass waste utilization and biomass wastes derived functional materials in last five years. The recent research interests mainly focus on the following three aspects: (1) extraction of natural polymers from biomass wastes, (2) reuse of biomass wastes, and (3) preparation of carbon-based materials as novel adsorbents, catalyst carriers, electrode materials, and functional composites. Various biomass wastes have been collected from agricultural and forestry wastes, animal wastes, industrial wastes and municipal solid wastes as raw materials with low cost; however, future studies are required to evaluate the quality and safety of biomass wastes derived products and develop highly feasible and cost-effective methods for the conversion of biomass wastes to enable the industrial scale production.

**Keywords:** biomass wastes, recycling, functional materials, value-added applications

## 2.2 Introduction

The disposal, utilization and management issues of biomass wastes are a burgeoning challenge to cities especially in developing countries due to the increasing generation of biomass wastes and the lack of feasible and efficient approaches recycling these biomass wastes resources. Therefore, the rational reuse of them has attracted much attention around the world [1-3]. Biomass is a stored source of solar energy initially collected by plants via the process of photosynthesis where CO<sub>2</sub> is captured and transferred to plant materials. It covers ranges of organic materials derived from plants and animals fed on the plant sand [4], and it can be converted into a variety of useful sources of bioenergy [5]. Nowadays, biomass energy has become the world's fourth largest energy source, following coal, oil and natural gas [1].

Biomass wastes commonly consist of forestry residues, agricultural wastes, animal wastes, industrial wastes, MSW, food processing wastes and so on [3,6]. Among various kinds of biomass wastes, biomass feedstock from agricultural and forestry wastes, animal wastes, industrial wastes, and MSW have been widely investigated in recent five years to extract natural polymers or to be converted into functional materials for value-added applications. Majority of biomass wastes are left in the field to naturally decompose, or discarded in landfill, or incinerated in the open for cooking, drying, and charcoal production, which not only are low efficient, but also lead to severe environmental pollution like greenhouse gas emissions and air quality deterioration. Thus, converting biomass wastes into value-added products for various applications such as medicine, materials, and food packaging has been drawn attention recently.

Although several literature reviews have discussed the importance of recycling biomass wastes, most of them merely focus on a certain kind of biomass wastes, for example wood biomass [7], agricultural waste peels [8], biochar [9,10], activated carbon for

adsorption of dye [11] and biomass waste cellulosic materials for nanocrystalline cellulose extraction [12]. Thus, this review systematically summarizes biomass wastes that have attracted most interest during the last five years. Biomass wastes are considered as biomass feedstock from the waste stream and are mainly derived from agricultural and forestry resources, animal resources, industrial resources and MSW. In one aspect, the recent research focuses on the recycling of natural polymers, such as cellulose, lignin, collagen, gelatin, keratin, and chitin/chitosan. They are extracted from various biomass wastes, including rice husk, peanut shell, corncob, head, skin, bones of fish, shrimp, crabs and wastepaper, and then used to fabricate functional materials with potential applications in biomaterials [13], coating for packaging [14], films for bioactive molecule delivery [15], water treatment [8], supercapacitor [16] and construction [10]. In another, biomass wastes could be directly applied, or converted into carbon-based materials as novel adsorbents, catalysts carriers, electrode materials, and functional composites.

### **2.3 Biomass wastes for functional material synthesis**

In last five years, agricultural and forestry residues, animal wastes, industrial wastes, and MSW have been frequently studied. Most of them are under-utilized for energy and material production, which means only a small amount of biomass wastes can be used as a feedstock for real industrial applications [6].

#### **2.3.1 Agricultural and forestry wastes**

It is estimated that the generation of rice straw, wheat straw, corn straw, sugarcane bagasse, and rice husk, the most abundant biomass wastes from agricultural wastes, is 731, 354, 204, 181 and 110 Mt per year, respectively [17]. In addition, the global production of wood biomass wastes is 4.6 Gt every year, with 20% being production loss [6]. Wastes from the olive oil industry are up to 30 Mt every year, and coffee industry produces 7.4 Mt of spent coffee grounds, coffee pulp, cherry hush [17], causing

severe disposal problems and low efficiency of utilization.

#### *2.3.1.1 Crop straw*

Crop straw is the dry stalk or stem produced in the field after removing the grain and chaff. The amount of crop straw is extremely huge all over the world. For example, the generation of crop straw in China has already reached about 600-800 Mt annually [18]. Burning is the commonest and cheapest method to eliminate crop straw for preparing land after harvesting crops, leading to the deteriorated air quality and other environmental problems [19]. Cellulose, hemicellulose, and lignin are the main constituents of crop straw. Crop straw is promising lignocellulosic raw materials to produce biofuel and some chemicals, but physico-chemical, bio and enzymatic pretreatments are needed due to its chemical constituents and the structure of lignocellulose. For example, biodiesel can be obtained by fast pyrolysis and catalytic liquefaction followed by hydrolysis, fermentation, and alkali catalysis processes [20]. The technology of producing fuel ethanol from straw mainly includes three steps: pretreatment, hydrolysis, and fermentation, among which are to degrade the carbohydrates in the plant cell wall and convert them into monosaccharides. On top of that, crop straw can be converted into biochar to immobilize metals [21].

#### *2.3.1.2 Rice husk*

Rice husk is one of the most abundant agricultural waste materials that is ecofriendly and biodegradable. It can be separated from rice grain during the rice milling. Rice husk consists of cellulose (25-35%), hemicellulose (18-21%), lignin (26-31%) and silica (15-17%). Apart from these structured components, some other nonstructural components such as pectin, waxes, and inorganic salts are also included [22]. The global rice production was estimated at 769.7 Mt in 2017 [23]. As a result of such huge production of rice, millions of tons of rice husk are formed annually, leading to disposal problems. Many attempts have been made to recycle rice husk, such as used as fodder for animals, energy generation for heat, and electricity and biogas by combustion and gasification

[24]. In recent five years, it is found that burning rice husk can produce different by-products such as rice husk ash and carbonized rice husk as sustainable additives to produce cement-based construction materials [23,25]. In addition, rice husk can be added into films as the filler, which can influence the properties of the filler-reinforced composites [26-28].

#### *2.3.1.3 Peanut shells*

The peanut industry is the main source for the generation of peanut shells. According to the Food and Agriculture Organization of the United Nations report [29], peanut shells account for 20% of the whole peanut and the peanut production is up to approximately 46 Mt every year. Majority of peanut shells are discarded or burnt as wastes during the process or used as fodder for animals. When they are added into fodder, they cannot be used directly unless they are crushed and processed by proper chemical treatments because they contain some harmful chemicals and the lignin in peanut shells is difficult to be digested [30]. In one aspect, the disposal problem of peanut shells is getting worse; in the other, the high-energy content of peanut shells is worth exploring. Many works have focused on recycling and taking advantage of peanut shells. It has been reported that peanut shells contained a large amount of total polyphenol, flavonoid, and amino acid substances, which endowed them with superior antioxidant capacity and functional properties [31]. Moreover, the porous structure of peanut shells makes it potential to form gas permeable packaging films for extending shelf life of food products [32]. It can also be utilized as carbon source for plant biomass-degrading enzymes, precursor for adsorbent to remove heavy metals [33], H<sub>2</sub> production, bio-carbon production, construction materials, and so on [34,35].

#### *2.3.1.4 Corncob*

Corncob is the central core of corns. It contains 39-45% of glucan, 25-35% of xylan, 17-21% of lignin, and low amounts of extractives [36]. Like the other agricultural wastes, corncob is usually incinerated for cooking and heating, causing serious

environmental pollution. Recently, the researchers are considering new applications to explore corncob's high energy content. However, corncob needs to be pretreated or hydrolyzed to break the links among cellulose, hemicellulose, and lignin for further applications due to its complex composition and structure. For example, due to the high lignocellulosic constituents of corncob, chemicals such as furfural, xylooligosaccharides and glucose can be produced [37]. In addition, biochar can be obtained by the pyrolysis of corncob for energy applications [38].

#### *2.3.1.5 Others*

In addition to the agricultural and forest wastes mentioned above, there are large numbers of other wastes in nature such as rattan, bagasse, and nutshells that have tremendous prospects for development. For example, shells from pecans, almonds, acorns, and bamboo have high porosity and are useful in the production of activated carbon by pyrolysis [39]. They can be applied as bio-fillers to reinforce thermoplastics via extrusion and injection molding processes as well [3]. In addition, the production of hydrogen from sunflower husk and bagasse and the conversion of levulinic acid to  $\gamma$ -valerolactone have been studied using Ni/NiO catalyst [40,41].

#### **2.3.2 Animal wastes**

Most animal wastes are generated from fishery, meat, leather and poultry industries such as fish/shrimp/crab wastes, animal and livestock manure, tannery wastes, feathers of chicken or other poultries, and so on. Among them, the seafood wastes, including shells, heads, skins, tails, fins, and bones, are the most abundant resources of biomaterials. During 2016-2017, the production of fish in India was up to 11.41 Mt, and 70% marine fish were processed before final sale, which left 20-80% fishing wastes [42]. In 2006, the total worldwide generation of shrimp reached 6 Mt, but only 60% were used as food, creating about 2.3 Mt of inedible wastes [43]. They were discarded nearby harbor or at the sea and were broken down by the aerobic bacteria living in the sea, resulting in the relative reduction of oxygen level under the sea [42]. In addition,

environmental problems such as higher mortality of marine organisms due to the production of toxic H<sub>2</sub>S, spreading pathogens that may make an adverse effect on human health, and emitting bad fishy smell that contaminates fresh air are increasing. Currently, the seafood, skin, bones, exoskeletons, and viscera are the most explored [44], which are considered as the great potential sources to recover natural substances (e.g. collagen, gelatin, chitin, and chitosan).

On the other hand, poultry and meat industries produce large amounts of inedible portions such as bones, feathers, tendons, and skins with the fast-growing rate due to the higher demand of consumers. It was reported that the annual generation of feather and offal was already up to  $8 \times 10^5$  tonnes over the world [45]. Pathogens exist in these wastes, so it is essential to treat them as soon as possible. The common treatments are incineration or composting them with manure, but several problems occur such as high-energy consumption, emission of carbon dioxide, odorous smell of H<sub>2</sub>S from composting, and so on.

Due to the above mentioned problems, the recent studies focused on developing sustainable high-value applications of animal waste, including extraction of biopolymers (e.g. collagen, keratin, and gelatin) [46], production of biogas [47], commercial crop (e.g. tomato) [48], and biodiesel [49].

### **2.3.3 Industrial wastes**

Black liquor and industrial sludge sewage from manufacturing are main constituents of industrial biomass wastes. Black liquor is a major pollution source in pulp and paper mills. It is consisted of 65-85% solid content, containing inorganic matters from cooking chemicals (e.g. sodium hydroxide, sodium sulfide) in the digester of processing and organic materials (e.g. lignin) from lignocellulosic biomass [50]. It is estimated that each ton of pulp generated by Kraft pulping process can produce approximately 10 tons

of black liquor [50], which accounts for 90% pollution of the pulp and paper industry [51]. Black liquor is traditionally treated to extract lignin by super-filtration, agglomeration and acid separation and recover alkali by combustion. However, these conventional methods have high operation cost and need huge pre-equipment investment [51]. Till now, many researchers have investigated the applications of black liquor derived products in functional fertilizer synergist [52], bio-fuel [53,54], and bio-plastic [50].

Industrial sewage sludge with high moisture content is generally produced from the industrial wastewater treatment facility. Because sewage sludge contains various hazardous matters, pathogens, heavy metals, and microplastics, it is difficult to properly treat it [55]. Expect from being recycled as fertilizer, new approaches have been proposed to generate valuable resources and materials from industrial sewage sludge over past five years, including the production of sludge pyrochar as adsorbent and soil conditioner [55], and sewage sludge ash for applications in heavy metal removal and construction of cement-based materials and cementitious binder [56-58].

#### **2.3.4 Municipal solid wastes**

Textile and wastepaper are major contributors to MSW with the generation of 16 Mt just in United States in 2014 for textile and 400 Mt globally for wastepaper [59]. However, the recycling of these wastes has not reached to a high rate. For example, textile accounts for about 5% of the landfill and global textile recycling is only about 13%, while recycling of wastepaper and cardboard stands for 58% [60]. The majority of wastes are discarded into landfill or incinerated, leading to negative impacts on the environment by contaminating ground water and generating greenhouse gases during decomposition [61]. Several attempts have been made to re-utilize wastepaper and cardboard, such as recycling of cellulose into antimicrobial packaging [59], producing biochar and bio-oil through pyrolysis [62] and obtaining cellulose nanocrystals [63]. In

terms of textile made from a variety of materials, novel recycling approaches have also gained attention, including recovering polyester fibers and glucose syrup from waste polyester cotton blends [64], recycling cellulosic fibers from cotton wastes [65], and preparing insulation materials [61].

## 2.4 Extraction of natural polymers

Most synthetic polymers are derived from fossil resources. The environmental and socioeconomic consequences have aroused much concern because many of synthetic polymers (e.g. polyethylene, polypropylene, and polystyrene) are non-renewable and non-biodegradable. Much attention has been paid to natural polymer-based materials, which are usually non-toxic, biodegradable, and biocompatible. Recently, a new trend has been found to recycle natural polymers from biomass wastes. The extraction of cellulose, lignin, collagen, gelatin, keratin, and chitin/chitosan from biomass wastes is summarized in Table 2.1. These natural polymers can be then used to prepare various films and hydrogels (Figure 2.1) for food packaging and biomedical applications.

**Table 2.1** Extraction of natural polymers from biomass wastes

Polymer	Raw material	Extraction method	Extraction yield (%)	Purity
Cellulose	Coconut shell [13]	Organosolv reaction with ethanol/HNO <sub>3</sub> followed by NaOH	70-95*	Free of lignin and hemicellulose
	OPF [66]	Different concentrations of NaOH solution under pressure and non-pressure	n.d.	91.33%
	Areca nut	Chemo-mechanical	22-26**	85.47%

	husk [14]	method: milling, homogenization, alkali treatment, acid hydrolysis, and bleaching			
Lignin	Rice straw [67]	Alkaline (sodium hydroxide) and acidic (formic acid/acetic acid) treatment	n.d.	n.d.	
	Corn stover [68]	Organic amine and organosolv synergetic pretreatment	81.7*	n.d.	
	Sugarcane bagasse [69]	Ionic liquid	90.1*	Almost in pure form	
Collagen	Skin/hide trimming wastes [70]	Propionic acid and acetic acid solubilization	93*	n.d.	
	Bovine hide [71]	Acid-solubilization and AES	n.d.	75.13%	
	Chicken sternal cartilage [72]	Pepsin and ultra-sonication treatment	~80*	High purity	
Gelatin	Atlantic mackerel skins [73]	Organic acids: acetic, citric, lactic, tartaric, or malic acid	29.6-31.8*	n.d.	
	Camel skins [74]	Calcium hydroxide and ammonium sulfate	36.8-42.2*	88.21-90.42%	
	Golden carp [75]	Prior-ultrasonication-acid treatment	62.12*	n.d.	

Keratin	Chicken feathers [45]	Thermo-chemical treatments with different reducing agents	82-94*	n.d.
	Red sheep's hair [76]	SMBS, urea with sodium dodecyl sulfate	96*	Higher than 90%
	Hog hair [77]	A two-step thermal hydrolysis process	68*	89.2%
Chitin	Shells of crab, crayfish and shrimp [78]	Twice NaClO treatments before demineralization and deproteinization	n.d.	n.d.
Chitosan	Shrimp shells [43]	Concentrated and diluted chloric acids, nitric acids, and sulfuric acids	n.d.	n.d.

---

‘\*’ Calculated by the weight of extracted polymer/the weight of polymer in raw material

‘\*\*’ Calculated by dry weight of extracted polymer/dry weight of raw material

‘n.d.’ Not determined

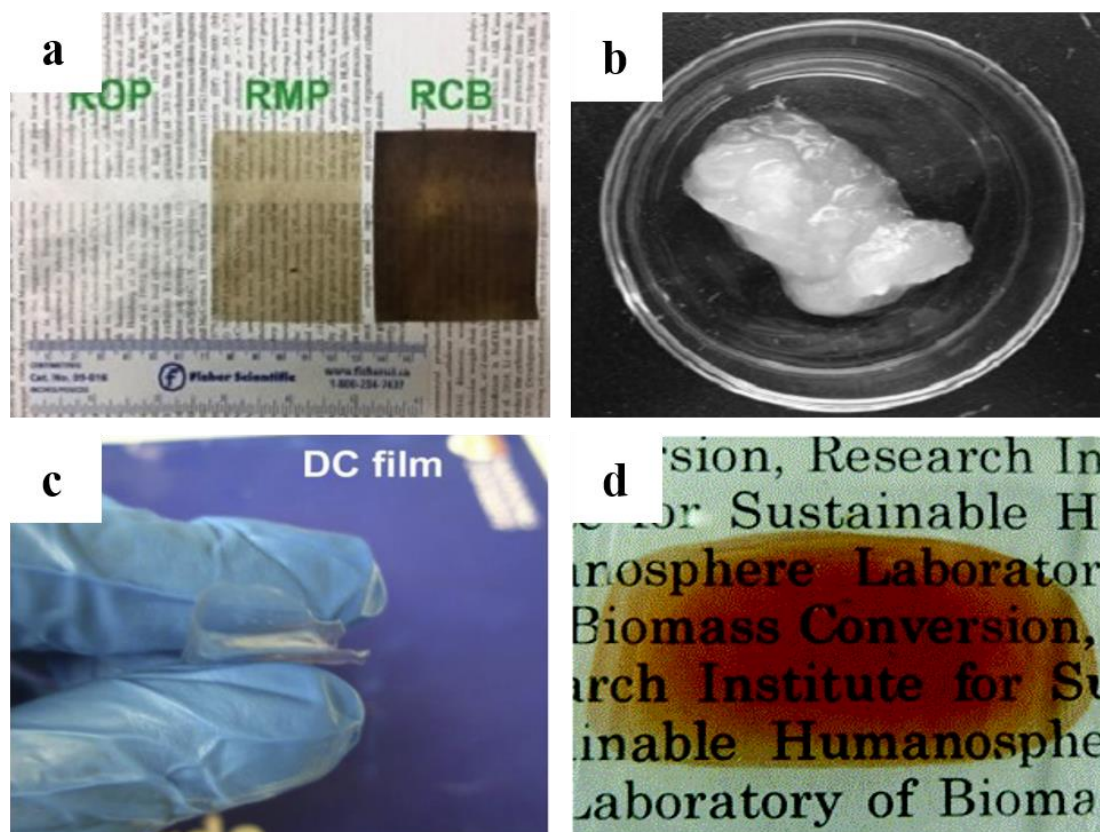


**Figure 2.1** Films and hydrogels derived from different biomass wastes: (a) films from wastepaper; (b) CNF hydrogel from waste sackcloth; (c) film from durian rind; and (d) film from *Eucalyptus globulus* wood chips [59,79-81] (Reproduced by permissions from [80], copyright [2014, The Royal Society of Chemistry], from [59], copyright [2020, Elsevier], from [79], copyright [2015, Elsevier] and from [81], copyright [2019, Elsevier])

### 2.4.1 Cellulose

Cellulose is the most abundant polymer, representing approximately 40-50% of plant and woody biomass by weight [82]. Cellulose exhibits a high strength and is renewable and biodegradable, so it is widely used for fabricating optical films, coatings, and controlled released systems, as well as in textile and paper industries [83]. Mechanical, chemical, biological, enzymatic, and their combination treatments are common methods to extract cellulose from biomass wastes [84]. Substances like hemicellulose and lignin are removed by multistep treatments and cellulose is then obtained with high

purity. Compared to single treatment, combination of mechanical, chemical, and biological treatments can increase the quality of cellulose; however, it increases the cost and causes high-energy consumption. For example, Kumneadklang et al. [66] treated OPF by NaOH solution with various concentrations under pressure of 7 bar and non-pressure (1.013 bar). It was found that  $\alpha$ -cellulose fibers with highest content (91.33%) and crystallinity (77.78%) were obtained by using 15 wt.% NaOH at 150 °C and 7 bar. Except from combination of treatments, it has been reported that organosolv process is a promising approach for the pretreatment of biomass wastes, because the lignocellulosic structure can be broken down and fragmented, and the constituents (e.g. cellulose, lignin, and hemicellulose) are subsequently isolated with high purity. For example, Amaral et al. [13] isolated cellulose from babassu coconut shells through organosolv with an acid catalyst, and the yield was about 70-95%. Comparison with conventional pulping processes (e.g. Kraft process and sulfite process) with yields of 50-60% [85], these new isolation processes are faster, more effective, and less harmful to the environment.

Apart from extracting cellulose by various methods, novel solvent systems have also been investigated recently to dissolve cellulose directly from biomass wastes, such as NMMO [86], LiCl/DMAc [87], ionic liquids [88], alkali/urea [89] and sulfuric acid solvents [90]. Compared to traditional cellulose dissolution namely viscose process, these novel systems are eco-friendly, and effective. For example, Oliva et al. [59] dissolved wastepaper within only 210 seconds through pre-cooled H<sub>2</sub>SO<sub>4</sub> aqueous solution and converted it into regenerated cellulose films with antimicrobial activity.

Additionally, celluloses with special structures such as CNF [79,91], CNC [92,93], and bamboo fibers [94], were also separated from textile waste, wastepaper, rattan, and so on. These nanocelluloses are well known as the reinforcing agents in building composite materials, textile engineering, musical instruments, food packaging, quality

sensors, and drug delivery systems [3,92]. Cao et al. [79] developed H<sub>2</sub>O<sub>2</sub>/HNO<sub>3</sub> solution as bleaching agent and hydrolysis medium to extract CNF from waste sackcloth. Non-cellulosic components were removed, and the obtained CNF possessed good dispersibility in different solvents. A chemo-mechanical method was developed to isolation of CNF from areca nut husk with the yield of 85.47% and the crystallinity of 73%. The chemical processes included alkali treatment, acid hydrolysis, and bleaching, while the mechanical treatment was involved grinding and homogenization [14]. Ahuja et al. [91] extracted both highly purified lignin and crystalline CNF simultaneously from jute bag waste. Soda cooking pretreatment was applied to reduce recalcitrance of lignocellulose, and then hemicellulose was hydrolyzed into sugar, leaving cellulose and lignin residues. Huang et al. [92] reviewed the extraction and modification of CNCs from biomass wastes in the past five years and highlighted the potential applications of CNCs in food-related areas. It was found that although novel extraction methods have been developed, sulfuric acid hydrolysis was still applied widely.

#### **2.4.2 Lignin**

Lignin is the key structural material in the formation of plant cell walls, especially in wood and bark due to its aromatic structure that enhances the strength and rigidity [3]. The content of lignin in different plants varies. For example, in hardwood, grass and softwood, the lignin content is 20-25%, 10-15%, and 25-35%, respectively [3]. Generally, lignin is obtained as a by-product through paper pulping process, and the production was about several million tons over the past few years. However, it has low-value and is usually burnt for heat and power [95]. Therefore, significant attention has been paid to extract lignin from plant-based biomass wastes and used as antioxidant, absorbent, binder, dispersant, and so on, which mostly rely on its structure with hydrophobic constituents [96,97].

The complex structure of lignin makes it difficult to be isolated and increases the

industry cost during the process. Lignin could present different physicochemical properties, which depend on the type of biomass and method of extraction [17]. Numerous methods have been applied for extracting lignin from biomass such as MWL, kraft pulping, sulfite pulping, soda process [17], organosolv process [68] and so on. The common way to derive lignin from wood is MWL, where plant materials are milled, and then extracted by dioxane and water. The disadvantage of this method is the low yield (10-60%) and structure change during the extraction process [98]. Kraft pulping and sulfite pulping are the traditional paper making processes, while the soda process is suitable for the extraction of lignin with low molecular weight and high purity from non-woody biomass [17]. Except from frequently used pulping process, the organosolv process can isolate lignin with high purity under mild conditions in a more environmentally friendly way. This method solubilizes lignin and hemicellulose from lignocellulosic biomass into water or an organic solvent (e.g. ethanol, methanol, acetone, acetic acid, ethylene glycol, etc.), leaving an insoluble cellulose pulp for enzymatic hydrolysis [99]. According to selected organic solvents, catalysts may be used in the processes as well, including acids, bases, Lewis acids, and ionic liquids [99,100]. For example, an organic amine catalytic organosolv treatment was performed to obtain high quality lignin from corn stover with the yield of 81.7% [68]. Ionic liquid [EMIM]OAc was also applied for the extraction of lignin from sugarcane bagasse with 90.1% yield [69]. Compare to traditional inorganic or solid base treatments, the solvent with catalyst in this system could be easily recycled and reused. However, these mono-phase solvents still require another processing step to separate lignin and hemicellulose [99]. Therefore, a two-phase system (water/1-butanol solvent) was introduced to extract lignin with a high quality [99,101]. Although these novel processes resulted in the high yield and purity, the relatively high cost and complicated operations limit their industrial-scale application.

### **2.4.3 Collagen**

Collagen is the major constituent of collagenous solid wastes (e.g. skin, muscle, and tendons) generated from the fishing processing [42], leather trimming [70], poultry [46], and other industries. It is a fibrous, biocompatible and biodegradable protein, which is rich in animals and, accounts for about 30% of the body's total protein [102]. There are several common methods to isolate collagen, including acid solution, acid solution with enzymes and neutral saline solutions [103]. For acid extraction, propionic acid solubilization approach could obtain collagen with higher yield (93%) from raw skin or hide trimming wastes [70], compared to acetic acid treatment with a yield of 85%. Another modified acid-enzyme solubilization method could extract collagen from cow hides with the highest yield of 75.13% [71]. Recently, several advanced technologies that are economical, effective and time saving have been springing up, including high pressure, electrical pulse, and ultra-sonication [72]. For example, Akram and Zhang [72] extracted collagen from chicken sternal cartilage through the 'green' method using pepsin and ultra-sonication treatments. The highest collagen-II content was approximately 80%. In addition, this method was proved to improve the physicochemical and functional properties such as thermal stability of collagen-II. To date, collagen derived from animal wastes has been applied in terms of tissue engineering, biomaterials, pharmaceutical and cosmetics industry [70]. Salim et al. [46] obtained collagen from chicken feet via a facile method of pepsin digestion and used it as a precursor to form low-cost porous carbon fibers in large quantities by wet spinning. Govindharaj et al. [42] treated waste eel skin with acetic acid, common salt and pepsin to obtain the collagen, which was then incorporated into alginate hydrogel to produce 3D scaffolds for tissue engineering application.

### **2.4.4 Gelatin**

Gelatin, a kind of hydrocolloid and high molecular weight peptide that contains most amino acids, is usually derived from collagen. Factors like different extraction methods,

extraction conditions (e.g. specifically the temperature, pH, pretreatments, and time), types of raw materials, and hydrolysis of collagen could relatively affect the yield, quality and functionalities of gelatin [74]. It has various applications in food industry (e.g. thickening agent, stabilizer, texturizer, and gelling agent), pharmaceutical industry and membrane technology because of its unique gel strength, rheological properties, and excellent film forming ability [44]. Boughriba et al. [44] extracted gelatin from fresh blackchin guitarfish through NaOH treatments, while Khiari et al. [73] recovered gelatin from Atlantic mackerel skins by various organic acids. No significant difference was observed among these organic acids, and the highest yield was 31.8%. Al-Hassan [74] used calcium hydroxide and ammonium sulfate to isolate gelatin from the skins of camels, and the yield of gelatin was up to 36.8-42.2%. However, these conventional methods generally obtained a low yield because the linkages among collagen molecules are quite stable. Therefore, ultrasound treatment has attracted much attention, which could improve the extraction efficiency and the functional properties of gelatin. For instance, Ali et al. [75] pretreated golden carp skin with different acids, with or without prior-ultrasonication, to extract gelatin. It was found that the method with sulfuric acid/acetic acid along with prior-ultrasonication improved the efficacy of extraction (highest yield of 62.2%) and gelling strength of the obtained gelatin.

#### **2.4.5 Keratin**

Keratin is a significant component in hair, chicken or bird's feathers, bristles, horns, hooves, and nails. Millions tonnes of keratin containing wastes are produced every year over the world, typically in poultry slaughterhouses and fabric textile industry [45]. The content of keratin in animal hair (including human hair) and poultry feathers is over 90% [104]. It is present as  $\alpha$ -keratin in hair, horns and hoofs and  $\beta$ -keratin in bird feathers, respectively. Keratin plays an important role in providing a tough matrix for substances due to its mechanically durable property. The extraction, purification and characterization of keratin from raw materials can facilitate the development of keratin-

based materials for tissue engineering [76], cosmetics, agriculture, and biodegradable packaging [45].

Soluble keratin can be obtained by hydrolysis (e.g. alkaline, acid, or enzyme), oxidation or reduction of disulfide bonds, thermal treatment, and steam flash explosion [45]. The yield of keratin through hydrolysis depends on temperature, pH, time, and type and concentration of alkaline, acid, and enzyme. Sinkiewicz et al. [45] used 2.5% NaOH pretreatment and thermo-chemical treatment with different reducing agents (e.g. 2-mercaptoethanol, dithiothreitol, sodium metabisulfite, and sodium hydroxide) to prepare keratin from chicken feathers, and the highest yield was 94%, while the yields of keratin through sodium sulfide and L-cysteine were about 88% and 66% in another study [105]. Ramya et al. [76] extracted keratin from red sheep's hair using sodium metabisulfite, urea and SMBS. This method had a yield of 96%, but the high cost for operation and chemicals, highly concentrated agents, long processing time, and potential health and environmental risks limited its application in industrial production. Therefore, Tasaki [77] developed a two-step thermal hydrolysis process without the use of chemicals to extract keratin from hog hair, and the yield was nearly 70%.

#### **2.4.6 Chitin/Chitosan**

Chitin and chitosan are commonly found in crustaceans, insects, and microorganisms [43]. Among them, the shells of crustaceans such as shrimp, crab, and lobster are the most significant sources. Through enzymatic or chemical deacetylation, chitin can be converted to its derivative, chitosan. Due to their hydroxyl, amino and carbonyl groups, they can be acylated, esterified, etherified, alkylated, oxidized, chelated, graft copolymerized, and crosslinked. Both chitin and chitosan are widely used in biomedicine, water treatment, enzyme immobilization, stabilization, purification, and so on [15,106,107].

The most common methods to isolate chitin are chemical and biological treatments that involve two steps, demineralization and deproteinization. Concentrated acids and bases are usually used in chemical treatments, while microorganisms including lactic acid bacteria and other microbial species are applied in biological route [108]. In recent years, these methods have been modified to reduce operation time, and improve the purity and thermal stability of chitin and chitosan. Kaya et al. [78] reported that repeating a NaClO treatment twice for 10 min before demineralization and deproteinization could speed up the isolation of chitin from the shells of crab, crayfish and shrimp, and save energy. In addition, the percentage chitin yields from biomass wastes through this new method were in the range of 13-14%, which were very similar to the previously reported yields by conventional way (10-20%). Eddy et al. [43] investigated the effect of acid concentration on the chitosan extraction efficiency from shrimp shell. The result showed that chitosan obtained from concentrated acid and base treatment was highly pure with the degree of deacetylation of 80% and had better heat resistance compared with commercial chitosan. Besides, chitin nanocrystals were also obtained from prawn shell (20% yield) [109], oceanic biomass wastes [110] and shrimp [111] by extraction and acid hydrolysis. These nanocrystals were then applied as Pickering emulsion stabilizers, and functional additives in bio-nanocomposites to enable good water treatment capacity, and antibacterial and antioxidant activities.

## **2.5 Functional materials derived from biomass wastes**

In spite of being good sources of natural polymers, biomass wastes also have functional groups and unique properties, so they can be directly reused, especially as adsorbents and construction materials [112,113]. In addition, they can be used as precursor or base to make functional carbon-based materials through pyrolysis and hydrothermal, physical, and chemical activations, which has attracted much attention in last five years.

Till now, various forms of carbon-based materials, including biochar, AC, graphitic

carbon, and so on, have been developed. Both biochar and AC are produced by pyrolysis, but there are fine distinctions between them, such as feedstock, pyrolysis conditions, activation treatments, porous structures, and applications [114]. The feedstock for biochar includes various biomass wastes, such as peanut shell, corn stalk, and some animal wastes. Biochar is obtained by the pyrolysis of organic materials at the temperature of below 700 °C and limited oxygen condition in a hot sealed reactor [115]. This process is eco-friendly, available, and efficient compared to the productions of other charcoals because the reactors are nontoxic and recyclable. The pyrolysis conditions, such as the temperature and ramping rate, have significant impact on the microstructures of biochar, resulting in various functional properties [116]. Therefore, biochar has shown great potentials in water treatment, soil amendment, and catalytic oxidation of organic pollutants [115]. However, if pyrolysis process is incomplete, pollutants such as NO<sub>x</sub>, SO<sub>x</sub>, smoke, aerosols, and unburned hydrocarbons will be formed and released, impacting environment and health [117]. AC can be produced from biomass or other carbonaceous substances (e.g. coal) through pyrolysis at the temperature above 700 °C. AC usually has larger specific surface area and smaller microporous structure compared to biochar. It is worth noting that biochar can be converted into AC with optimized porous structure and specific surface area by activation process (e.g. KOH and NaOH chemical and physical activation). Thus, the biochar-based AC was prepared and applied in EDLC [16].

Graphitic carbon is commonly obtained from soft carbons (e.g. petroleum coke) via heating above 2100 °C [118]. The in-plane structure of graphene layers in the graphitic carbon is almost similar to that in graphite. It is produced by various synthetic methods to increase the degree of graphitization, including direct heating of porous carbons at 2500-3000 °C, and catalytic graphitization where in-situ graphitic nanostructure was obtained by metal catalysts [119].

These carbon-based materials not only possess high specific surface area, porous structure, and abundant surface functional groups, but also exhibit favorable chemical stability, great performance, and regeneration capacity [120]. Their SEM images are shown in Figure 2.2. Many efforts have been made to investigate their potential applications as adsorbents, catalyst carriers, electrode materials, and functional composites.

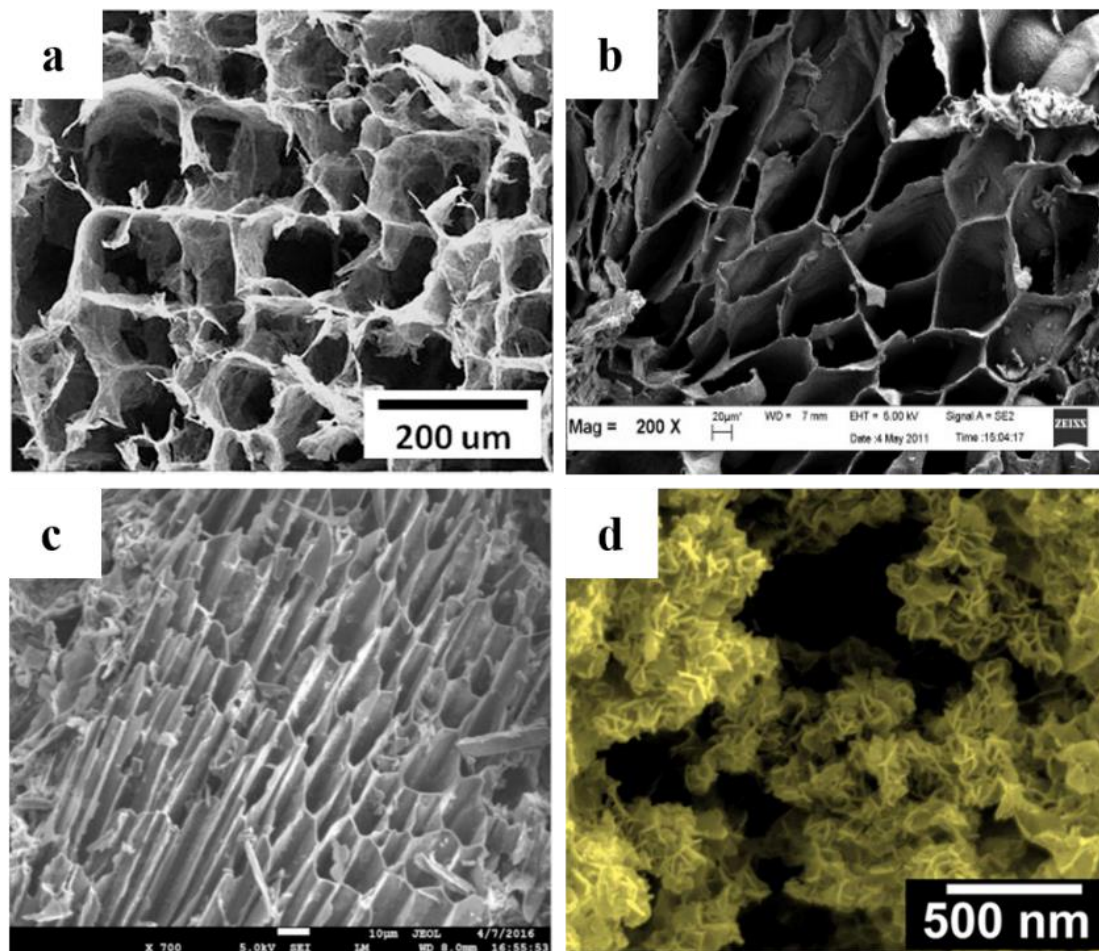


**Figure 2.2** SEM images of carbon-based materials derived from biomass wastes: (a) lignin-modified graphene aerogel from corncob; (b) activated carbon from rambutan peel; (c) biochar from wheat straw; and (d) graphitic-carbon nanoflakes from green tea waste [2,97,121,122] (Reproduced by permissions from [2], copyright [2016, Elsevier], from [97], copyright [2018, Elsevier], from [121], copyright [2014, Elsevier] and from [122], copyright [2019, Elsevier])

### 2.5.1 Adsorbent materials

Functional groups including carboxyl, hydroxyl, sulfhydryl, and amide of biomass wastes play an important role in adsorbing contaminants from liquid phase or natural gas. The adsorption of heavy metals by directly utilizing the raw biomass wastes, such as leaves [112], orange peel [8], tea waste [123], crop shells [113], and ESM [124], has been studied. It can not only lower the production cost of adsorbents but also improve the recovery efficiency of biomass wastes. Lee and Choi [125] used RPL and DPL as adsorbents to remove heavy metals ( $\text{Pb}^{2+}$ ,  $\text{Cu}^{2+}$  and  $\text{Cd}^{2+}$ ), because persimmon leaves have numerous hydroxyl groups that can bind with heavy metals. The study revealed that both RPL and DPL displayed high removal efficiencies (over 98%) towards  $\text{Pb}^{2+}$ ,  $\text{Cu}^{2+}$  and  $\text{Cd}^{2+}$  at the concentrations of adsorbates below 1 mg/L. Compared to RPL, the removal rate of DPL was 10-15% higher, and the removal efficiency of  $\text{Pb}^{2+}$  was highest among three heavy metals, followed by  $\text{Cu}^{2+}$  and  $\text{Cd}^{2+}$ . In terms of adsorption performance, the maximum adsorption capacity of  $\text{Pb}^{2+}$ ,  $\text{Cu}^{2+}$  and  $\text{Cd}^{2+}$  was 22.59 mg/g, 19.42 mg/g, and 18.26 mg/g, respectively. Monteiro et al. [126] reported that seafood waste, crab carapace and clam shell, could be used to remove  $\text{Hg}^{2+}$  and  $\text{Cd}^{2+}$  from wastewater, and the  $\text{Hg}^{2+}$  removal efficiency of both adsorbents were higher than 80% in monometallic solutions, while the uptake of  $\text{Hg}^{2+}$  was limited due to high kinetic and equilibrium selectivity for  $\text{Cd}^{2+}$  in binary solutions. Feizi and Jalali [113] investigated competitive adsorption of heavy metals ( $\text{Cd}^{2+}$ ,  $\text{Cu}^{2+}$ ,  $\text{Ni}^{2+}$ ,  $\text{Zn}^{2+}$ ,  $\text{Fe}^{3+}$ , and  $\text{Mn}^{2+}$ ) by sunflower, potato, canola, and walnut shell. The study showed that the adsorption capacities of biosorbents were as followed: sunflower > potato > canola > walnut shell. Among various heavy metals, the adsorption capacity towards  $\text{Cd}^{2+}$  was highest, up to 50-70 mg/g at the concentration of adsorbate of around 150 mg/L. ESM also has good adsorbent properties for the removal of heavy metals and dyes from wastewater. Choi [124] esterified carboxylic groups to endow ESM with a high cationic charge density, and thus improved the capacity to remove negatively charged sulfur dye. The results revealed that methyl-esterified ESM showed over 98% removal of sulfur dye at optimal

condition, and 0.68-0.73 mg/L sulfur dye could be adsorbed by 1 mg/L adsorbent.

However, there are some drawbacks for directly using raw biomass wastes as adsorbents. For example, the removal rate of heavy metals is relatively low due to the slow diffusion or limited surface-active sites. It is also difficult to separate the adsorbents from solutions and recycle them for multiple usage. As a result, the conversion of biomass wastes into different forms of carbon-based materials with better adsorption capacities has been investigated in the past five years.

Biochar is widely used as adsorbents for removing heavy metals from wastewater. Yu et al. [2] made three kinds of biochars from peanut shell, corn stalk and wheat straw to remove hydrophilic ionic liquid, [BMIM][Cl]. It was found that these biochars exhibited similar microporous structures and a large number of oxygen-containing functional groups. All of them showed higher removal rates ( $q_{\max}$  of 0.644~0.888) than those of other reported carbon-based materials (e.g.  $q_{\max}$  of 0.170~0.520). As well, Sattar et al. [127] used peanut shell as feedstock material for the production of biochar to remove  $As^{5+}$  and  $As^{3+}$  from water. The  $As^{5+}$  and  $As^{3+}$  removal rates of PSB were up to 99% (at pH 6.2) and 95% (at pH 7.2) with 0.6 g/L adsorbent dose, 5 mg/L initial As ion concentration, and 2 h equilibrium time, which was due to its abundant surface functional groups. In order to further improve the adsorption capacity, biochars are modified with special functional groups through chemical treatments. Chen et al. [128] prepared CFCP from chicken feather, whose functional groups and super surface area were beneficial to its adsorption capacities of  $Cd^{2+}$  and  $Pb^{2+}$ . The results showed that, compared to the biochar without modification, CFCP had faster adsorption rate probably due to the increased N-containing heterocycles. Gao et al. [129] prepared biochar from grapefruit endothelium and modified it by iron ion and polyaniline through biosorption-pyrolysis method. This novel biochar displayed superior removal capacity towards  $Cr^{6+}$  (up to 100% within 135 min at initial  $Cr^{6+}$  concentration of 50

$\mu\text{M}$ , 30 mL) mainly due to the synergistic effect of polyaniline and iron ion. Peng et al. [130] obtained biochars from corn stalk, almond shell, and dairy manure with Fe/Al (hydr)oxides via co-precipitation. These biochars displayed better performance for removing phosphate than other adsorbents possibly due to the synergistic effects of Fe/Al oxides and biochar with larger surface area, higher pore volume, and more reactive surface hydroxyl sites. However, the application of biochar in water treatment still faces the struggle of the inconvenient separation [115].

Biomass-derived AC also can be used as adsorbents for environmental remediation. The adsorption capacity of AC usually depends on the precursor, activation methods, physical and chemical pre-treatments, type of activating agents, and gasification time [131]. Especially, after thermal or chemical pre-treatments, the surface functional groups and physical and chemical structures of AC can be improved, resulting in the better adsorption performance. Mehrvarz et al. [131] generated AC from the broom sorghum stalk, followed by the treatment with triethylenetetramine to functionalize the surface of AC. The study showed that the modified AC dramatically enhanced the selectivity of  $\text{CO}_2/\text{CH}_4$  and the adsorption of  $\text{CO}_2$  was up to 3.20 mmol/g. Njoku et al. [121] used microwave heating for KOH activation to obtain AC from rambutan peel, which was different from conventional heating methods. This method could shorten the activation time significantly (12 min for this study but 60 min for others) and the adsorption capacity of the resultant AC for acid yellow 17 dye was in the range of 49.14 and 215.05 mg/g at dye concentrations from 50-400 mg/L. Georgin et al. [35] investigated the adsorption capacity of AC derived from peanut shell through conventional pyrolysis and MW-P. It was found that AC obtained by MW-P presented stronger adsorption capacity for organic dyes at pH 2.5 due to its higher total pore volume ( $0.210 \text{ cm}^3/\text{g}$ ) and larger surface area ( $395.80 \text{ m}^2/\text{g}$ ) compared to the conventionally pyrolyzed samples. The adsorptions towards direct black 38 and reactive red 141 dyes were between 56.7-96.6 mg/g and 165.7-260.3 mg/g, respectively,

at the concentrations of dyes of 100-350 mg/L.

Overall, the direct use of biomass wastes as adsorbents is a simple and cost-effective way to remove the heavy metals. Through modifying the structure or surface functional groups of biomass wastes, the adsorption capacity could be improved. Additionally, carbon-based adsorbents obtained from biomass wastes usually have higher adsorption capacities due to their larger surface area and higher porosity. However, these processes increased the cost, and the recyclability of adsorbents needs to be improved.

### **2.5.2 Catalytic materials**

The conversion of biomass wastes into value-added biochar as catalysis matrix is another attractive option. Liu et al. [115] studied the performance of nitrogen doped magnetic biochar produced from rice straw in catalytic oxidation of metolachlor. The study showed that the doped nitrogen atoms could significantly increase the surface basicity and facilitate the catalytic degradation of metolachlor along with peroxymonosulfate. In addition, adding proper transition metals into biomass-derived biochar has been illustrated to be beneficial to endow it with good catalytic capacity. Liu et al. [132] explored a one-pot method to make an Ag loaded biochar hybrid material via fast pyrolysis from the fir sawdust and studied its catalytic capacity of the HCOOH-induced  $\text{Cr}^{6+}$  reduction.  $\text{Ag}@$ biochar could facilitate the reduction from  $\text{Cr}^{6+}$  to  $\text{Cr}^{3+}$  in liquid within 20 min with the efficiency of 93%, which revealed its good catalytic activity to this reaction. Considering the adverse environmental effect on land caused by uncontrolled release of caffeine in spent coffee ground, Cho et al. [133] fabricated Co-loaded waste coffee grounds to produce value-added Co-biochar catalyst in one-step. It was found that the catalyst presented superior catalytic capacity to reduce 70.1% of 0.17 mM PNP within 5 min.

AC is another option as a catalyst support due to its great internal surface area, high

inertness, and versatility. However, biomass waste-derived AC usually displays the low recoverability and reutilization. Thus, Huang et al. [134] chose *Enteromorpha prolifera* (a kind of marine green alga) and  $K_2FeO_4$  as bases to fabricate  $Fe_3C/C$  composite (an improving Fenton-like catalyst) via a simple one-step calcination synthesis method (Figure 2.3). The results revealed that the catalyst exhibited great catalytic and adsorption capacities, which could decrease the COD volume (below 50) in actual plant wastewater and be catalytic for NOR degradation. It also presented perfect stability and recyclability.

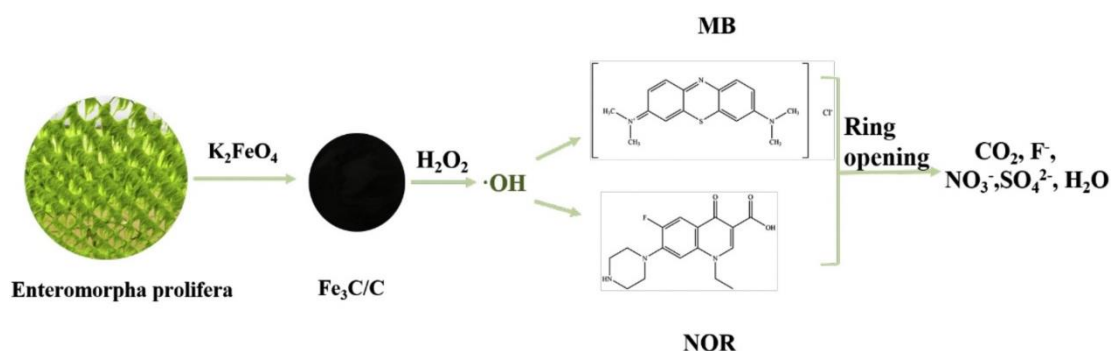


**Figure 2.3** Schematic diagram of  $Fe_3C/C$  composite for methylene blue removal and NOR degradation [134] (Reproduced by permission from [134], copyright [2019, Elsevier])

### 2.5.3 Electrode materials

Over the past few years, many researches have focused on converting biomass wastes into energy-storage materials. The carbon-based materials derived from biomass wastes with high specific surface area can facilitate the process of interfacial interactions between the electrode and electrolyte ions by decreasing ions delivering resistance and diffusion distance [119]. Table 2.2 shows the specific properties of electrode materials derived from different biomass wastes.

**Table 2.2** Electrode porous carbons derived from biomass wastes

Raw Material	Treatment	Electrolyte	Specific capacitance

Rice husks [135]	KOH activation, at temperatures between 400 and 900 °C	6 M KOH	367 F/g at 5 mV/s*
		1.5 M TEA-BF <sub>4</sub> in acetonitrile	174 F/g at 5 mV/s*
Loblolly pine chips [16]	Different carbonization methods and NaOH activation	6 M KOH	74 F/g at 20 mV/s*
Tissue paper produced by wood pulp [136]	One-step carbonization and activation treatment	6 M KOH	~200 F/g at 1 mV/s*
Tissue paper produced by straw [136]			~150 F/g at 1 mV/s*
Dawn redwood cone [137]	Pre-carbonization and chemical activation	6 M KOH	197 F/g at 1.0 A/g*
Starch-based packing peanuts [119]	KOH activation	1 M TEA-BF <sub>4</sub> in acetonitrile	149 F/g at 0.5 mA/cm <sup>2</sup> *
Cherry stones [138]	Pretreatment of lignin dissolution-precipitation	6 M KOH	370.5 F/g at 0.5 A/g**
Palm-shell [139]	Graphitic carbon prepared by dispersion of AC in the graphene layers	1 M HCl	54.6 F/g**

Green tea waste [140]	KOH activation with 1 M H <sub>2</sub> SO <sub>4</sub> water or hydrochloric acid treatment	~162 F/g at 0.5 A/g**
-----------------------	---	--------------------------

---

‘\*’ Tested in two-electrode system

‘\*\*’ Tested in three-electrode system

EDLC and pseudo capacitors are two device schemes of supercapacitors. However, the applications of pseudo capacitor are limited because of their poor cycle stability and low electrical conductivity [138]. Due to the high-power density and superior charge-discharge stability of EDLC, more studies are focusing on them. Generally, different forms of carbon-based electrode materials include AC [135], biochar-based AC [16], graphitic carbon [119], microporous carbons [136], and so on. Gao et al. [135] transformed rice husk into AC through KOH activation. Because SiO<sub>2</sub> nanocrystals were encompassed by a carbon matrix in the rice husk, the AC kept the size and shape, and had an increased ordering degree of carbon which showed great high-power solving performance and electrochemical cycle capacity. Moreover, He et al. [16] recycled loblolly pine chips to fabricate biochar-based ACs by NaOH activation and then assembled it into EDLCs as electrode materials due to its high surface area and huge pore volume.

Many factors have the impact on the electrochemical capacity such as the structure of raw materials, carbonization temperature, activation and pretreatments, which lead to various pore structure, SSA and high porosity of carbon materials [136]. For example, two kinds of tissue papers (from wood pulp and straw) were converted into carbon materials by one-step carbonization and activation treatment. It was revealed that the carbon with microporous structure obtained from wood pulp at 700 °C displayed better capacitance (~200 F/g at 1 mV/s), while the carbon derived from straw presented hierarchical porous structure with decreased capacitance at 900 °C [136]. Jia et al. [137]

prepared nitrogen-doped porous carbon from dawn redwood waste through carbonization combination with chemical activation. It displayed a large SSA of 1831 m<sup>2</sup>/g and superior performance with the specific capacitance of 326 F/g at current density of 0.5 A/g. Zhang et al. [138] fabricated the nitrogen-doped carbon from cherry stones which showed hierarchical porous structure through the lignin dissolution-precipitation pretreatment and molten salt activation. It was found that the material possessed the excellent specific capacitance of 370.5 F/g at the current density of 0.5 A/g, and about 99% of this capacitance was kept after 5,000 cycles.

Among these carbon-based electrode materials, graphitic carbon has been considered as a promising electrode material due to its low cost, superior electrochemical stability, large SSA (1000-3000 m<sup>2</sup>/g), high specific capacitance and eco-friendliness [122]. Sankar et al. [122] successfully prepared ultrathin mesoporous graphitic carbon from green tea via KOH activation, with either water or hydrochloric acid treatments. It was shown that water-treated graphitic-carbon nanoflakes presented higher specific capacitance of 162 F/g at 0.5 A/g.

It is worth noting that electrode materials can also be used to treat wastewater through capacitive deionization. Chong et al. [139] prepared graphitic activated carbon from palm-shell, which displayed high electrical conductivity and better electrosoption stability compared to AC electrodes.

#### **2.5.4 Composite materials**

In general, two or more components that possess distinctive properties can consist of composite materials, and the properties of composites are not attainable with the separated components [141]. In recent years, the use of biomass wastes like rice husk [25], rice straw [142], flax [143], and fly ash [23], as unconventional construction materials is an interesting solution, since the construction department should always

face the issues about greenhouse gas emission, the disposal and recycling of raw materials and sustainable development [25]. Hu et al. [23] prepared reactive rice husk ash using the self-designed combustion system and applied it in cement-base materials. It was found that the compressive strength of mortars was improved with the increase of the rice husk ash content. As well, this approach to utilize rice husk ash was environmentally friendly, which was indicated by sustainability analysis. Martinez-Lage et al. [10] also reported that with the addition of biomass ash, the flexural strength decreased, but the compressive strength of all the composite mortars increased.

Despite of the construction applications, the carbon-based materials derived from biomass wastes were also widely used to endow the composites with other functional properties, such as conductivity, adsorption, hydrophobicity, and so on. Zhu et al. [144] developed an interfacial catalytic engineering protocol to prepare carbon microtube anodes for Li batteries that were graphitic, porous and co-doped with heteroatoms from hair waste. During the biomass graphitization, Ni-based nanofilm played an important catalytic role in  $\text{Li}^+$  diffusions and formation of deep pores. It was revealed that the microtube presented superior anodic behaviors on recycling capacity, active utilization efficiency, long-term cyclic stability, and rate capabilities. However, the complicated preparation and the existence of toxic and non-sustainable chemicals limit its application [145]. Hence, the interlayer is proposed, which is a carbon film placed between the separator and sulfur cathode to improve the rate ability and cyclic stability in Li-S batteries [145]. The introduction of interlayer is beneficial to reuse the active compounds during energy storage. Zhu et al. [146] prepared NB-PPCA from pomelo peel by hydrothermal process, freeze-drying, and pyrolysis process (Figure 2.4). It was used as an interlayer on pristine separator in Li batteries, and showed superior initial discharge capacity, high specific capacity, and better cyclic stability and rate ability compared to other cells with PPCA separator and pristine separator.

In terms of adsorption capacity enhancement, apart from chemical modification, the incorporation of nanoparticles is another effective way. Li et al. [147] assembled nHAP and wood-processing residues, wheat straw and Chinese medicine residues to prepare nHAP@biochar. The nHAP particles had a large surface area, and the calcium on their surface could be easily replaced by heavy metals. It was found that tylosin and  $\text{Cu}^{2+}$  could be removed by nHAP@biochar simultaneously but the adsorption quantities for the antibiotic and heavy metal were affected by the pyrolysis temperature. Zhao et al. [148] reported the effect of adding silica particles in bamboo-derived biochar on its stability and adsorption capacities for tetracycline (Figure 2.4). The total pore volume, thermal stability, and adsorption capacity of biochar obviously increased after adding silica, which was attributed to the structure of silica and interaction between silica and biochar. Fan et al. [149] fabricated a magnetic tea waste/ $\text{Fe}_3\text{O}_4$  composite via a chemical co-precipitation method. Loading tea waste with nano- $\text{Fe}_3\text{O}_4$  particles not only could enhance the stability of nanoparticles but also endowed the material with excellent superparamagnetic property for easy separation. The chromium adsorption test revealed that this composite presented high adsorption capacity of up to 75.76 mg/g. It also had a good reusability, and the removal rate was still higher than 70% after five recycling cycles.

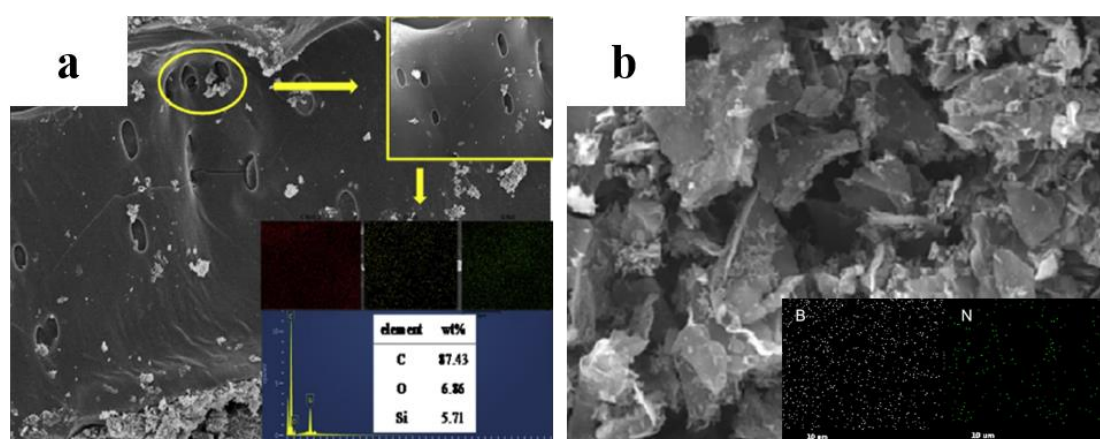


**Figure 2.4** SEM images and elemental mapping of composite materials derived from biomass wastes: (a) silica-loaded biochars from bamboo; and (b) nitrogen and boron dual-doped aerogel from pomelo peel [146,148] (Reproduced by permissions from [146])

and [148], copyright [2019, Elsevier]).

The hydrophobic property of composite is worth noting as well because it is relevant to the functionalities such as catalytic property and self-cleaning. Chen et al. [97] modified graphene aerogel by mixing lignin from corncob through one-step hydrothermal treatment. This kind of aerogel showed good capacity of adsorbing petroleum oils and toxic solvents (e.g. toluene, chloroform, carbon tetrachloride), owing to the hydrophobic constituents in lignin skeletons and porous structure of graphene aerogels. Besides, the aerogel could be reused by repeated heat treatment and compression. Fitria et al. [150] used coffee bean waste to produce hydrophobic layer, which was obtained through carbonization method, dispersed in acetic acid, and then coated with PVA binder. It was shown that the ratio of carbon and PVA could affect the hydrophobicity property. The composite possessed comparable hydrophobicity compared to that of other well-known materials.

## **2.6 Conclusion and future perspectives**

This review highlights the research work on the biomass wastes reuse and recycling in recent five years, where agricultural and forestry residues, animal wastes, industrial wastes, and municipal solid wastes have been frequently studied. Instead of treating these biomass wastes in traditional methods (e.g. incineration and landfill), many researchers intended to extract natural polymers such as cellulose, lignin, gelatin, chitin and so on from biomass wastes through various approaches for further applications in food, agriculture, and medicine. Compared to conventional extraction approaches, novel methods such as organosolv process (especially two-phase system), combination of mechanical, chemical and biological treatments, and incorporation of pressure or ultrasonication have been proposed to isolate natural polymers in a more efficient and eco-friendly way. These technologies also aim to improve the yields and purities of extracted products, simplify the extraction processes, and enhance the functional

properties of extracts. Several efforts have been made to directly reuse biomass wastes as adsorbents for water contaminant removal or additives of composite materials in a simple and cost-effective way, but more attention has been paid to convert them into carbon-based materials (e.g. biochar, AC, and graphitic carbon) with large surface area, porous structure, favorable chemical stability, great performance, and regeneration capacity. Various methods such as thermal and chemical pretreatments and incorporation of nanoparticles have been applied to further improve the functionalities of carbon-based materials so as to enable their applications as adsorbents, catalyst carriers, electrode materials, and functional composites.

It is believed that biomass wastes are a promising source of natural building blocks, and the reuse and recycling of biomass wastes could relieve the environmental pressure. However, future research in the following areas is required to promote their practical applications:

1. Quality control is the key to future development. Current biomass wastes derived products are prepared in research labs, so it is easy to get enough raw materials from the certain suppliers. Once the production scale is enlarged, the required biomass wastes collected from different seasons and locations may vary. Therefore, the quality control is necessary to determine the compositions of biomass wastes and the molecular structure of targeted natural polymers, so as to ensure the desirable properties of final products.
2. Feasible and cost-effective approaches for the conversion of biomass wastes into value-added products are expected in future studies. For the extraction of natural polymers, more works should focus on the development and optimization of extraction methods that are able to scale up and can generate products with high yields and purities for each major biomass wastes. In terms of functional materials derived from biomass wastes, systematically study is needed to better modulate the properties of carbon-based materials by actively designing and controlling their structures. Moreover, a wider

vision should be encouraged to develop other types of materials (rather than carbon) so as to facilitate the reuse and recycling of biomass wastes.

3. Safety issues of biomass wastes derived products need to be investigated. Although the major components in biomass wastes are biocompatible and nontoxic, there are still certain amounts of 'impurities' or contaminants existed. Moreover, various nanoparticles are incorporated to improve the performance of composite materials, which also cause some concerns. Therefore, it is necessary to study case-by-case the fate of these minorities in materials and their potential safety issues.

## 2.7 References

1. Tong, X. C., *Introduction to materials for advanced energy systems*. Springer: Cham, Switzerland, **2019**.
2. Yu, F.; Sun, L.; Zhou, Y.; Gao, B.; Gao, W.; Bao, C.; Feng, C.; Li, Y., Biosorbents based on agricultural wastes for ionic liquid removal: An approach to agricultural wastes management. *Chemosphere* **2016**, *165*, 94-99.
3. Hakeem, K. R.; Jawaid, M.; Alothman, O. Y., *Agricultural biomass based potential materials*. Springer: Cham, Switzerland, **2015**.
4. McKendry, P., Energy production from biomass (part 1): Overview of biomass. *Bioresource Technology* **2002**, *83* (1), 37-46.
5. Kour, S.; Mishra, A.; Sinha, A.; Kaur, P.; Singh, H., The development of mesoporous ni-based catalysts and evaluation of their catalytic and photocatalytic applications. *ChemistrySelect* **2020**, *5* (12), 3710-3723.
6. Tripathi, N.; Hills, C. D.; Singh, R. S.; Atkinson, C. J., Biomass waste utilisation in low-carbon products: Harnessing a major potential resource. *npj Climate and Atmospheric Science* **2019**, *2* (1), 35.
7. Danish, M.; Ahmad, T., A review on utilization of wood biomass as a sustainable precursor for activated carbon production and application. *Renewable Sustainable Energy Reviews* **2018**, *87*, 1-21.
8. Bhatnagar, A.; Sillanpaa, M.; Witek-Krowiak, A., Agricultural waste peels as versatile biomass for water purification - a review. *Chemical Engineering Journal* **2015**, *270*, 244-271.
9. Ok, Y. S.; Tsang, D. C. W.; Boland, N.; Novak, J. M., *Biochar from biomass and waste: Fundamentals and applications*. Elsevier: Chambridge, **2019**.
10. Martinez-Lage, I.; Velay-Lizancos, M.; Vazquez-Burgo, P.; Rivas-Fernandez, M.; Vazquez-Herrero, C.; Ramirez-Rodriguez, A.; Martin-Cano, M., Concretes and mortars with waste paper industry: Biomass ash and dregs. *Journal of Environmental*

*Management* **2016**, *181*, 863-873.

11. Bello, O. S.; Adegoke, K. A.; Olaniyan, A. A.; Abdulazeez, H., Dye adsorption using biomass wastes and natural adsorbents: Overview and future prospects.

*Desalination and Water Treatment* **2015**, *53* (5), 1292-1315.

12. Mishra, S.; Kharkar, P. S.; Pethe, A. M., Biomass and waste materials as potential sources of nanocrystalline cellulose: Comparative review of preparation methods (2016 - till date). *Carbohydrate Polymers* **2019**, *207*, 418-427.

13. Amaral, H. R.; Cipriano, D. F.; Santos, M. S.; Schettino, M. A., Jr.; Ferreti, J. V. T.; Meirelles, C. S.; Pereira, V. S.; Cunha, A. G.; Emmerich, F. G.; Freitas, J. C. C., Production of high-purity cellulose, cellulose acetate and cellulose-silica composite from babassu coconut shells. *Carbohydrate Polymers* **2019**, *210*, 127-134.

14. C.S, J. C.; George, N.; Narayanankutty, S. K., Isolation and characterization of cellulose nanofibrils from arecanut husk fibre. *Carbohydrate Polymers* **2016**, *142*, 158-166.

15. Uranga, J.; Etxabide, A.; Cabezudo, S.; de la Caba, K.; Guerrero, P., Valorization of marine-derived biowaste to develop chitin/fish gelatin products as bioactive carriers and moisture scavengers. *Science of the Total Environment* **2020**, *706*, 10.

16. He, N.; Yoo, S.; Meng, J.; Yildiz, O.; Bradford, P. D.; Park, S.; Gao, W., Engineering biorefinery residues from loblolly pine for supercapacitor applications. *Carbon* **2017**, *120*, 304-312.

17. Cho, E. J.; Trinh, L. T. P.; Song, Y.; Lee, Y. G.; Bae, H.-J., Bioconversion of biomass waste into high value chemicals. *Bioresource Technology* **2020**, *298*, 122386.

18. Sun, D.; Ge, Y.; Zhou, Y., Punishing and rewarding: How do policy measures affect crop straw use by farmers? An empirical analysis of jiangsu province of china. *Energy Policy* **2019**, *134*, 110882.

19. Seglah, P. A.; Wang, Y.; Wang, H.; Bi, Y.; Zhou, K.; Wang, Y.; Wang, H.; Feng, X., Crop straw utilization and field burning in northern region of ghana. *Journal of Cleaner Production* **2020**, *261*, 121191.

20. Passoth, V.; Sandgren, M., Biofuel production from straw hydrolysates: Current achievements and perspectives. *Applied Microbiology and Biotechnology* **2019**, *103* (13), 5105-5116.
21. Xiao, R.; Wang, P.; Mi, S. S.; Ali, A.; Liu, X. Y.; Li, Y. M.; Guan, W. D.; Li, R. H.; Zhang, Z. Q., Effects of crop straw and its derived biochar on the mobility and bioavailability in cd and zn in two smelter-contaminated alkaline soils. *Ecotoxicology and Environmental Safety* **2019**, *181*, 155-163.
22. Luduena, L.; Fasce, D.; Alvarez, V. A.; Stefani, P. M., Nanocellulose from rice husk following alkaline treatment to remove silica. *Bioresources* **2011**, *6* (2), 1440-1453.
23. Hu, L.; He, Z.; Zhang, S., Sustainable use of rice husk ash in cement-based materials: Environmental evaluation and performance improvement. *Journal of Cleaner Production* **2020**, *264*, 121744.
24. Yaseri, S.; Masoomi Verki, V.; Mahdikhani, M., Utilization of high volume cement kiln dust and rice husk ash in the production of sustainable geopolymer. *Journal of Cleaner Production* **2019**, *230*, 592-602.
25. Chabi, E.; Doko, V.; Hounkpè, S. P.; Adjovi, E. C., Study of cement composites on addition of rice husk. *Case Studies in Construction Materials* **2020**, *12*, e00345.
26. Kong, J.; Gao, S.; Liu, Y.; Jin, X.; Wei, D.; Jiang, S.; Ye, K.; Wang, J.; Xing, P.; Luo, X., Recycling of carbonized rice husk for producing high purity silicon by the combination of electric arc smelting and slag refining. *Journal of Hazardous Materials* **2019**, *380*, 120827.
27. Liou, T. H.; Wang, P. Y., A sustainable route to synthesize graphene oxide/ordered mesoporous carbon as effect nanocomposite adsorbent. *Journal of Nanoscience and Nanotechnology* **2020**, *20* (5), 2867-2877.
28. Majeed, K.; Hassan, A.; Abu Bakar, A., Influence of maleic anhydride-grafted polyethylene compatibiliser on the tensile, oxygen barrier and thermal properties of rice husk and nanoclay-filled low-density polyethylene composite films. *Journal of Plastic Film & Sheeting* **2014**, *30* (2), 120-140.

29. Carneiro, A. P.; Rodriguez, O.; Macedo, E. A., Dissolution and fractionation of nut shells in ionic liquids. *Bioresource Technology* **2017**, *227*, 188-196.
30. Hill, G. M., Peanut by-products fed to cattle. *The Veterinary clinics of North America. Food animal practice* **2002**, *18* (2), 295-315.
31. Adhikari, B.; Dhungana, S. K.; Waqas Ali, M.; Adhikari, A.; Kim, I.-D.; Shin, D.-H., Antioxidant activities, polyphenol, flavonoid, and amino acid contents in peanut shell. *Journal of the Saudi Society of Agricultural Sciences* **2019**, *18* (4), 437-442.
32. Zhang, X.; Lian, H.; Shi, J.; Meng, W.; Peng, Y., Plant extracts such as pine nut shell, peanut shell and jujube leaf improved the antioxidant ability and gas permeability of chitosan films. *International Journal of Biological Macromolecules* **2020**, *148*, 1242-1250.
33. Arumugam, N.; Biely, P.; Puchart, V.; Singh, S.; Pillai, S., Structure of peanut shell xylan and its conversion to oligosaccharides. *Process Biochemistry* **2018**, *72*, 124-129.
34. Qi, N.; Hu, X.; Xin, X.; Ye, S.; Fu, Z.; Zhao, X., Mechanisms of biohydrogen recovery enhancement from peanut shell by *C. guangxiense*: Temperature pretreatment ranges from -80 to 100 °C. *Bioresource Technology* **2020**, *304*, 123026.
35. Georjgin, J.; Dotto, G. L.; Mazutti, M. A.; Foletto, E. L., Preparation of activated carbon from peanut shell by conventional pyrolysis and microwave irradiation-pyrolysis to remove organic dyes from aqueous solutions. *Journal of Environmental Chemical Engineering* **2016**, *4* (1), 266-275.
36. Ling, H.; Cheng, K.; Ge, J.; Ping, W., Corncob mild alkaline pretreatment for high 2,3-butanediol production by spent liquor recycle process. *BioEnergy Research* **2017**, *10* (2), 566-574.
37. Han, J.; Cao, R.; Zhou, X.; Xu, Y., An integrated biorefinery process for adding values to corncob in co-production of xylooligosaccharides and glucose starting from pretreatment with gluconic acid. *Bioresource Technology* **2020**, *307*, 123200.
38. Yu, J. S.; Zhao, Y. C.; Li, Y. D., Utilization of corn cob biochar in a direct carbon fuel cell. *Journal of Power Sources* **2014**, *270*, 312-317.

39. Nithya, R.; Ragupathy, S.; Sakthi, D.; Arun, V.; Kannadasan, N., Photocatalytic efficiency of brilliant green dye on zno loaded on cotton stalk activated carbon. *Materials Research Express* **2020**, *7* (7), 075002.
40. Singh, H.; Yadav, R.; Farooqui, S. A.; Dudnyk, O.; Sinha, A. K., Nanoporous nickel oxide catalyst with uniform Ni dispersion for enhanced hydrogen production from organic waste. *International Journal of Hydrogen Energy* **2019**, *44* (36), 19573-19584.
41. Singh, H.; Iyengar, N.; Yadav, R.; Rai, A.; Sinha, A. K., Facile conversion of levulinic acid to  $\gamma$ -valerolactone using a high surface area magnetically separable Ni/NiO catalyst. *Sustainable Energy & Fuels* **2018**, *2* (8), 1699-1706.
42. Govindharaj, M.; Roopavath, U. K.; Rath, S. N., Valorization of discarded Marine Eel fish skin for collagen extraction as a 3D printable blue biomaterial for tissue engineering. *Journal of Cleaner Production* **2019**, *230*, 412-419.
43. Eddy, M.; Tibb, B.; El-Hami, K., A comparison of chitosan properties after extraction from shrimp shells by diluted and concentrated acids. *Heliyon* **2020**, *6* (2), e03486.
44. Boughriba, S.; Souissi, N.; Jridi, M.; Li, S. M.; Nasri, M., Thermal, mechanical and microstructural characterization and antioxidant potential of rhinobatos cemiculus gelatin films supplemented by titanium dioxide doped silver nanoparticles. *Food Hydrocolloids* **2020**, *103*, 12.
45. Sinkiewicz, I.; Śliwińska, A.; Staroszczyk, H.; Kołodziejka, I., Alternative methods of preparation of soluble keratin from chicken feathers. *Waste and Biomass Valorization* **2017**, *8* (4), 1043-1048.
46. Salim, N. V.; Jin, X.; Mateti, S.; Lin, H.; Glattauer, V.; Fox, B.; Ramshaw, J. A. M., Porous carbon fibers made from collagen derived from an animal by-product. *Materials Today Advances* **2019**, *1*, 100005.
47. Khalil, M.; Berawi, M. A.; Heryanto, R.; Rizalie, A., Waste to energy technology: The potential of sustainable biogas production from animal waste in indonesia. *Renewable and Sustainable Energy Reviews* **2019**, *105*, 323-331.

48. Ravindran, B.; Lee, S. R.; Chang, S. W.; Nguyen, D. D.; Chung, W. J.; Balasubramanian, B.; Mupambwa, H. A.; Arasu, M. V.; Al-Dhabi, N. A.; Sekaran, G., Positive effects of compost and vermicompost produced from tannery waste-animal fleshing on the growth and yield of commercial crop-tomato (*lycopersicon esculentum* L.) plant. *Journal of Environmental Management* **2019**, *234*, 154-158.
49. Idowu, I.; Pedrola, M. O.; Wylie, S.; Teng, K. H.; Kot, P.; Phipps, D.; Shaw, A., Improving biodiesel yield of animal waste fats by combination of a pre-treatment technique and microwave technology. *Renewable Energy* **2019**, *142*, 535-542.
50. Al-Kaabi, Z.; Pradhan, R.; Thevathasan, N.; Gordon, A.; Chiang, Y. W.; Dutta, A., Bio-carbon production by oxidation and hydrothermal carbonization of paper recycling black liquor. *Journal of Cleaner Production* **2019**, *213*, 332-341.
51. Wang, Z.; Shen, T.; Yang, Y.; Gao, B.; Wan, Y.; Li, Y. C.; Yao, Y.; Liu, L.; Tang, Y.; Xie, J.; Ding, F.; Chen, J., Fulvic acid-like substance and its characteristics, an innovative waste recycling material from pulp black liquor. *Journal of Cleaner Production* **2020**, *243*, 118585.
52. Stoica, A.; Sandberg, M.; Holby, O., Energy use and recovery strategies within wastewater treatment and sludge handling at pulp and paper mills. *Bioresource technology* **2009**, *100* (14), 3497-505.
53. Li, H.; Wu, S.; Dang, C.; Yang, G.; Cao, Y.; Wang, H.; Peng, F.; Yu, H., Production of high-purity hydrogen from paper recycling black liquor via sorption enhanced steam reforming. *Green Energy & Environment* **2020**.
54. Al-Kaabi, Z.; Pradhan, R. R.; Thevathasan, N.; Chiang, Y. W.; Gordon, A.; Dutta, A., Potential value added applications of black liquor generated at paper manufacturing industry using recycled fibers. *Journal of Cleaner Production* **2017**, *149*, 156-163.
55. Li, J.; Pan, L.; Yu, G.; Li, C.; Xie, S.; Wang, Y., Synthesis of an easily recyclable and safe adsorbent from sludge pyrochar for ciprofloxacin adsorption. *Environmental Research* **2021**, *192*, 110258.
56. Wang, Q.; Li, J.-s.; Poon, C. S., Recycling of incinerated sewage sludge ash as an

adsorbent for heavy metals removal from aqueous solutions. *Journal of Environmental Management* **2019**, *247*, 509-517.

57. Chen, Z.; Li, J. S.; Poon, C. S., Combined use of sewage sludge ash and recycled glass cullet for the production of concrete blocks. *Journal of Cleaner Production* **2018**, *171*, 1447-1459.

58. Zhou, Y.-f.; Li, J.-s.; Lu, J.-x.; Cheeseman, C.; Poon, C. S., Recycling incinerated sewage sludge ash (ISSA) as a cementitious binder by lime activation. *Journal of Cleaner Production* **2020**, *244*, 118856.

59. Oliva, C.; Huang, W.; El Badri, S.; Lee, M. A. L.; Ronholm, J.; Chen, L.; Wang, Y., Concentrated sulfuric acid aqueous solution enables rapid recycling of cellulose from waste paper into antimicrobial packaging. *Carbohydrate Polymers* **2020**, *241*, 116256.

60. Hole, G.; Hole, A. S., Improving recycling of textiles based on lessons from policies for other recyclable materials: A minireview. *Sustainable Production and Consumption* **2020**, *23*, 42-51.

61. Islam, S.; Bhat, G., Environmentally-friendly thermal and acoustic insulation materials from recycled textiles. *Journal of Environmental Management* **2019**, *251*, 109536.

62. Sotoudehnia, F.; Baba Rabiou, A.; Alayat, A.; McDonald, A. G., Characterization of bio-oil and biochar from pyrolysis of waste corrugated cardboard. *Journal of Analytical and Applied Pyrolysis* **2020**, *145*, 104722.

63. Orue, A.; Santamaria-Echart, A.; Eceiza, A.; Peña-Rodriguez, C.; Arbelaz, A., Office waste paper as cellulose nanocrystal source. *Journal of Applied Polymer Science* **2017**, *134* (35), 45257.

64. Subramanian, K.; Chopra, S. S.; Cakin, E.; Li, X.; Lin, C. S. K., Environmental life cycle assessment of textile bio-recycling – valorizing cotton-polyester textile waste to pet fiber and glucose syrup. *Resources, Conservation and Recycling* **2020**, *161*, 104989.

65. Ütebay, B.; Çelik, P.; Çay, A., Effects of cotton textile waste properties on recycled fibre quality. *Journal of Cleaner Production* **2019**, *222*, 29-35.

66. Kumneadklang, S.; O-Thong, S.; Larpkiattaworn, S., Characterization of cellulose fiber isolated from oil palm frond biomass. *Materials Today: Proceedings* **2019**, *17*, 1995-2001.
67. De, S.; Mishra, S.; Poonguzhali, E.; Rajesh, M.; Tamilarasan, K., Fractionation and characterization of lignin from waste rice straw: Biomass surface chemical composition analysis. *International Journal of Biological Macromolecules* **2020**, *145*, 795-803.
68. Tang, C.; Shan, J.; Chen, Y.; Zhong, L.; Shen, T.; Zhu, C.; Ying, H., Organic amine catalytic organosolv pretreatment of corn stover for enzymatic saccharification and high-quality lignin. *Bioresource Technology* **2017**, *232*, 222-228.
69. Saha, K.; Dasgupta, J.; Chakraborty, S.; Antunes, F. A. F.; Sikder, J.; Curcio, S.; dos Santos, J. C.; Arafat, H. A.; da Silva, S. S., Optimization of lignin recovery from sugarcane bagasse using ionic liquid aided pretreatment. *Cellulose* **2017**, *24* (8), 3191-3207.
70. Masilamani, D.; Madhan, B.; Shanmugam, G.; Palanivel, S.; Narayan, B., Extraction of collagen from raw trimming wastes of tannery: A waste to wealth approach. *Journal of Cleaner Production* **2016**, *113*, 338-344.
71. Noorzai, S.; Lay, M. C.; Swan, J.; Verbeek, C. J. R., Collagen extraction from various waste bovine hide sources. *Waste and Biomass Valorization* **2020**, *11*, 5687-5698.
72. Akram, A. N.; Zhang, C., Extraction of collagen-II with pepsin and ultrasound treatment from chicken sternal cartilage; physicochemical and functional properties. *Ultrasonics Sonochemistry* **2020**, *64*, 105053.
73. Khiari, Z.; Rico, D.; Martin-Diana, A. B.; Barry-Ryan, C., Valorization of fish by-products: Rheological, textural and microstructural properties of mackerel skin gelatins. *Journal of Material Cycles and Waste Management* **2017**, *19* (1), 180-191.
74. Al-Hassan, A. A., Gelatin from camel skins: Extraction and characterizations. *Food Hydrocolloids* **2020**, *101*, 8.
75. Ali, A. M. M.; Kishimura, H.; Benjakul, S., Physicochemical and molecular

properties of gelatin from skin of golden carp (*Probarbus Jullieni*) as influenced by acid pretreatment and prior-ultrasonication. *Food Hydrocolloids* **2018**, *82*, 164-172.

76. Ramya, K. R.; Thangam, R.; Madhan, B., Comparative analysis of the chemical treatments used in keratin extraction from red sheep's hair and the cell viability evaluations of this keratin for tissue engineering applications. *Process Biochemistry* **2020**, *90*, 223-232.

77. Tasaki, K., A novel thermal hydrolysis process for extraction of keratin from hog hair for commercial applications. *Waste Management* **2020**, *104*, 33-41.

78. Kaya, M.; Baran, T.; Karaarslan, M., A new method for fast chitin extraction from shells of crab, crayfish and shrimp. *Natural Product Research* **2015**, *29* (15), 1477-1480.

79. Cao, Y.; Jiang, Y.; Song, Y.; Cao, S.; Miao, M.; Feng, X.; Fang, J.; Shi, L., Combined bleaching and hydrolysis for isolation of cellulose nanofibrils from waste sackcloth. *Carbohydrate Polymers* **2015**, *131*, 152-158.

80. Nishiwaki-Akine, Y.; Watanabe, T., Dissolution of wood in  $\alpha$ -keto acid and aldehydic carboxylic acids and fractionation at room temperature. *Green Chemistry* **2014**, *16* (7), 3569-3579.

81. Zhao, G.; Lyu, X.; Lee, J.; Cui, X.; Chen, W.-N., Biodegradable and transparent cellulose film prepared eco-friendly from durian rind for packaging application. *Food Packaging and Shelf Life* **2019**, *21*, 100345.

82. Anwar, Z.; Gulfraz, M.; Irshad, M., Agro-industrial lignocellulosic biomass a key to unlock the future bio-energy: A brief review. *Journal of Radiation Research and Applied Sciences* **2014**, *7* (2), 163-173.

83. Klemm, D.; Heublein, B.; Fink, H. P.; Bohn, A., Cellulose: Fascinating biopolymer and sustainable raw material. *Angewandte Chemie-International Edition* **2005**, *44* (22), 3358-3393.

84. Kucharska, K.; Rybarczyk, P.; Hołowacz, I.; Łukajtis, R.; Glinka, M.; Kamiński, M., Pretreatment of lignocellulosic materials as substrates for fermentation processes. *Molecules* **2018**, *23* (11), 2937.

85. Ma, Y.; Stubb, J.; Kontro, I.; Nieminen, K.; Hummel, M.; Sixta, H., Filament spinning of unbleached birch kraft pulps: Effect of pulping intensity on the processability and the fiber properties. *Carbohydrate Polymers* **2018**, *179*, 145-151.
86. Zhang, Y.; Tian, Z.; Fu, Y.; Wang, Z.; Qin, M.; Yuan, Z., Responsive and patterned cellulose nanocrystal films modified by N-methylmorpholine-N-oxide. *Carbohydrate Polymers* **2020**, *228*, 115387.
87. Han, Q.; Gao, X.; Zhang, H.; Chen, K.; Peng, L.; Jia, Q., Preparation and comparative assessment of regenerated cellulose films from corn (zea mays) stalk pulp fines in DMAc/LiCl solution. *Carbohydrate Polymers* **2019**, *218*, 315-323.
88. Amalini, A. N.; Haida, M. K. N.; Imran, K.; Haafiz, M. K. M., Relationship between dissolution temperature and properties of oil palm biomass based-regenerated cellulose films prepared via ionic liquid. *Materials Chemistry and Physics* **2019**, *221*, 382-389.
89. Cai, J.; Zhang, L., Rapid dissolution of cellulose in LiOH/urea and NaOH/urea aqueous solutions. *Macromolecular Bioscience* **2005**, *5* (6), 539-48.
90. Huang, W.; Wang, Y.; Zhang, L.; Chen, L., Rapid dissolution of spruce cellulose in H<sub>2</sub>SO<sub>4</sub> aqueous solution at low temperature. *Cellulose* **2016**, *23* (6), 3463-3473.
91. Ahuja, D.; Kaushik, A.; Singh, M., Simultaneous extraction of lignin and cellulose nanofibrils from waste jute bags using one pot pre-treatment. *International Journal of Biological Macromolecules* **2018**, *107*, 1294-1301.
92. Huang, S.; Liu, X.; Chang, C.; Wang, Y., Recent developments and prospective food-related applications of cellulose nanocrystals: A review. *Cellulose* **2020**, *27* (6), 2991-3011.
93. Fath, M. T. A.; Nasution, H., Process optimization of manufacturing nanocrystalline cellulose from rattan biomass using sulfuric acid. *AIP Conference Proceedings* **2018**, *2024* (1, Proceedings of the 4th International Symposium on Applied Chemistry 2018), 020020/1-020020/6.
94. Chin, S. C.; Tee, K. F.; Tong, F. S.; Ong, H. R.; Gimbin, J., Thermal and mechanical

properties of bamboo fiber reinforced composites. *Materials Today Communications* **2020**, *23*, 100876.

95. Supanchaiyamat, N.; Jetsrisuparb, K.; Knijnenburg, J. T. N.; Tsang, D. C. W.; Hunt, A. J., Lignin materials for adsorption: Current trend, perspectives and opportunities. *Bioresource Technology* **2019**, *272*, 570-581.

96. Upton, B. M.; Kasko, A. M., Strategies for the conversion of lignin to high-value polymeric materials: Review and perspective. *Chemical Reviews* **2016**, *116* (4), 2275-2306.

97. Chen, C.; Li, F.; Zhang, Y.; Wang, B.; Fan, Y.; Wang, X.; Sun, R., Compressive, ultralight and fire-resistant lignin-modified graphene aerogels as recyclable absorbents for oil and organic solvents. *Chemical Engineering Journal* **2018**, *350*, 173-180.

98. Min, D.-y.; Waters Smith, S.; Chang, H.-m.; Jameel, H., Influence of isolation condition on structure of milled wood lignin characterized by quantitative <sup>13</sup>C nuclear magnetic resonance spectroscopy. *BioResources* **2013**, *8* (2), 1790-1800.

99. Lancefield, C. S.; Panovic, I.; Deuss, P. J.; Barta, K.; Westwood, N. J., Pre-treatment of lignocellulosic feedstocks using biorenewable alcohols: Towards complete biomass valorisation. *Green Chemistry* **2017**, *19* (1), 202-214.

100. Başakçılardan Kabakcı, S.; Tanış, M. H., Pretreatment of lignocellulosic biomass at atmospheric conditions by using different organosolv liquors: A comparison of lignins. *Biomass Conversion and Biorefinery* **2020**, 1-12.

101. Kawamata, Y.; Yoshikawa, T.; Aoki, H.; Koyama, Y.; Nakasaka, Y.; Yoshida, M.; Masuda, T., Kinetic analysis of delignification of cedar wood during organosolv treatment with a two-phase solvent using the unreacted-core model. *Chemical Engineering Journal* **2019**, *368*, 71-78.

102. Hong, H.; Fan, H. B.; Chalamaiah, M.; Wu, J. P., Preparation of low-molecular-weight, collagen hydrolysates (peptides): Current progress, challenges, and future perspectives. *Food Chemistry* **2019**, *301*, 125222.

103. Schmidt, M. M.; Dornelles, R. C. P.; Mello, R. O.; Kubota, E. H.; Mazutti, M. A.;

Kempka, A. P.; Demiate, I. M., Collagen extraction process. *International Food Research Journal* **2016**, *23* (3), 913-922.

104. Coward-Kelly, G.; Agbogbo, F. K.; Holtzapple, M. T., Lime treatment of keratinous materials for the generation of highly digestible animal feed: 2. Animal hair. *Bioresource Technology* **2006**, *97* (11), 1344-1352.

105. Pourjavaheri, F.; Ostovar Pour, S.; Jones, O. A. H.; Smooker, P. M.; Brkljača, R.; Sherkat, F.; Blanch, E. W.; Gupta, A.; Shanks, R. A., Extraction of keratin from waste chicken feathers using sodium sulfide and l-cysteine. *Process Biochemistry* **2019**, *82*, 205-214.

106. Choi, C.; Nam, J. P.; Nah, J. W., Application of chitosan and chitosan derivatives as biomaterials. *Journal of Industrial and Engineering Chemistry* **2016**, *33*, 1-10.

107. Muley, A. B.; Chaudhari, S. A.; Mulchandani, K. H.; Singhal, R. S., Extraction and characterization of chitosan from prawn shell waste and its conjugation with cutinase for enhanced thermo-stability. *International Journal of Biological Macromolecules* **2018**, *111*, 1047-1058.

108. Arbia, W.; Arbia, L.; Adour, L.; Amrane, A., Chitin extraction from crustacean shells using biological methods - a review. *Food Technology and Biotechnology* **2013**, *51* (1), 12-25.

109. Barkhordari, M. R.; Fathi, M., Production and characterization of chitin nanocrystals from prawn shell and their application for stabilization of pickering emulsions. *Food Hydrocolloids* **2018**, *82*, 338-345.

110. Salaberria, A. M.; Diaz, R. H.; Labidi, J.; Fernandes, S. C. M., Preparing valuable renewable nanocomposite films based exclusively on oceanic biomass - chitin nanofillers and chitosan. *Reactive and Functional Polymers* **2015**, *89*, 31-39.

111. Gopi, S.; Balakrishnan, P.; Divya, C.; Valic, S.; Govorcin Bajsic, E.; Pius, A.; Thomas, S., Facile synthesis of chitin nanocrystals decorated on 3D cellulose aerogels as a new multi-functional material for waste water treatment with enhanced anti-bacterial and anti-oxidant properties. *New Journal of Chemistry* **2017**, *41* (21), 12746-

12755.

112. Lee, S.-Y.; Choi, H.-J., Persimmon leaf bio-waste for adsorptive removal of heavy metals from aqueous solution. *Journal of Environmental Management* **2018**, *209*, 382-392.

113. Feizi, M.; Jalali, M., Removal of heavy metals from aqueous solutions using sunflower, potato, canola and walnut shell residues. *Journal of the Taiwan Institute of Chemical Engineers* **2015**, *54*, 125-136.

114. Tomczyk, A.; Sokołowska, Z.; Boguta, P., Biochar physicochemical properties: Pyrolysis temperature and feedstock kind effects. *Reviews in Environmental Science and Bio/Technology* **2020**, *19* (1), 191-215.

115. Liu, C.; Chen, L.; Ding, D.; Cai, T., From rice straw to magnetically recoverable nitrogen doped biochar: Efficient activation of peroxymonosulfate for degradation of metolachlor. *Applied Catalysis, B: Environmental* **2019**, *254*, 312-320.

116. He, N. F.; Yoo, S.; Meng, J. J.; Yildiz, O.; Bradford, P. D.; Park, S.; Gao, W., Engineering biorefinery residues from loblolly pine for supercapacitor applications. *Carbon* **2017**, *120*, 304-312.

117. Fang, J.; Leavey, A.; Biswas, P., Controlled studies on aerosol formation during biomass pyrolysis in a flat flame reactor. *Fuel* **2014**, *116*, 350-357.

118. Zheng, T. A. O.; Dahn, J. R., Chapter 11 - applications of carbon in lithium-ion batteries. In *Carbon materials for advanced technologies*, Burchell, T. D., Ed. Elsevier Science Ltd: Oxford, **1999**; pp 341-387.

119. Kim, M. H.; Tang, J. L.; Jang, S. J.; Pol, V. G.; Roh, K. C., Porous graphitic activated carbon sheets upcycled from starch-based packing peanuts for applications in ultracapacitors. *Journal of Alloys and Compounds* **2019**, *805*, 1282-1287.

120. Zhu, L.; Jiang, H. T.; Ran, W. X.; You, L. J.; Yao, S. S.; Shen, X. Q.; Tu, F. Y., Turning biomass waste to a valuable nitrogen and boron dual-doped carbon aerogel for high performance lithium-sulfur batteries. *Applied Surface Science* **2019**, *489*, 154-164.

121. Njoku, V. O.; Foo, K. Y.; Asif, M.; Hameed, B. H., Preparation of activated carbons

- from rambutan (*Nephelium lappaceum*) peel by microwave-induced KOH activation for acid yellow 17 dye adsorption. *Chemical Engineering Journal* **2014**, *250*, 198-204.
122. Sankar, S.; Ahmed, A. T. A.; Inamdar, A. I.; Im, H.; Im, Y. B.; Lee, Y.; Kim, D. Y.; Lee, S., Biomass-derived ultrathin mesoporous graphitic carbon nanoflakes as stable electrode material for high-performance supercapacitors. *Materials & Design* **2019**, *169*, 107688.
123. Mondal, M. K., Removal of Pb(II) ions from aqueous solution using activated tea waste: Adsorption on a fixed-bed column. *Journal of Environmental Management* **2009**, *90* (11), 3266-3271.
124. Choi, H. J., Use of methyl esterified eggshell membrane for treatment of aqueous solutions contaminated with anionic sulfur dye. *Water Science and Technology* **2017**, *76* (10), 2638-2646.
125. Lee, S. Y.; Choi, H. J., Persimmon leaf bio-waste for adsorptive removal of heavy metals from aqueous solution. *Journal of Environmental Management* **2018**, *209*, 382-392.
126. Monteiro, R. J. R.; Lopes, C. B.; Rocha, L. S.; Coelho, J. P.; Duarte, A. C.; Pereira, E., Sustainable approach for recycling seafood wastes for the removal of priority hazardous substances (Hg and Cd) from water. *Journal of Environmental Chemical Engineering* **2016**, *4* (1), 1199-1208.
127. Sattar, M. S.; Shakoor, M. B.; Ali, S.; Rizwan, M.; Niazi, N. K.; Jilani, A., Comparative efficiency of peanut shell and peanut shell biochar for removal of arsenic from water. *Environmental Science and Pollution Research* **2019**, *26* (18), 18624-18635.
128. Chen, H. Y.; Li, W. Y.; Wang, J. J.; Xu, H. J.; Liu, Y. L.; Zhang, Z.; Li, Y. T.; Zhang, Y. L., Adsorption of cadmium and lead ions by phosphoric acid-modified biochar generated from chicken feather: Selective adsorption and influence of dissolved organic matter. *Bioresource Technology* **2019**, *292*, 121948.
129. Gao, J.; Wu, Z.; Chen, L.; Xu, Z.; Gao, W.; Jia, G.; Yao, Y., Synergistic effects of iron ion and PANI in biochar material for the efficient removal of Cr(VI). *Materials*

*Letters* **2019**, *240*, 147-149.

130. Peng, Y. T.; Sun, Y. Q.; Sun, R. Z.; Zhou, Y. Y.; Tsang, D. C. W.; Chen, Q., Optimizing the synthesis of Fe/Al (Hydr)oxides-biochars to maximize phosphate removal via response surface model. *Journal of Cleaner Production* **2019**, *237*, 117770.

131. Mehrvarz, E.; Ghoreyshi, A. A.; Jahanshahi, M., Surface modification of broom sorghum-based activated carbon via functionalization with triethylenetetramine and urea for Co<sub>2</sub> capture enhancement. *Frontiers of Chemical Science and Engineering* **2017**, *11* (2), 252-265.

132. Liu, W.-J.; Ling, L.; Wang, Y.-Y.; He, H.; He, Y.-R.; Yu, H.-Q.; Jiang, H., One-pot high yield synthesis of Ag nanoparticle-embedded biochar hybrid materials from waste biomass for catalytic Cr(VI) reduction. *Environmental Science: Nano* **2016**, *3* (4), 745-753.

133. Cho, D. W.; Tsang, D. C. W.; Kim, S.; Kwon, E. E.; Kwon, G.; Song, H., Thermochemical conversion of cobalt-loaded spent coffee grounds for production of energy resource and environmental catalyst. *Bioresource Technology* **2018**, *270*, 346-351.

134. Huang, W.; Wang, F.; Qiu, N.; Wu, X.; Zang, C.; Li, A.; Xu, L., Enteromorpha prolifera-derived Fe<sub>3</sub>C/C composite as advanced catalyst for hydroxyl radical generation and efficient removal for organic dye and antibiotic. *Journal of Hazardous Materials* **2019**, *378*, 120728.

135. Gao, Y.; Li, L.; Jin, Y.; Wang, Y.; Yuan, C.; Wei, Y.; Chen, G.; Ge, J.; Lu, H., Porous carbon made from rice husk as electrode material for electrochemical double layer capacitor. *Applied Energy* **2015**, *153*, 41-47.

136. Luo, Y.; Luo, C.; Zhang, S.-W.; Wei, J.; Lv, W.; Yang, Q.-H., Porous carbons derived from carbonization of tissue papers for supercapacitors. *Journal of Materials Science: Materials in Electronics* **2019**, *30* (12), 11250-11256.

137. Jia, H.; Wang, S.; Sun, J.; Yin, K.; Xie, X.; Sun, L., Nitrogen-doped microporous carbon derived from a biomass waste-metasequoia cone for electrochemical capacitors.

*Journal of Alloys and Compounds* **2019**, 794, 163-170.

138. Zhang, J.; Chen, H.; Ma, Z.; Li, H.; Dong, Y.; Yang, H.; Yang, L.; Bai, L.; Wei, D.; Wang, W., A lignin dissolution-precipitation strategy for porous biomass carbon materials derived from cherry stones with excellent capacitance. *Journal of Alloys and Compounds* **2020**, 832, 155029.

139. Chong, L. G.; Chen, P. A.; Huang, J. Y.; Huang, H. L.; Wang, H. P., Capacitive deionization of a RO brackish water by AC/graphene composite electrodes. *Chemosphere* **2018**, 191, 296-301.

140. Sankar, S.; Ahmed, A. T. A.; Inamdar, A. I.; Im, H.; Bin Im, Y.; Lee, Y.; Kim, D. Y.; Lee, S., Biomass-derived ultrathin mesoporous graphitic carbon nanoflakes as stable electrode material for high-performance supercapacitors. *Materials & Design* **2019**, 169, 107688.

141. Vasiliev, V. V.; Morozov, E. V., Chapter 1 - introduction. In *Advanced mechanics of composite materials (third edition)*, Vasiliev, V. V.; Morozov, E. V., Eds. Elsevier: Boston, **2013**; pp 1-27.

142. Xie, X.; Gou, G.; Wei, X.; Zhou, Z.; Jiang, M.; Xu, X.; Wang, Z.; Hui, D., Influence of pretreatment of rice straw on hydration of straw fiber filled cement based composites. *Construction and Building Materials* **2016**, 113, 449-455.

143. Khazma, M.; Goullieux, A.; Dheilly, R.-M.; Rougier, A.; Quéneudec, M., Optimization of flax shive-cementitious composites: Impact of different aggregate treatments using linseed oil. *Industrial Crops and Products* **2014**, 61, 442-452.

144. Zhu, J.; Liu, S.; Liu, Y.; Meng, T.; Ma, L.; Zhang, H.; Kuang, M.; Jiang, J., Graphitic, porous, and multiheteroatom codoped carbon microtubes made from hair waste: A superb and sustained anode substitute for Li-ion batteries. *ACS Sustainable Chemistry & Engineering* **2018**, 6 (11), 13662-13669.

145. Yang, J.; Chen, F.; Li, C.; Bai, T.; Long, B.; Zhou, X., A free-standing sulfur-doped microporous carbon interlayer derived from luffa sponge for high performance lithium-sulfur batteries. *Journal of Materials Chemistry A* **2016**, 4 (37), 14324-14333.

146. Zhu, L.; Jiang, H.; Ran, W.; You, L.; Yao, S.; Shen, X.; Tu, F., Turning biomass waste to a valuable nitrogen and boron dual-doped carbon aerogel for high performance lithium-sulfur batteries. *Applied Surface Science* **2019**, *489*, 154-164.
147. Li, Z.; Li, M. A.; Zheng, T. L.; Li, Y. D.; Liu, X., Removal of tylosin and copper from aqueous solution by biochar stabilized nano-hydroxyapatite. *Chemosphere* **2019**, *235*, 136-142.
148. Zhao, Z. D.; Nie, T. T.; Zhou, W. J., Enhanced biochar stabilities and adsorption properties for tetracycline by synthesizing silica-composited biochar. *Environmental Pollution* **2019**, *254*, 113015.
149. Fan, S.; Wang, Y.; Li, Y.; Tang, J.; Wang, Z.; Tang, J.; Li, X.; Hu, K., Facile synthesis of tea waste/Fe<sub>3</sub>O<sub>4</sub> nanoparticle composite for hexavalent chromium removal from aqueous solution. *RSC Advances* **2017**, *7* (13), 7576-7590.
150. Fitria, D.; Al Baroroh, L. A.; Destyorini, F.; Widayatno, W. B.; Amal, M. I.; Wismogroho, A. S., Identification of potential hydrophobic properties of carbon layer from the coffee bean waste. *Journal of Physics: Conference Series* **2018**, *985* (3rd International Symposium on Frontier of Applied Physics, 2017), 012031/1-012031/6.

## CONNECTING STATEMENT I

**Chapter 2** reviewed the research on biomass wastes utilization and functional materials derived from biomass wastes in the past five years. The review covered the current situation of biomass wastes for functional material synthesis, extraction of natural polymers from biomass wastes, and preparation of carbon-based materials as novel adsorbents, catalyst carriers, electrode materials, and functional composites. **Chapter 3** summarized a mechano-bactericidal strategy for eliminating surface foodborne bacteria. The mechanism of action and the formation of natural and synthetic nanopillared surfaces were presented in this review. In addition, factors that affect the mechano-bactericidal efficiency were highlighted as well.

## CHAPTER 3 LITERATURE REVIEW 2

### 3.1 Abstract

Contamination of food by bacterial pathogens is one of the biggest concerns in the food industry as it can result in serious human illnesses and death. Approaches to eliminate bacteria from outer surfaces of food products would be an effective way to safeguard against bacterial contamination. Nanopillars found on natural surfaces have been shown to mechanically damage cell membranes of foodborne bacteria. Therefore, fabricating bio-inspired mechano-bactericidal nanostructures into food packaging and processing materials could be a promising strategy to reduce surface bacterial contamination, to improve food safety. In this review, we summarize the formation of natural and synthetic nanopillared surfaces and their mechanism of action, and highlight the factors that influence their mechano-bactericidal activities.

**Keywords:** mechano-bactericidal, nanostructured surfaces, bio-inspired, bactericidal mechanisms, food safety

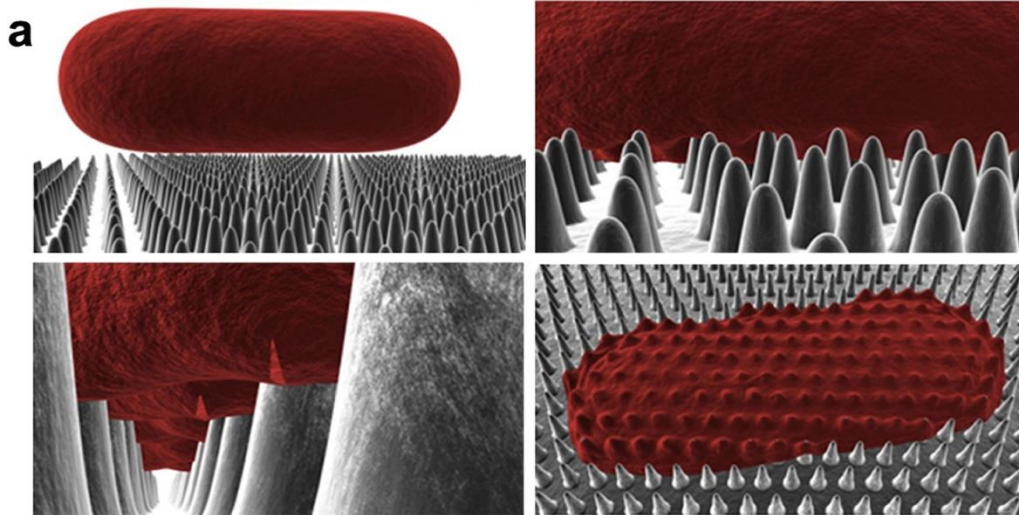
## 3.2 Introduction

Adhesion of pathogenic bacteria to food-contacting surfaces and subsequent biofilm formation can result in food safety issues. Biofilms facilitate cell-cell and cell-surface attachment and provide a protective environment for bacterial pathogens to withstand cleaning efforts and persist in food-processing environments, leading to foodborne outbreaks [1]. Traditional approaches entail either chemically modifying or physically coating the surface with antibacterial agents in order to eliminate the attachment of bacteria to the surface [2]. However, designs that use antibacterial release to eliminate surface bacteria are problematic since the active agents often do not reach required concentrations [3], while the overuse of antibacterial agents can lead to antimicrobial resistance. Additionally, antibacterial agents may also introduce undesired toxins into food products.

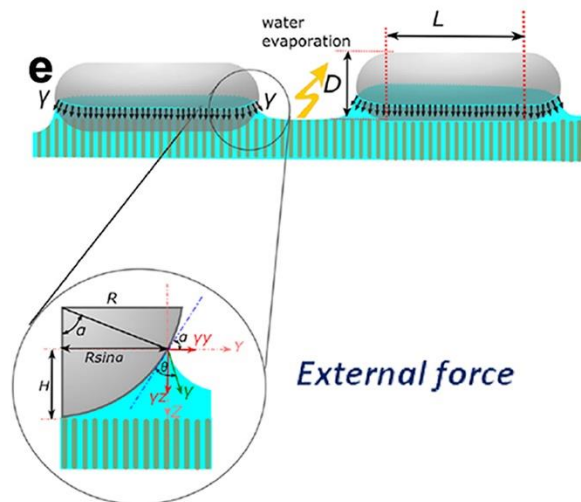
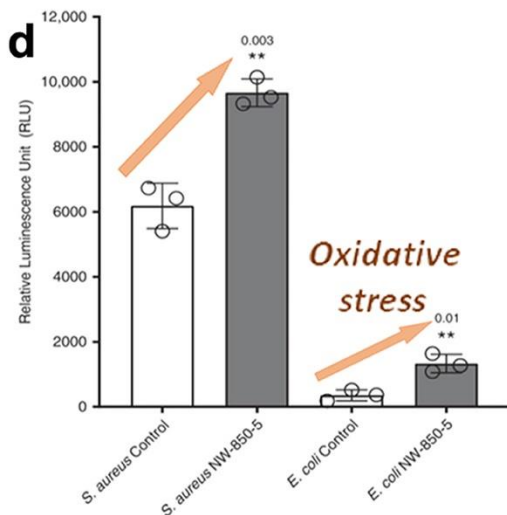
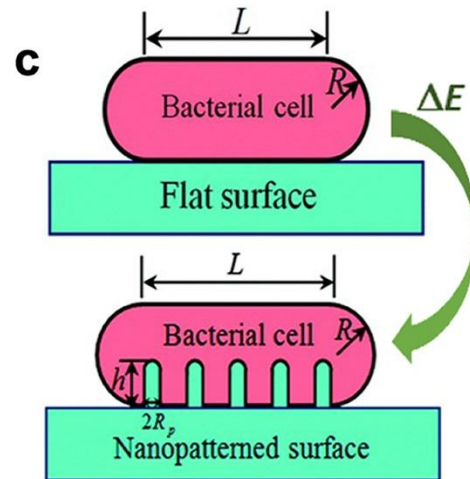
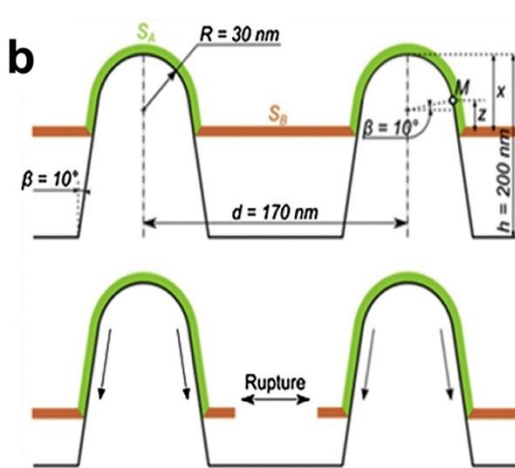
Inspired by the naturally occurring surfaces such as insect wings and gecko skin, a novel mechano-bactericidal approach has been developed in recent years. Hierarchical nanofeatures including pillars, hairs, and needles exist on these surfaces, and bacterial cells are inhibited, injured, and even killed when they directly contact surface nanotopography [4,5]. Synthetic surfaces capable of mimicking this physical biocidal mechanism have been fabricated and some exhibit promising antibacterial properties. Therefore, this mechano-bactericidal approach may overcome the drawbacks of traditional antibacterial treatments and be applied in food packaging and processing to improve food safety. In this review, we have summarized different mechano-bactericidal nanostructured surfaces, found both in nature and synthesized by various fabrication techniques, as well as their theoretical mechanisms of action. Factors that affect mechano-bactericidal activity are highlighted, including characteristics of the bacteria as well as surface nanofeatures such as spacing, contact area, and aspect ratio. Finally, future opportunities, challenges, and research directions are described.

### **3.3 Bactericidal mechanism of nanostructured surfaces**

The bactericidal effects of nanopillars require bacterial cells to adhere to the surface (Figure 3.1a). Bacterial surficial attachment is mediated by microbe structure, surface charge, hydrophobicity, production of extracellular substances, and cellular appendages such as fimbria or pili [6]. Higher adhesion forces between bacteria and nano-textured surfaces induce a higher probability of cellular rupture [7]. Two models, the biophysical model and the analytical thermodynamic model, have been developed to describe the mechanism of cell death on nano-patterned surfaces [8]. However, neither of these two models explain the up-regulation of oxidative stress proteins in bacterial cells exposed to nanopillared surfaces, so a third model regarding oxidative stress has been proposed [9]. In addition to these commonly accepted models, other possible mechanisms such as external forces have also been proposed to further explain the interactions between bacteria and nanopillared surfaces [10].



## Mechano-bactericidal activity



## Mechano-bactericidal mechanisms

**Figure 3.1** Schematic diagram of mechano-bactericidal activity on nanopillar surface (a) and different bactericidal mechanism models (b-e): (b) biophysical model; (c) thermodynamic model; (d) H<sub>2</sub>O<sub>2</sub> production in response to nanopillar surfaces in oxidative stress model; and (e) sketch of the capillary meniscus on bacterium during water evaporation and analysis of capillary forces [9,11,12,14]

### 3.3.1 Biophysical model

The bactericidal mechanism of nano-textured surfaces is the physical stretching of the cell membrane upon direct contact with the surface resulting in rupture. This effect is dependent on the rigidity of bacterial cell membrane [11]. The exact interactions of bacterial adsorption on a nanopillared surface can be divided into two regions: areas in direct contact with the pillars ( $S_A$ ) and areas between pillars ( $S_B$ ) (Figure 3.1b). Mathematical modeling describes cell wall stretching dynamics within the two regions by calculating the total free energy ( $E$ ):

$$E = \frac{\epsilon n_0 S_A}{1+\alpha_A} + \frac{k}{2} \left( \frac{\alpha_A^2 S_A}{1+\alpha_A} + \frac{\alpha_B^2 S_B}{1+\alpha_B} \right) + \lambda k \left( \frac{S_A}{1+\alpha_A} + \frac{S_B}{1+\alpha_B} - \frac{S_i}{1+\alpha_i} \right) \quad (1)$$

Where  $\epsilon$  is the energy gains per adsorption site on nanopillar surface;  $n_0$  is the surface density of the sites on relaxed layer;  $\alpha_A$  is the stretching of adsorbed region of layer;  $\alpha_B$  is the stretching of suspended region of layer;  $k$  is the stretching modulus;  $\lambda$  is Lagrange multiplier;  $S_i$  is the total initial area of unperturbed membrane; and  $\alpha_i$  is the initial stretching degree [11]. Once  $\alpha_B$  reaches a critical value, the membrane ruptures.

When a bacterial cell contacts nanopillars, it adsorbs onto the nanopillars, resulting in the increased surface area and the stretching of the regions between pillars. Once beyond the maximum stretchable potential, the cell membrane ruptures and leaks cytoplasmic contents, leading to eventual cell death [11]. The shortcoming of this model is that it does not incorporate information on bacterial shape or composition, or the mechanical properties of the nanopillars.

### 3.3.2 Thermodynamic model

This model suggests that the bactericidal activity is related to the balance between the deformation energy and contact adhesion energy [9]. Interactions between bacterial cells and surfaces are defined through analyzing the total free energy change of adherent bacteria (Figure 3.1c) [12]. It is calculated by comparing a nanopillared surface to a flat surface where the primary differences are the deformation of the cell membrane and the contact adhesion interface in the attached area. The total free energy change ( $\Delta E$ ) on a nanopillared surface is given by:

$$\Delta E = \frac{1}{2} \delta \frac{\Delta S^2}{S_0} + (E_{edge}^{Bend} + E_{ad}^{Bend} - E_0^{Bend}) - \gamma S_{ad} \quad (2)$$

Where  $\delta$  is the stretching modulus of membrane;  $S_0$  and  $\Delta S$  are the initial area and the area change of cell membrane;  $E_{edge}^{Bend}$  is the deformed bending energy of the membrane at the edge of bacterial cell;  $E_{ad}^{Bend}$  is the deformed bending energy of contact adhesion membrane;  $E_0^{Bend}$  is the deformed bending energy of initial cell membrane;  $\gamma$  is the contact adhesion energy density between flat surface and cell membrane; and  $S_{ad}$  is the contact area [12].

This model also assumes the bacterial membrane is a thin elastic layer and neglects the membrane composition. The higher density and larger radius and height of nanopillars increase the contact adhesion energy, resulting in a large degree of bacterial membrane stretching [12]. If the degree of stretching is sufficient, it will lead to rupture and death of bacterial cells. According to this model, bacterial cells with larger stretching capacity will have greater resistance to the bactericidal action of nanopillars [13].

### 3.3.3 Oxidative stress model

Although cell membrane deformation and penetration have been observed in many studies, such events do not lyse bacteria. Thus, interactions mentioned above cannot

solely account for the reduction in bacterial viability. The oxidative stress model is proposed to explain why up-regulation of oxidative stress proteins and time-dependent decrease in cell viability are observed in both Gram-positive and Gram-negative bacteria when the cells come to contact with nanopillared surfaces (Figure 3.1d) [9]. Due to the effect of nanopillars, increased levels of ROS and hydrogen peroxide were observed. Upregulation of ROS and hydrogen peroxide triggered bacterial oxidative stress leading to damage of DNA, lipids, and proteins. Such damages altered the bacterial cell envelope morphology and might enhance cell rupture [9].

### **3.3.4 Other models**

No consensus has been reached on the bactericidal mechanism, and more factors such as external forces have been considered. Li et al. proposed the mechanism to explain the death of small, long, and thin bacteria on nanopillared side edges. Surface adhesion, gravity, or a combination of both accounted for the stretching, compression, tearing or disrupting of bacterial cell wall [13]. Bandara et al. [10] found that the strong adhesion and shearing stress were imposed by nanopillars, contributing to the damage of bacterial membrane. A recent study demonstrated that bacteria on multiple hydrophilic “mechano-bactericidal” surfaces remained viable unless exposed to a critical level of external force that could rapidly deform and rupture bacteria (Figure 3.1e) [14].

## **3.4 Naturally occurring nanotopography**

Natural nanotextured surfaces evolve as a strategy to inhibit bacterial growth and biofilm formation. For example, cicada [15], damselfly [16] and dragonfly [10] wings, and gecko skin [13] are coated with nanopillars (Figure 3.2). Such micro- and nano-structures on biological surfaces endow characteristic properties of self-cleaning, superhydrophobicity [17], antireflection [18], and bactericidal activity [19]. Among these properties, bactericidal behavior towards *Staphylococcus aureus*, *Escherichia coli*, and *Pseudomonas aeruginosa*, common pathogens that cause foodborne infections, has

drawn significant amount of attention [20]. Bactericidal activities of various natural nanostructured surfaces are shown in Table 3.1.

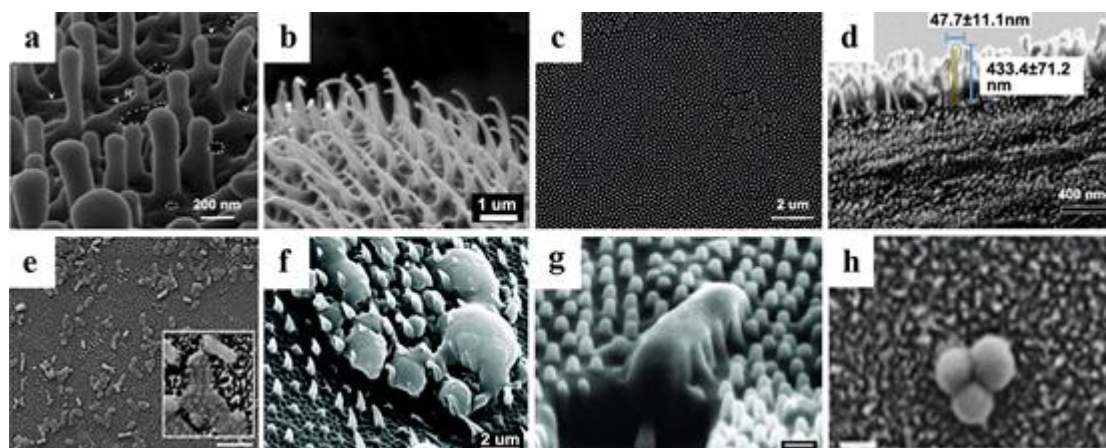


**Figure 3.2** SEM images of natural bactericidal nanotopographies (top) and bacteria on surfaces (bottom): (a, e) *E. coli* on dragonfly wing; (b, f) *Porphyromonas gingivalis* on gecko skin; (c, g) *P. aeruginosa* on cicada wing; and (d, h) *S. aureus* on damselfly wing [10,13,15,16]

**Table 3.1** Bactericidal activities of various natural and synthetic nanostructured surfaces

Nanostructured surfaces	Bactericidal mechanisms	Bacterial species	Bactericidal effects
Gecko hairs [13]	Surface adhesion / external forces	<i>Streptococcus mutans</i>	90-95% cell death
Dragonfly wings [10]	Adhesion / shear force	<i>E. coli</i>	Reduction of $4.99 \times 10^5$ cells/min·cm <sup>2</sup>
Damselfly wings [16]	n.d.	<i>S. aureus</i> <i>P. aeruginosa</i>	89.7% cell death 97.7% cell death
Titanium dioxide nanopillars [9]	Oxidative stress	<i>S. aureus</i> / <i>E. coli</i>	n.d.

Spear-type titanium surface [50]	Sharp tips of nano spears caused cell lysis	<i>S. epidermidis</i>	37% cell death
Pocket-type titanium surface [50]	Cell deformation between nano spears inside the pocket	<i>S. epidermidis</i>	47% cell death
Polystyrene and chitosan duplicates from gecko skin [19]	Compression, stretching, tearing and piercing	<i>Lactobacillus</i>	95% cell death
Positively charged MOF nano-dagger arrays mimicked from cicada wing [48]	Oxidative stress; electrostatic and hydrophobic interactions	<i>E. coli</i> <i>S. aureus</i>	<i>Log</i> reduction of 7 <i>Log</i> reduction of 8
Silicon nanopillars [36]	Stretching	<i>P. aeruginosa</i> <i>S. aureus</i>	85% cell death 8% cell death
Silicon nanopillars [14]	External force / nanopillared surface	<i>P. aeruginosa</i>	Over 99.9% cell death
Graphene oxide nanosheets [38]	Electrostatic / van der Waals forces	<i>E. coli</i> <i>M. smegmatis</i> <i>S. aureus</i>	80% cell death 70% cell death 80% cell death

“n.d.” not determined.

### 3.4.1 Insect wings

Nanopillars on the surface of cicada (*Psaltoda claripennis*) wings are able to structurally deform *P. aeruginosa* cells beyond repair within 3 min and are therefore bactericidal [15]. To identify the role of surface chemistry in the bactericidal effects, cicada wings were coated with a 10 nm-thick gold film to decrease the hydrophobicity

without changing topography. The bactericidal effect of gold-coated wings was preserved, indicating that the physical structure, rather than the surface chemistry, was responsible for bacterial inactivation [15]. Subsequent studies revealed that subtle nanoscale differences could cause substantial changes in bactericidal action [21]. Long sharp nanopillars had broader antibacterial activity against both Gram-positive and Gram-negative bacteria, while short blunt nanopillars were only bactericidal against specific species [22]. The bactericidal selectivity based on different nanopillars was also observed in nature. Dragonfly wings nanopillars have random shapes, sizes, and distribution, and are effective against both Gram-positive and Gram-negative bacteria, while the nanopillars on cicada wings are more consistent and are only effective against Gram-negative bacteria [11,15,21].

### **3.4.2 Gecko skin**

Geckos have a uniform array of nano-tipped spinule (hairs) hierarchical structures on their skin, capable of killing bacterial cells [23]. The hairs are approximately 1-4  $\mu\text{m}$  in length and taper into 50 nm nanotips that are composed of two length tiers. They can curve significantly due to their flexibility and elasticity [19] and have displayed a high efficiency in eliminating pathogenic bacteria on the skin even after multiple exposures [13]. Multi-tiered nanostructures also play an important role in the death of bacteria, due to synergistic stresses on cells [13].

### **3.5 Synthetic bactericidal surfaces**

To mimic nanostructured surfaces found in nature, many synthetic nanopillars (Figure 3.3) have been fabricated from various materials including black silicon [24], graphene [25], titanium [26], copper [27], and gold [28], and have exhibited remarkable bactericidal capabilities (Table 3.1).

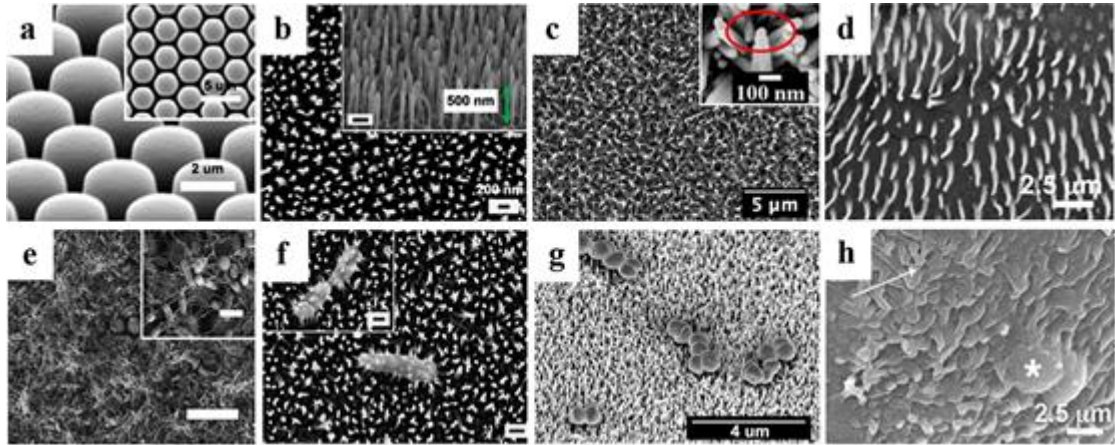


**Figure 3.3** SEM images of synthetic bactericidal nanotopographies (top) and bacteria on surfaces (bottom): (a, e) *E. coli* on polydimethylsiloxane; (b, f) *P. aeruginosa* on black silicon; (c, g) *Staphylococcus epidermidis* on titanium; and (d, h) *Lactobacillus* on chitosan [19,29,49,50]

### 3.5.1 Black silicon and silicon materials

BSi was the first material used to mimic nanopillars found on *Diplacodes bipunctata* dragonfly wings [29]. Various techniques such as plasma etching [24,30], electrochemical etching [31,32], and laser treatment [33] have been used to fabricate bSi nanotextured surfaces, which were bactericidal against foodborne bacteria such as *S. aureus*, *P. aeruginosa*, and *E. coli* [24,34]. May et al. [24] fabricated a BDD electrode material using bSi as a substrate. The bSi surface consisted of short needles and was bactericidal against approximately 13% of *P. aeruginosa* cells. In another study, it was found that the reactive-ion etching process endowed Si structures with high aspect ratio nano-protrusions [34]. Nanostructured Si prepared by tetrafluoromethane/hydrogen plasma technique could significantly decrease the bacterial loads of *E. coli*, *S. aureus*, and *Bacillus cereus* with >5 log reductions. By controlling the processing time, plasma etching can form various surface topographies. Linklater et al. [35] produced different surface nanostructures with increasing heights of 280, 430, and 610 nm through plasma etching using 15, 30, and 45 min etching intervals, respectively. It was shown that shorter and denser nanopillars exhibited better bactericidal properties with 85% and 89%

inhibition of *S. aureus* and *P. aeruginosa*. Using plasma etching and deep UV immersion lithography, a Si nanopillar array with an average height of 380 nm and a diameter of 35 nm was engineered [36]. The bactericidal efficacy towards *P. aeruginosa* was 85%, but only 8% against *S. aureus*.

### 3.5.2 Graphene and graphene-derived materials

Graphene and graphene-derived materials (e.g. GO and rGO) possess high bactericidal efficacies. Sengupta et al. [37] found that GO inhibited *S. aureus* and *P. aeruginosa* by 93.7% and 48.6%, while rGO killed 67.7% and 93.3%, respectively. Highly wrinkled GO films can be produced by simple vacuum filtration and drying of GO suspension through a pre-strained filter [38]. The sharp edges found on atomically thin layers of graphene are responsible for the deformation of bacterial cells and the subsequent release of cytoplasmic material [5]. Moreover, the oxidative environment induced by nanosheets could likely damage surrounding bacteria cells.

Nanostructures with improved mechano-bactericidal activities can be fabricated by decorating GO with nanoparticles. Selim et al. [39] developed GO sheets with blade-like structure decorated by nano-Cu<sub>2</sub>O and SiC nanocomposites, where GO/Cu<sub>2</sub>O exhibited higher bactericidal activity than GO/SiC towards Gram-negative bacterial strains (*P. aeruginosa* and *E. coli*). Graphene sponge decorated with copper nanoparticles also displayed high antibacterial efficiency against *E. coli* [40].

### 3.5.3 Titanium surfaces

Titanium-based nanotextured surfaces produced by a hydrothermal etching process exhibited the bactericidal activities of 80.7% and 86.8% against methicillin- and gentamicin-susceptible and resistant *S. aureus* strains, respectively [41]. Since the nanosheet topology produced by hydrothermal etching is random, processing parameters (e.g. etching time) were controlled to obtain optimal surface structure for

bactericidal activity [26\*]. The results showed that titanium treated for 6 h had the best bactericidal capacity against *P. aeruginosa* (99%) and *S. aureus* (90%) [42].

In addition to hydrothermal etching, other methods were also used to develop nanotextured titanium surfaces. Sjöström et al. [43] used thermal oxidation to fabricate nanospikes on a titanium alloy and observed a 40% reduction of *E. coli*. The reduction was attributed to the sharp tips or edges of nanospikes on alloy surface. Similarly, Hasan, et al. [44] fabricated a black titanium surface through a chlorine-based reactive ion etching processing. The anisotropic nanostructures trapped the light to make the surface appear black and displayed antimicrobial efficiency of killing 95% of *E. coli*, 98% of *P. aeruginosa*, 92% of *Mycobacterium smegmatis*, and 22% of *S. aureus* within 4 h of contact. Furthermore, titanium surfaces with hierarchical nanostructures have been produced by maskless plasma etching [45], where micron-sized pillars were likely responsible for trapping the cells and the second tier of pillars acted to kill the cells. The bactericidal efficiencies against *P. aeruginosa* and *S. aureus* were 87.2% (30 min of etching) and 72.5% (40 min of etching), respectively.

#### **3.5.4 Other bioinspired nanostructured surfaces**

Singh et al. [27] prepared a copper nanowhisker surface deposited by molecular beam epitaxy and proposed the behavior ‘pinning effect of water drops’ on the surface would encourage mechanical bacteria killing. Rosenzweig et al. [46] fabricated the nanopillar surfaces by nanoimprint lithography, which were able to reduce the motility and attachment of *P. aeruginosa*. The technique is time-efficient, scalable, precise, and low-cost, since it can produce large numbers of replicates from one master mold. The same method was also used to prepare polydimethylsiloxane (PDMS) pillar arrays against *E. coli* and *S. aureus* [47], and a similar rapid and accurate bio-templating technique was developed by casting material onto the surface of gecko skin as a negative mold [19]. Furthermore, Yuan et al. [48] reported positively charged MOF nano-dagger surfaces

that displayed superior bactericidal activity, because the positive charge enhanced bacteria adhesion and sharp nano-dagger tips promoted bacteria killing.

### **3.6 Factors influencing bactericidal activity**

In addition to the fabrication parameters, properties of certain bacteria and nanofeatures including protrusion diameter, height, and spacing can also influence the bactericidal efficacy.

#### **3.6.1 Bacterial cell properties**

The bactericidal activity of a nanotextured surface is dependent on bacterial adhesion, which involves an initial attraction and subsequent attachment of bacterial cells. Many factors can affect the attachment of bacteria to a given substrate, namely cell surface hydrophobicity and cell surface charge [51]. Cell surface hydrophobicity is a physical force that can increase or decrease the propensity of microbial adhesion, depending on the surface and bacterial cell wall composition [52]. Bacteria are generally hydrophilic, and therefore can adhere more readily to hydrophilic surfaces [53]. However, microorganisms can switch between hydrophilic and hydrophobic phenotypes depending on environmental conditions and growth phases, meaning that they may not always attach [52]. Cell surface charge may also be a factor responsible for influencing bacterial attachment. While the degree of charge varies between species and strains, the majority of bacterial cells are negatively charged due to an excess of carboxyl and phosphate groups within their cell walls [54]. A positively charged nanostructured surface tends to display higher bactericidal efficiency and selectivity due to the stronger interaction with negatively charged bacterial cell membranes [48].

Differences in Gram-positive and Gram-negative bacteria cell wall compositions can affect their rigidity. The type of bonds (covalent vs. electrostatic) between the peptidoglycan and outer membrane layer also contributes to overall cell rigidity [22].

Gram-negative bacteria contain a 2-3 nm peptidoglycan layer, while Gram-positive bacteria have a 20-80 nm peptidoglycan layer, giving Gram-positive bacteria more rigidity. Higher rigidity results in higher resistance towards deformational stresses imparted from protrusions on the surface [55].

Bacterial size and shape can dictate interactions with nanotextured surfaces. Larger bacterial cells settle on top of pillars and penetrate gradually, while smaller bacteria tend to settle in the interspace between two pillars, interacting more with edges [13]. It has been proposed that, if the spacing among pillars was comparable to the size of bacteria, the cells would orient themselves in order to maximize the contact area [56]. For example, rod-shaped bacterial cells were found to settle perpendicularly between pillars, and the contact area increased when the spacing decreased. When cell membrane attaches and adsorbs onto the surface, extensive stretching causes the rupture of membrane and finally cell death, albeit only when external forces exceed the maximum elasticity of membrane [34].

Bacterial growth cycle plays a key role in the bactericidal activity of nano-pillared surfaces. Truong et al. [16] investigated the bactericidal action of damselfly wings to lag, log, and stationary *S. aureus* and *P. aeruginosa* cells. It was found that *S. aureus* (89.7% at log phase) and *P. aeruginosa* (97.9% at stationary phase) were most inhibited.

### **3.6.2 Surface features**

#### *3.6.2.1 Nanostructured surface shape*

Besides pillars, alternative structures have also been fabricated in recent years. For example, Cao et al. [50] produced spear-like and pocket-like structures through hydrothermal treatments. The spear type could not prevent the formation of biofilms, while the pocket type, which was the network of intertwined spears, delayed biofilm growth and killed up to 47% of adherent bacteria. It was proposed that bacteria slid in

between arranged spears inside the pocket, resulting in the increased contact area and subsequent cell penetration. Similarly, Linklater et al. [45] suggested that nanopillar clusters were able to rapidly trap and damage more bacteria than single pillar due to the presence of many sharp and dense tips that enhanced membrane stretching. Moreover, Zou et al. [38] demonstrated that GO nanosheets containing wrinkled structures with a 500 nm roughness grade displayed the strongest antibacterial effect against *E. coli* and *S. aureus*, trapping size matched bacteria with a large contact area. Other studies have shown that the edge of nanostructure is an important factor in determining bactericidal activity. Wandiyanto et al. [26] fabricated titanium nanosheets with sharp and blade-like nano-edges of about 10 nm, which demonstrated the highest mechano-bactericidal efficacy against *P. aeruginosa* (99%) and *S. aureus* (90%). Zeolitic imidazolate framework nano-dagger arrays were taller, larger, more rigid, and sharper at the tips than common nanopillars [48]. These positively charged nano-daggers led to a stronger interaction with bacteria, and thus increased bactericidal activity. However, the bactericidal efficiencies of nano-pillars, nano-rings, and nano-nuggets with the same height of 100 nm and diameter of 50 nm were similar [28].

#### 3.6.2.2 Other features

It has been found that spacing, height, aspect ratio, and diameter of nanostructured surfaces can influence mechano-bactericidal activity. By decreasing height, spacing and diameter, the number of bacterial cells attached to the surface decreases [35]. For instance, the pillar arrays with a pitch of 1100 nm only showed antifouling behavior against large bacteria, such as *E. coli*, whereas those with a pitch of 480 nm displayed both bactericidal activity and antifouling behavior [47]. In addition, pillars with spacing under 60 nm could effectively kill *S. aureus* [35]. Smaller spacing was thought to induce more localized forces on cells, causing intensive stretching of membranes and finally cell lysis [11]. However, too small spacing between nanopillars would not allow bacterial cells to settle, providing additional chances for bacterial attachment [49]. This

was supported by the result that surfaces with approximately 40 pillars/ $\mu\text{m}^2$  had higher bactericidal effects than that with very high density ( $\sim 70$  pillars/ $\mu\text{m}^2$ ) [57].

Bactericidal activity is also related to the height of nanopillars. For example, nanopillars with a height of 50 nm were not effective at killing *S. aureus*, but 400 nm nanopillars were highly bactericidal [28]. Extremely long nanopillars ( $>7 \mu\text{m}$ ) exhibited superior bactericidal action against various bacterial species, while short ones ( $<2 \mu\text{m}$ ) killed species selectively [22]. However, if nanopillars were too long ( $\sim 1000$  nm), they could not be well separated, resulting in a low bactericidal activity [58].

### 3.7 Conclusions and outlook

Several natural surfaces with nanostructures display antibacterial properties against common pathogens including foodborne bacteria. Inspired by these natural structures, synthetic surfaces have been fabricated from black silicon, graphene, graphene-derived materials, and titanium. Factors such as the cell properties of bacteria and surface features (e.g. spacing, height, aspect ratio) significantly influence the interactions between surfaces and bacteria. However, current models cannot explain the mechano-bactericidal mechanisms of different nanotopographies.

Compared to traditional antimicrobial strategies, mechano-bactericidal nanostructures have demonstrated exciting potential in the field of food safety and are promising to be applied in various food supply chain stages. Future research is required to fully realize their applications:

1. The mechanism of mechano-bactericidal properties is key to future development. It is difficult to conclude how nanoscale surface features affect the bactericidal activity due to multiple parameters that need to be considered. Increased nanopillar contact area, density, and aspect ratio, as well as sharper edges and tips possibly contribute to improved bactericidal efficiency. More research is needed to further understand how

each parameter influences the bactericidal properties. This will then allow us to better design and optimize the nanotopographies to achieve the broader bactericidal activity.

2. Bacterial adhesion compromises food quality and safety. To address this problem, nanostructures can be produced using various materials (not only inorganic compounds) or formed on different surfaces such as food packaging and food processing devices for applications in food preservation, antibacterial coating, water disinfection, etc. Feasible and cost-effective approaches to fabricate mechano-bactericidal nanostructures on an industrial scale are necessary.

3. The efficacy of most mechano-bactericidal surfaces is not comparable to other bactericidal approaches, which may hinder their applications. The bactericidal activity can be further improved by combining the physical optimization of structures, chemically surface modifications with recognition elements (e.g. aptamers, enzymes, and antibodies), and involvement of external forces.

### 3.8 References

1. Gomes, L. C.; Moreira, J. M. R.; Araujo, J. D. P.; Mergulhao, F. J., Surface conditioning with *Escherichia Coli* cell wall components can reduce biofilm formation by decreasing initial adhesion. *AIMS Microbiology* **2017**, *3* (3), 613-628.
2. Elbourne, A.; Crawford, R. J.; Ivanova, E. P., Nano-structured antimicrobial surfaces: From nature to synthetic analogues. *Journal of Colloid and Interface Science* **2017**, *508*, 603-616.
3. Lin, N.; Berton, P.; Moraes, C.; Rogers, R. D.; Tufenkji, N., Nanodarts, nanoblades, and nanospikes: Mechano-bactericidal nanostructures and where to find them. *Advances in Colloid and Interface Science* **2018**, *252*, 55-68.
4. Anselme, K.; Davidson, P.; Popa, A. M.; Giazson, M.; Liley, M.; Ploux, L., The interaction of cells and bacteria with surfaces structured at the nanometre scale. *Acta Biomaterialia* **2010**, *6* (10), 3824-3846.
5. Linklater, D. P.; Juodkazis, S.; Ivanova, E. P., Nanofabrication of mechano-bactericidal surfaces. *Nanoscale* **2017**, *9* (43), 16564-16585.
6. An, Y. H.; Friedman, R. J., Concise review of mechanisms of bacterial adhesion to biomaterial surfaces. *Journal of Biomedical Materials Research* **1998**, *43* (3), 338-348.
7. Nowlin, K.; Boseman, A.; Covell, A.; LaJeunesse, D., Adhesion-dependent rupturing of *saccharomyces cerevisiae* on biological antimicrobial nanostructured surfaces. *Journal of The Royal Society Interface* **2015**, *12* (102), 20140999.
8. Jagessar, A.; Shahali, H.; Mathew, A.; Yarlagadda, P. K. D. V., Bio-mimicking nano and micro-structured surface fabrication for antibacterial properties in medical implants. *Journal of Nanobiotechnology* **2017**, *15* (1), 1-20.
9. Jenkins, J.; Mantell, J.; Neal, C.; Gholinia, A.; Verkade, P.; Nobbs, A. H.; Su, B., Antibacterial effects of nanopillar surfaces are mediated by cell impedance, penetration and induction of oxidative stress. *Nature Communications* **2020**, *11* (1), 1626.
10. Bandara, C. D.; Singh, S.; Afara, I. O.; Wolff, A.; Tesfamichael, T.; Ostrikov, K.;

- Oloyede, A., Bactericidal effects of natural nanotopography of dragonfly wing on *Escherichia Coli*. *ACS Applied Materials & Interfaces* **2017**, *9* (8), 6746-6760.
11. Pogodin, S.; Hasan, J.; Baulin, Vladimir A.; Webb, Hayden K.; Truong, Vi K.; Phong Nguyen, The H.; Boshkovikj, V.; Fluke, Christopher J.; Watson, Gregory S.; Watson, Jolanta A.; Crawford, Russell J.; Ivanova, Elena P., Biophysical model of bacterial cell interactions with nanopatterned cicada wing surfaces. *Biophysical Journal* **2013**, *104* (4), 835-840.
12. Li, X., Bactericidal mechanism of nanopatterned surfaces. *Physical Chemistry Chemical Physics* **2016**, *18* (2), 1311-6.
13. Li, X.; Cheung, G. S.; Watson, G. S.; Watson, J. A.; Lin, S.; Schwarzkopf, L.; Green, D. W., The nanotipped hairs of gecko skin and biotemplated replicas impair and/or kill pathogenic bacteria with high efficiency. *Nanoscale* **2016**, *8* (45), 18860-18869.
14. Cheeseman, S.; Truong, V. K.; Walter, V.; Thalmann, F.; Marques, C. M.; Hanssen, E.; Vongsvivut, J.; Tobin, M. J.; Baulin, V. A.; Juodkazis, S.; Maclaughlin, S.; Bryant, G.; Crawford, R. J.; Ivanova, E. P., Interaction of giant unilamellar vesicles with the surface nanostructures on dragonfly wings. *Langmuir* **2019**, *35* (6), 2422-2430.
15. Ivanova, E. P.; Hasan, J.; Webb, H. K.; Truong, V. K.; Watson, G. S.; Watson, J. A.; Baulin, V. A.; Pogodin, S.; Wang, J. Y.; Tobin, M. J.; L b be, C.; Crawford, R. J., Natural bactericidal surfaces: Mechanical rupture of *Pseudomonas aeruginosa* cells by cicada wings. *Small* **2012**, *8* (16), 2489-2494.
16. Truong, V. K.; Geeganagamage, N. M.; Baulin, V. A.; Vongsvivut, J.; Tobin, M. J.; Luque, P.; Crawford, R. J.; Ivanova, E. P., The susceptibility of *Staphylococcus aureus* CIP 65.8 and *Pseudomonas Aeruginosa* ATCC 9721 cells to the bactericidal action of nanostructured *Calopteryx haemorrhoidalis* damselfly wing surfaces. *Applied Microbiology and Biotechnology* **2017**, *101* (11), 4683-4690.
17. Nishimoto, S.; Bhushan, B., Bioinspired self-cleaning surfaces with superhydrophobicity, superoleophobicity, and superhydrophilicity. *RSC Advances* **2013**, *3* (3), 671-690.

18. Morikawa, J.; Ryu, M.; Seniutinas, G.; Balčytis, A.; Maximova, K.; Wang, X.; Zamengo, M.; Ivanova, E. P.; Juodkazis, S., Nanostructured antireflective and thermoisolative cicada wings. *Langmuir* **2016**, *32* (18), 4698-4703.
19. Green, D. W.; Lee, K. K.-H.; Watson, J. A.; Kim, H.-Y.; Yoon, K.-S.; Kim, E.-J.; Lee, J.-M.; Watson, G. S.; Jung, H.-S., High quality bioreplication of intricate nanostructures from a fragile gecko skin surface with bactericidal properties. *Scientific Reports* **2017**, *7* (1), 41023.
20. Jay, J. M.; Loessner, M. J.; Golden, D. A., *Modern food microbiology*. 7th ed. ed.; Springer: New York, **2005**.
21. Mainwaring, D. E.; Nguyen, S. H.; Webb, H.; Jakubov, T.; Tobin, M.; Lamb, R. N.; Wu, A. H. F.; Marchant, R.; Crawford, R. J.; Ivanova, E. P., The nature of inherent bactericidal activity: Insights from the nanotopology of three species of dragonfly. *Nanoscale* **2016**, *8* (12), 6527-6534.
22. Michalska, M.; Gambacorta, F.; Divan, R.; Aranson, I. S.; Sokolov, A.; Noiro, P.; Laible, P. D., Tuning antimicrobial properties of biomimetic nanopatterned surfaces. *Nanoscale* **2018**, *10* (14), 6639-6650.
23. Watson, G. S.; Cribb, B. W.; Schwarzkopf, L.; Watson, J. A., Contaminant adhesion (aerial/ground biofouling) on the skin of a gecko. *Journal of The Royal Society Interface* **2015**, *12* (108), 20150318.
24. May, P. W.; Clegg, M.; Silva, T. A.; Zanin, H.; Fatibello-Filho, O.; Celorrio, V.; Fermin, D. J.; Welch, C. C.; Hazell, G.; Fisher, L.; Nobbs, A.; Su, B., Diamond-coated 'black silicon' as a promising material for high-surface-area electrochemical electrodes and antibacterial surfaces. *Journal of Materials Chemistry B* **2016**, *4* (34), 5737-5746.
25. Linklater, D. P.; Ivanova, E. P.; Linklater, D. P.; Juodkazis, S.; Baulin, V. A., Mechano-bactericidal mechanism of graphene nanomaterials. *Interface Focus* **2018**, *8* (3), 20170060.
26. Wandiyanto, J. V.; Tamanna, T.; Linklater, D. P.; Truong, V. K.; Al Kobaisi, M.; Baulin, V. A.; Juodkazis, S.; Thissen, H.; Crawford, R. J.; Ivanova, E. P., Tunable

morphological changes of asymmetric titanium nanosheets with bactericidal properties. *Journal of Colloid Interface Science* **2020**, *560*, 572-580.

27. Singh, A. V.; Baylan, S.; Park, B.-W.; Richter, G.; Sitti, M., Hydrophobic pinning with copper nanowhiskers leads to bactericidal properties. *PLOS One* **2017**, *12* (4), e0175428/1-e0175428/14.

28. Wu, S.; Zuber, F.; Brugger, J.; Maniura-Weber, K.; Ren, Q., Antibacterial on nanostructured surfaces. *Nanoscale* **2016**, *8* (5), 2620-2625.

29. Ivanova, E. P.; Hasan, J.; Webb, H. K.; Gervinskas, G.; Juodkazis, S.; Truong, V. K.; Wu, A. H. F.; Lamb, R. N.; Baulin, V. A.; Watson, G. S.; Watson, J. A.; Mainwaring, D. E.; Crawford, R. J., Bactericidal activity of black silicon. *Nature Communications* **2013**, *4* (1), 2838.

30. Hazell, G.; May, P. W.; Taylor, P.; Nobbs, A. H.; Welch, C.; Su, B., Studies of black silicon and black diamond as materials for antibacterial surfaces. *Biomaterials science* **2018**, *6* (6), 1424-1432.

31. Ma, L. L.; Zhou, Y. C.; Jiang, N.; Lu, X.; Shao, J.; Lu, W.; Ge, J.; Ding, X. M.; Hou, X. Y., Wide-band "black silicon" based on porous silicon. *Applied Physics Letters* **2006**, *88* (17), 171907.

32. Jang, Y.; Choi, W. T.; Johnson, C. T.; García, A. J.; Singh, P. M.; Breedveld, V.; Hess, D. W.; Champion, J. A., Inhibition of bacterial adhesion on nanotextured stainless steel 316L by electrochemical etching. *ACS Biomaterials Science & Engineering* **2018**, *4* (1), 90-97.

33. Žukauskas, A.; Malinauskas, M.; Kadys, A.; Gervinskas, G.; Seniutinas, G.; Kandasamy, S.; Juodkazis, S., Black silicon: Substrate for laser 3D micro/nanopolymerization. *Optics Express* **2013**, *21* (6), 6901-6909.

34. Vassallo, E.; Pedroni, M.; Silvetti, T.; Morandi, S.; Toffolatti, S.; Angella, G.; Brasca, M., Bactericidal performance of nanostructured surfaces by fluorocarbon plasma. *Materials Science and Engineering: C* **2017**, *80*, 117-121.

35. Linklater, D. P.; Nguyen, H. K. D.; Bhadra, C. M.; Juodkazis, S.; Ivanova, E. P.,

Influence of nanoscale topology on bactericidal efficiency of black silicon surfaces. *Nanotechnology* **2017**, *28* (24), 245301.

36. Nguyen, D. H. K.; Loebbe, C.; Linklater, D. P.; Xu, X.; Vrancken, N.; Katkus, T.; Juodkazis, S.; Maclaughlin, S.; Baulin, V.; Crawford, R. J.; Ivanova, E. P., The idiosyncratic self-cleaning cycle of bacteria on regularly arrayed mechano-bactericidal nanostructures. *Nanoscale* **2019**, *11* (35), 16455-16462.

37. Sengupta, I.; Bhattacharya, P.; Talukdar, M.; Neogi, S.; Pal, S. K.; Chakraborty, S., Bactericidal effect of graphene oxide and reduced graphene oxide: Influence of shape of bacteria. *Colloid and Interface Science Communications* **2019**, *28*, 60-68.

38. Zou, F.; Zhou, H.; Jeong, D. Y.; Kwon, J.; Eom, S. U.; Park, T. J.; Hong, S. W.; Lee, J., Wrinkled surface-mediated antibacterial activity of graphene oxide nanosheets. *ACS Applied Materials & Interfaces* **2017**, *9* (2), 1343-1351.

39. Selim, M. S.; Mo, P. J.; Hao, Z.; Fatthallah, N. A.; Chen, X., Blade-like structure of graphene oxide sheets decorated with cuprous oxide and silicon carbide nanocomposites as bactericidal materials. *Journal of Colloid and Interface Science* **2020**, *578*, 698-709.

40. Deng, C.-H.; Gong, J.-L.; Zeng, G.-M.; Zhang, P.; Song, B.; Zhang, X.-G.; Liu, H.-Y.; Huan, S.-Y., Graphene sponge decorated with copper nanoparticles as a novel bactericidal filter for inactivation of *Escherichia Coli*. *Chemosphere* **2017**, *184*, 347-357.

41. Wandiyanto, J. V.; Cheeseman, S.; Truong, V. K.; Kobaisi, M. A.; Bizet, C.; Juodkazis, S.; Thissen, H.; Crawford, R. J.; Ivanova, E. P., Outsmarting superbugs: Bactericidal activity of nanostructured titanium surfaces against methicillin- and gentamicin-resistant *Staphylococcus Aureus* ATCC 33592. *Journal Materials Chemistry B* **2019**, *7* (28), 4424-4431.

42. Wandiyanto, J. V.; Al, K. M.; Truong, V. K.; Bazaka, O.; Crawford, R. J.; Ivanova, E. P.; Juodkazis, S.; Thissen, H.; Bazaka, K., The fate of osteoblast-like MG-63 cells on pre-infected bactericidal nanostructured titanium surfaces. *Materials* **2019**, *12* (10),

1575.

43. Sjöström, T.; Nobbs, A. H.; Su, B., Bactericidal nanospikes via thermal oxidation of Ti alloy substrates. *Materials Letters* **2016**, *167*, 22-26.

44. Hasan, J.; Jain, S.; Chatterjee, K., Nanoscale topography on black titanium imparts multi-biofunctional properties for orthopedic applications. *Scientific Reports* **2017**, *7* (1), 41118.

45. Linklater, D. P.; Juodkakis, S.; Crawford, R. J.; Ivanova, E. P., Mechanical inactivation of *Staphylococcus Aureus* and *Pseudomonas Aeruginosa* by titanium substrata with hierarchical surface structures. *Materialia* **2019**, *5*, 100197.

46. Rosenzweig, R.; Perinbam, K.; Ly, V. K.; Ahrar, S.; Siryaporn, A.; Yee, A. F., Nanopillared surfaces disrupt *Pseudomonas Aeruginosa* mechanoresponsive upstream motility. *ACS Applied Materials & Interfaces* **2019**, *11* (11), 10532-10539.

47. Heckmann, T. S.; Schiffman, J. D., Spatially organized nanopillar arrays dissimilarly affect the antifouling and antibacterial activities of *Escherichia Coli* and *Staphylococcus Aureus*. *ACS Applied Nano Materials* **2020**, *3* (2), 977-984.

48. Yuan, Y.; Zhang, Y., Enhanced biomimetic bactericidal surfaces by coating with positively-charged ZIF nano-dagger arrays. *Nanomedicine: Nanotechnology, Biology and Medicine* **2017**, *13* (7), 2199-2207.

49. Friedlander, R. S.; Vlamakis, H.; Kim, P.; Khan, M.; Kolter, R.; Aizenberg, J., Bacterial flagella explore microscale hummocks and hollows to increase adhesion. *Proceedings of the National Academy of Sciences* **2013**, *110* (14), 5624.

50. Cao, Y.; Su, B.; Chinnaraj, S.; Jana, S.; Bowen, L.; Charlton, S.; Duan, P.; Jakubovics, N. S.; Chen, J., Nanostructured titanium surfaces exhibit recalcitrance towards *Staphylococcus Epidermidis* biofilm formation. *Scientific Reports* **2018**, *8* (1), 1071.

51. Elbourne, A.; Chapman, J.; Gelmi, A.; Cozzolino, D.; Crawford, R. J.; Truong, V. K., Bacterial-nanostructure interactions: The role of cell elasticity and adhesion forces. *Journal of Colloid and Interface Science* **2019**, *546*, 192-210.

52. Krasowska, A.; Sigler, K., How microorganisms use hydrophobicity and what does this mean for human needs? *Front Cell Infect Microbiol* **2014**, *4*, 112-112.
53. Krekeler, C.; Ziehr, H.; Klein, J., Physical methods for characterization of microbial cell surfaces. *Experientia* **1989**, *45* (11), 1047-1055.
54. Goulter, R. M.; Gentle, I. R.; Dykes, G. A., Issues in determining factors influencing bacterial attachment: A review using the attachment of *Escherichia Coli* to abiotic surfaces as an example. *Letters in Applied Microbiology* **2009**, *49* (1), 1-7.
55. Silhavy, T. J.; Kahne, D.; Walker, S., The bacterial cell envelope. *Cold Spring Harbor perspectives in biology* **2010**, *2* (5), a000414.
56. Hsu, L. C.; Fang, J.; Borca-Tasciuc, D. A.; Worobo, R. W.; Moraru, C. I., Effect of micro- and nanoscale topography on the adhesion of bacterial cells to solid surfaces. *Applied and Environmental Microbiology* **2013**, *79* (8), 2703.
57. Wu, S.; Zuber, F.; Maniura-Weber, K.; Brugger, J.; Ren, Q., Nanostructured surface topographies have an effect on bactericidal activity. *Journal of Nanobiotechnology* **2018**, *16* (1), 20.
58. Bhadra, C. M.; Werner, M.; Baulin, V. A.; Truong, V. K.; Al Kobaisi, M.; Nguyen, S. H.; Balcytis, A.; Juodkazis, S.; Wang, J. Y.; Mainwaring, D. E.; Crawford, R. J.; Ivanova, E. P., Subtle variations in surface properties of black silicon surfaces influence the degree of bactericidal efficiency. *Nano-Micro Lett.* **2018**, *10* (2), 36/1-36/8.

## CONNECTING STATEMENT II

A literature review in **Chapter 3** highlighted a novel mechano-bactericidal strategy to eliminate the attachment of bacterial pathogens. Cell membranes of bacteria are physically damaged by nanopillars on the surfaces, leading to the cell death. Both naturally occurring and synthetic surfaces and their mechano-bactericidal mechanisms were summarized in the review. Moreover, factors to affect the bactericidal efficiency such as cell properties and surface features were also covered. **Chapter 4** investigated the dissolution of three typical WCFs (t-shirts, bed sheet and jeans) in three solvent systems ( $\text{H}_2\text{SO}_4$  aqueous solution, NaOH/urea aqueous solution, and LiCl/DMAc solvent). The properties of regenerated cellulose films (e.g. the optical transmittance, mechanical property, thermal stability, and water vapor barrier property) were investigated as well.

## **CHAPTER 4. RECYCLING OF WASTE COTTON FABRICS INTO REGENERATED CELLULOSE FILMS THROUGH THREE SOLVENT SYSTEMS: A COMPARISON STUDY**

### **4.1 Abstract**

Large amounts of textile waste are generated every year and disposed of through landfill or incineration, leading to numerous environmental and social issues. In this work, the dissolution of three typical waste cotton fabrics (t-shirts, bed sheets and jeans) in NaOH/urea aqueous solution, H<sub>2</sub>SO<sub>4</sub> aqueous solution, and LiCl/DMAc solution was investigated. Compared to different types of cotton fabrics, the effects of three solvents on the dissolution of fabrics were more obvious, leading to the significant changes in the structure and properties of regenerated cellulose films. Cotton fabrics (about 2-5%) were rapidly dissolved (8 min) in H<sub>2</sub>SO<sub>4</sub> and NaOH/urea solvents after acid pretreatment, while the dissolution in LiCl/DMAc solvent did not need any pretreatment, but a lower cellulose concentration (1%), higher dissolution temperature (80 °C), and longer dissolution time (24 h) were required. The films produced from bed sheets in NaOH/urea solution exhibited the highest tensile strength, thermal stability, and water vapor barrier property. It was because of the stronger cellulose chain entanglement and hydrogen bonds induced by the higher cellulose concentration in NaOH/urea solution. Therefore, this work proves the feasibility to recycle waste cotton fabrics into biodegradable cellulose films, which can be potentially used in various food and agricultural applications.

**Keywords:** waste cotton fabrics, cellulose dissolution, sulfuric acid, NaOH/urea, LiCl/DMAc

## 4.2 Introduction

Due to the increase in world population, fast changing fashion cycles and higher quality of life, large amounts of textile waste are generated every year and have become a global issue [1]. It was estimated that only 15-16 % of textile waste were recycled or reused in the United States in 2015, while the rest were commonly landfilled, discarded or incinerated [2]. It has led to multiple environmental and social problems, including increased production of greenhouse gas emission (1.2 billion tonnes of carbon dioxide each year), ground water contamination, hazardous chemical generation, and limited landfilling space especially in cities [1,3]. Therefore, efforts on recycling textile waste have gained attention such as carbonizing textile waste into biochar, extracting CNCs, recovering cotton fibers and polyester, and producing ethanol, biogas and cellulose acetate [3-7]. For example, Yousef et al. [4] recovered cotton and polyester fibers from textile waste using a sustainable technology, achieving \$1,629/ton economic returns and a 96% recycling rate. Huang and Wang [5] directly extracted CNCs from textile waste and evaluated their application as reinforcing agents of soybean protein isolate films.

Cotton is one of the most utilized fibers in textile industry, which consists of over 90% cellulose [8]. The dissolution and regeneration of cellulose is a promising way to recycle WCFs. However, it is difficult to dissolve cellulose in water and common organic solvents, because cellulose molecules are tightly linked by numerous intramolecular and intermolecular hydrogen bonds [9]. In the last few years, several eco-friendly solvents have been reported to dissolve cellulose, such as LiCl/DMAc [10], NMMO [11], ionic liquids [12,13], NaOH/urea aqueous solution [14], and sulfuric acid aqueous solution [15]. Among them, sulfuric acid aqueous solution could directly dissolve wood cellulose with high molecular weight at low temperature in 5 min [9], while NaOH/urea aqueous solvent proposed by Cai and Zhang [14] is able to rapidly

dissolve cellulose with molecular weight less than  $1.0 \times 10^5 \text{ g mol}^{-1}$  when pre-cooled to  $-12.6 \text{ }^\circ\text{C}$  by fast dynamic self-assembly among solvent molecules and cellulose macromolecules. LiCl/DMAc is the most popular solvent that is capable of dissolving different types of cellulose without severely degradation, and the obtained cellulosic suspension can be regenerated easily in water [10]. These three solvent systems are relatively more cost-effective and have been widely studied to dissolve cellulose from different sources such as wastepaper, toilet paper, pulp, bamboo, and durian rind [15-18]. Nevertheless, their capacities and applications in recycling WCFs are seldom reported.

In order to determine a feasible way to recycle WCFs, in this work, t-shirts, bed sheets, and jeans made of 100% cotton were selected and their dissolution in sulfuric acid aqueous solution, NaOH/urea aqueous solution, and LiCl/DMAc was investigated and compared. The structure and morphology of regenerated cellulose films were characterized by Fourier transform infrared spectroscopy, X-ray diffraction, and scanning electron microscopy. Additionally, the optical transmittance, mechanical property, thermal stability, and water vapor permeability of regenerated cellulose films were studied via ultraviolet-visible spectroscope, tensile test, thermogravimetric analysis, and modified cup method.

### **4.3 Materials and methods**

#### **4.3.1 Materials**

T-shirts and bed sheets (100% cotton) were collected from the secondhand shop in Montreal, Canada, and jeans (100% cotton) were kindly provided by Renaissance (Montreal, QC Canada). Sulfuric acid (95.0-98.0%) and sodium hydroxide were purchased from Sigma-Aldrich (MO, USA). Urea, lithium chloride, acetone and N, N-dimethylacetamide were purchased from Fisher Chemical (Ontario, Canada). Distilled

water is used unless specific mentioned.

### **4.3.2 Cotton fabric dissolution and regeneration**

#### *4.3.2.1 H<sub>2</sub>SO<sub>4</sub> aqueous solvent*

A grinding machine (KRUPS, Ontario, Canada) was applied to break cotton fabrics, and the pretreatment conditions were optimized in our preliminary experiment. The fabrics (5 g) were pretreated in 250 mL 20% (w/v) H<sub>2</sub>SO<sub>4</sub> at 25 °C, where t-shirts were soaked for 48 h, and bed sheets and jeans were soaked for 72 h. They were then washed thoroughly with water and dried in the oven. The desired amounts of fabrics (listed in Table 4.1) were added into 50 ml 64% (w/v) H<sub>2</sub>SO<sub>4</sub> aqueous solutions that were pre-cooled to -20 °C, and then stirred at 750 rpm for 8 min using IKA<sup>®</sup> Eurostar 60 digital mixer in ice bath [9]. The obtained solutions were centrifuged at 6500 rpm for 5 min by Centrifuge 5430 (Eppendorf, USA) to remove bubbles. After centrifugation, the transparent and homogenous solutions were immediately poured onto glass plate and immersed in a coagulation bath with 10% (w/v) NaOH for 15 min. The regenerated films were then soaked in water for 24 h and finally dried in air at room temperature. Cellulose films prepared from t-shirts, bed sheets, and jeans in H<sub>2</sub>SO<sub>4</sub> aqueous solution were coded as T-H, B-H, and J-H, respectively.

#### *4.3.2.2 NaOH/urea aqueous solvent*

After grinded into cotton wool, t-shirts (5 g) were soaked in 250 mL 20% (w/v) H<sub>2</sub>SO<sub>4</sub> at 25 °C for 6 days, while bed sheets and jeans were soaked for 7 days. The pretreated fabrics (2 g) were added into 7% NaOH/12% urea aqueous solutions and kept at -20 °C for 12 h. After thawing, 5% (w/w) transparent cellulose solutions were obtained through vigorously stirring at 2000 rpm for 8 min [14], followed by centrifugation at 6500 rpm for 5 min. Then, the solutions were quickly spread on a glass plate and immersed in a coagulation bath with 5% (w/v) H<sub>2</sub>SO<sub>4</sub> for 15 min. After washing with water, the regenerated films were dried in air at room temperature. Cellulose films prepared from

t-shirts, bed sheets and jeans in NaOH aqueous solution were coded as T-N, B-N, and J-N, respectively.

#### *4.3.2.3 LiCl/DMAc solvent*

Cotton fabrics were grinded into cotton wools, and washed with water, acetone, and finally DMAc for activation to open up the chains. The fabrics (0.25 g) were added in mixed solutions of DMAc (23 g) and LiCl (2 g), and stirred for 6 h at 80 °C and then for 18 h at room temperature [19]. After dissolution, cellulose solutions were centrifuged at 6500 rpm for 5 min and spread on a glass plate, followed by thoroughly water washing. Finally, the regenerated films were dried in air at room temperature. Cellulose films prepared from t-shirts, bed sheets and jeans in LiCl/DMAc were coded as T-D, B-D, and J-D, respectively.

### **4.3.3 Regenerated cellulose film characterization**

#### *4.3.3.1 Fourier transform infrared spectroscopy*

The structures of cotton fabrics and regenerated films were investigated by Nicolet 6700 spectrophotometer (Thermo Fisher Scientific Inc., MA, USA) equipped with an ATR accessory (Specac, Prpington, UK). The FT-IR spectra were recorded as the average of 64 scans with 4 cm<sup>-1</sup> resolution from 400-4000 cm<sup>-1</sup> at 25 °C, using the empty accessory as background.

#### *4.3.3.2 X-ray diffraction*

XRD patterns of cotton fabrics and regenerated films were collected through a Bruker D8 Discovery diffractometer (Bruker, Billerica, MA, USA), using Cu K $\alpha$  radiation ( $\lambda=0.1542$  nm) generated at 40 kV and 44 mA with the speed of 2°/min ( $2\theta$  was from 4° to 45°).

#### *4.3.3.3 Scanning electron microscopy*

The morphology of cotton fabrics and regenerated films was observed by a Hitachi

TM1000 SEM (New Jersey, USA) with an acceleration voltage of 4 kV at  $\times 1000$  magnification. Samples were sputtered with gold with the thickness of 5 nm by a Leica EM ACE200 low vacuum coater (Ontario, Canada) prior to observation.

#### *4.3.3.4 Optical transmittance*

The optical transmittance of regenerated films at a wavelength of 800 nm (the thickness was around 0.03 mm) was measured by a DU 800 UV/vis spectrophotometer (Beckman Coulter, Brea, CA, USA), using air as background.

#### *4.3.3.5 Mechanical property*

The tensile strength, elongation at break, and Young's modulus of regenerated films were tested on an Instron 5967 universal testing machine (Instron Corp., MA, USA) at the crosshead speed of 5 mm/min. The initial grip separation distance was set as 20 mm. Five strips were cut from films with the dimension of 6 cm $\times$ 1 cm (length  $\times$  width). The thickness of each strip was measured using a digital micrometer with a precision of 1  $\mu$ m.

#### *4.3.3.6 Thermogravimetric analysis*

TGA of regenerated films was performed using the thermogravimetric analyzer Q50 (TA instruments, DE, USA). Thermograms of samples were collected from 50  $^{\circ}$ C to 600  $^{\circ}$ C with a heating rate of 10  $^{\circ}$ C/min in nitrogen (40 mL/min) [10]. Universal analysis 2000 software was used to calculate DTG and the percentage of weight loss.

#### *4.3.3.7 Water vapor permeability*

A modified cup method was performed to measure the WVP of regenerated films according to ASTM E96-92 standard [20]. A dried film was taped on the top of a glass cup containing anhydrous calcium chloride. The sealed glass cup was then placed in a desiccator that contained saturated sodium chloride solution (75% RH). The weight change of the cup was recorded periodically at 25  $^{\circ}$ C. The WVP ( $\text{g m}^{-1} \text{h}^{-1} \text{Pa}^{-1}$ ) of films

was calculated by the following equation [20]:

$$WVP = \frac{\Delta m \times k}{A \times \Delta T \times \Delta P} \quad (3)$$

Where  $\Delta m$  is the weight change of the cup (g) during time  $\Delta T$  (h),  $k$  is the thickness of each film (m),  $A$  is the exposed area of the film ( $7.85 \times 10^{-5} \text{ m}^2$ ), and  $\Delta P$  is the partial water vapor pressure difference between two sides of the film (Pa).

#### 4.3.4 Statistical analysis

The experimental results were presented as the mean of three batches  $\pm$  SD. Statistical evaluation was performed by analysis of variance (ANOVA) followed by multiple comparison tests by Duncan's multiple range test. All of analyses were carried out through SPSS statistical software (IBM, New York, NY, USA) with significant differences within samples at  $p < 0.05$ .

### 4.4 Results and discussion

#### 4.4.1 Dissolution of cotton fabrics in three solvent systems

Three solvent systems were used to dissolve cotton fabrics. Due to their different dissolution capacities, chemical pretreatment (sulfuric acid hydrolysis) was applied to reduce the molecular weight and increase the internal surface area of cellulose, resulting in easier and faster dissolution [21]. The dissolution conditions were optimized by changing the hydrolysis time and cotton fabric concentration in our preliminary experiment and are summarized in Table 4.1.

**Table 4.1** Optimized dissolution conditions of cotton fabrics in three solvent systems

Regenerated films	Pretreatments	Fabric concentrations	Dissolution Time	Dissolution Temperature
T-H	48 h in 20% (w/v) H <sub>2</sub> SO <sub>4</sub>	3%	8 min	0 °C
B-H	72 h in 20%	2%	8 min	0 °C

	(w/v) H <sub>2</sub> SO <sub>4</sub>			
J-H	72 h in 20%	2%	8 min	0 °C
	(w/v) H <sub>2</sub> SO <sub>4</sub>			
T-N	6 days in 20%	5%	8 min	0 °C
	(w/v) H <sub>2</sub> SO <sub>4</sub>			
B-N	7 days in 20%	5%	8 min	0 °C
	(w/v) H <sub>2</sub> SO <sub>4</sub>			
J-N	7 days in 20%	5%	8 min	0 °C
	(w/v) H <sub>2</sub> SO <sub>4</sub>			
T-D	/	1%	~1 day	80 °C
B-D	/	1%	~1 day	80 °C
J-D	/	1%	~1 day	80 °C

The pretreatments were required for all the samples dissolved in H<sub>2</sub>SO<sub>4</sub> and NaOH/urea aqueous solvent systems. However, an obviously longer acid hydrolysis time was needed for NaOH/urea aqueous solution. It indicated that its dissolution capacity is not as strong as that of concentrated H<sub>2</sub>SO<sub>4</sub> aqueous solution. Similar phenomena were observed when spruce cellulose was dissolved in these two solvent systems [22]. Compared to them, LiCl/DMAc solvent was able to directly dissolve cotton fabrics without sulfuric acid pretreatment, but the fabrics required multiple steps of activation (washed with water, acetone and DMAc) before dissolution. In addition, only 1% fabrics could be dissolved in LiCl/DMAc solvent, and the considerably longer dissolution time and higher dissolution temperature were needed. For both H<sub>2</sub>SO<sub>4</sub> and NaOH/urea aqueous solvent systems, viscous and transparent cellulose solutions were rapidly obtained in only 8 min. However, cellulose molecules in H<sub>2</sub>SO<sub>4</sub> solution were not as stable as in the other two solvent systems. The cotton fabrics dissolved in NaOH/urea solvent underwent the longest acid hydrolysis pretreatments, which resulted in the lowest molecular weight and solution viscosity at the same concentration

[10]. Therefore, a relatively higher fabric content was necessary to obtain the solutions with suitable viscosity for regeneration of cellulose films. It was worth noting that the pretreatment durations for bed sheets and jeans were longer than those for t-shirts, but all the samples were successfully dissolved in three solvent systems at the optimized conditions.

#### 4.4.2 Structure of regenerated films

To investigate the structure change of cotton fabrics before and after dissolution and regeneration in three solvent systems, FT-IR spectra were collected. As shown in Figure 4.1, all samples displayed similar characteristic IR spectra, and no new peaks appeared after dissolution and regeneration, indicating that the processes were a direct physical dissolution and no chemical reaction happened [18]. However, minor differences between the spectra of cotton fabrics and regenerated cellulose films were observed. For example, the absorption peak at  $1427\text{ cm}^{-1}$  was attributed to whiskers of cellulose crystalline I [9], while the peak at  $898\text{ cm}^{-1}$  represented amorphous regions [23]. The ratio of these two bands ( $I_{1430}/I_{900}$ ) that was established as “crystallinity index” and closely corresponded to the portion of cellulose I structure decreased after dissolution and regeneration [23]. Moreover, cotton fabrics exhibited two peaks at 3330 and 3269  $\text{cm}^{-1}$  and the former was related to the O(3)H-O(5) intramolecular hydrogen bonds in cellulose I structure [24]. In the regenerated films, these two peaks were flattened and broadened, which suggested the loss of cellulose crystallinity and the change from cellulose I crystals in cotton fabrics to cellulose II crystals after dissolution and regeneration [15]. The change of cellulose polymorph was demonstrated by XRD (Figure 4.2). Cotton fabrics displayed diffraction peaks at ca.  $14.8^\circ$  ( $11\bar{0}$ ),  $16.4^\circ$  (110),  $22.5^\circ$  (200), and  $34^\circ$  (040), which were typical for cellulose I crystals [25]. However, some of these peaks disappeared in the regenerated films, which exhibited a new broad diffraction at about  $20.6^\circ$ . Especially, another peak at  $12^\circ$  was observed in the films produced from NaOH/urea solutions. It indicated that the cellulose I crystals

transformed to cellulose II crystals during the process [9,26]. It was worth noting that there were some other diffraction peaks, for example at  $20^\circ$ ,  $25.7^\circ$  and  $36^\circ$ , appeared in the XRD patterns of jeans, which might be attributed to the additives or dyes in textiles (Figure 4.2c). Some of them were removed from the regenerated films (e.g. the considerable decreases of these diffraction peaks in the films prepared from NaOH/urea and LiCl/DMAc solvent systems), while some constituents might be wrapped in cellulose matrix during regeneration [15].

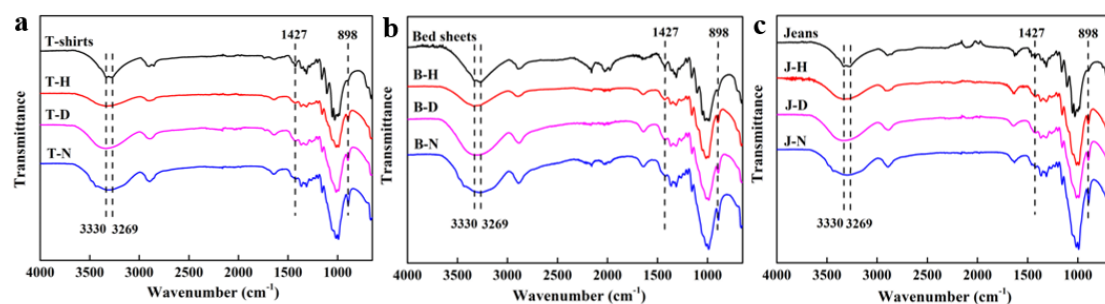


**Figure 4.1** FT-IR spectra of cotton fabrics and regenerated cellulose films prepared in three solvent systems

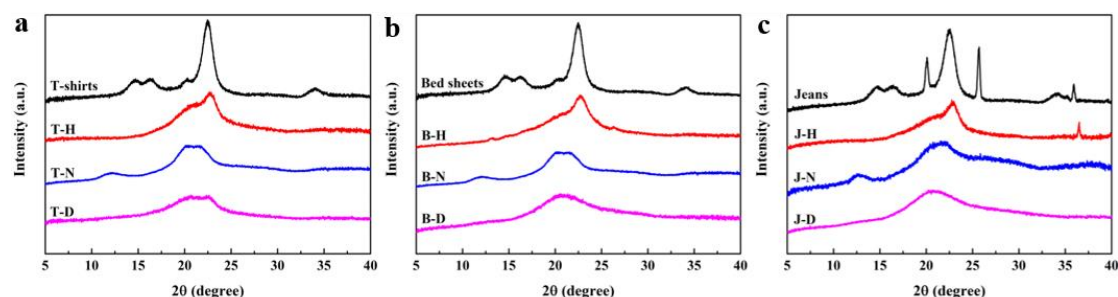


**Figure 4.2** X-ray diffraction patterns of cotton fabrics and regenerated cellulose films prepared in three solvent systems

The surface morphology of regenerated cellulose films prepared in three solvent systems were observed by SEM. As shown in Figure 4.3, no cotton fibers existed in all the films, which indicated the successful dissolution at our optimized conditions. Similar dense structures were also reported when cotton linter was dissolved in 6 wt% NaOH/4 wt% urea aqueous solution and regenerated in 2 M acetic acid and 2%  $H_2SO_4$

aqueous solution [27], and would contribute to the mechanical and barrier properties. No obvious difference could be distinguished among the films from t-shirts, bed sheets and jeans. However, the surfaces of regenerated films prepared in NaOH/urea solvent were relatively rougher than the others, which might be due to the rapid and uneven shrinkage during regeneration triggered by high cellulose concentration. A few particles were found in the films derived from LiCl/DMAc solvent, but it should be reminded that the raw materials were dissolved without any chemical pretreatment.

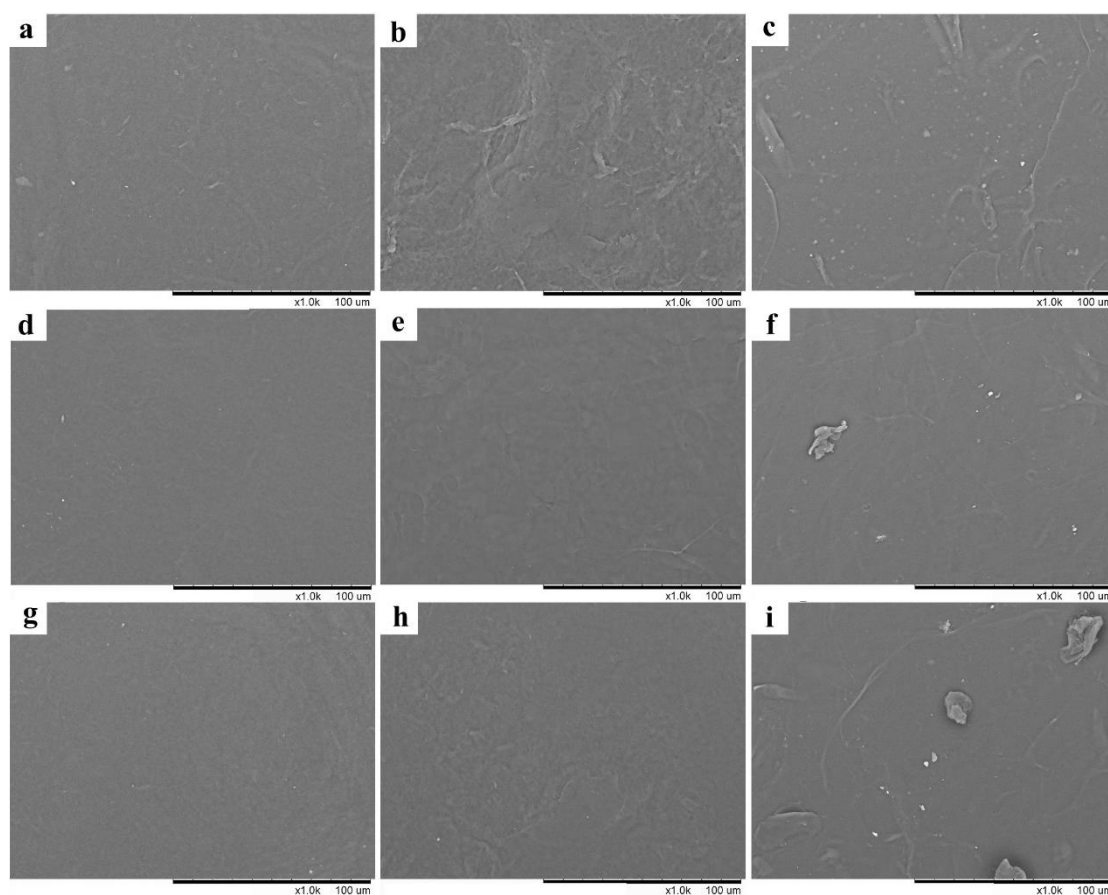


**Figure 4.3** SEM images of regenerated cellulose films prepared in three solvent systems: (a) T-H, (b) T-N, (c) T-D, (d) B-H, (e) B-N, (f) B-D, (g) J-H, (h) J-N, and (i) J-D

#### 4.4.3 Properties of regenerated films

The Tr of regenerated cellulose films at a wavelength of 800 nm is shown in Figure 4.4a. All the films were translucent (Figure 4.4b), and the Tr values depended on the

types of cotton fabrics and solvent systems. Generally speaking, the regenerated films prepared in  $\text{H}_2\text{SO}_4$  aqueous solution displayed the highest transmittance at the wavelength of 800 nm, followed by the films from LiCl/DMAc and NaOH/urea solvents. The Tr value of regenerated cellulose films could be affected by the following factors: firstly, it decreases with the increasing content of cellulose because higher cellulose content leads to more compact structure [28]; secondly, the presence of undissolved cellulose particles causes optical scattering and internal reflection and result in the decrease of Tr value [24]; and thirdly, the additives in cotton fabrics such as dyes may have significant absorption of visible light [29].

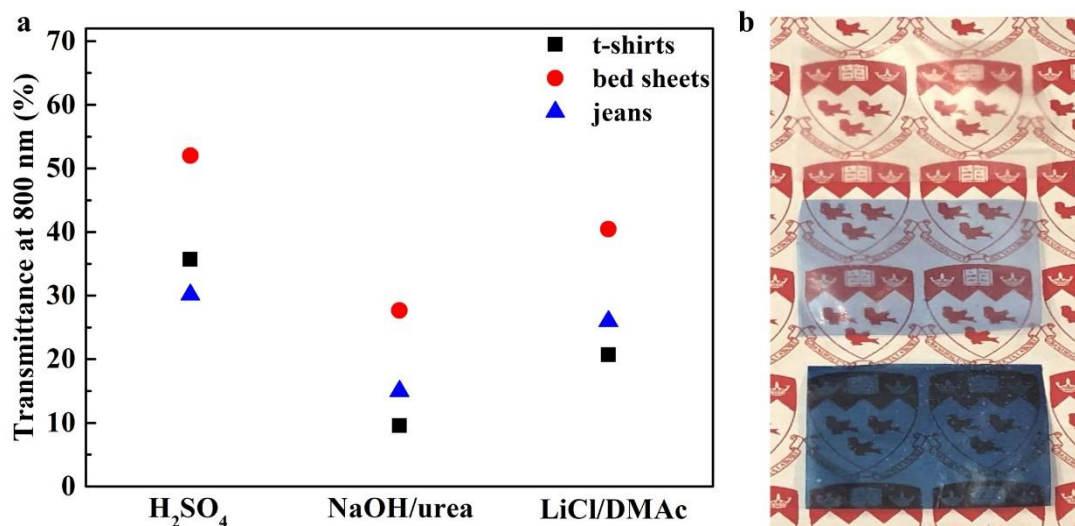


**Figure 4.4** (a) Tr of regenerated cellulose films prepared in three solvent systems at the wavelength of 800 nm; and (b) transparencies of B-H, T-H, and J-H (from top to bottom)

Mechanical properties of regenerated cellulose films were investigated by tensile test (Figure 4.5). It was found that the films from different raw materials using the same solvent displayed similar mechanical properties. However, the tensile strength and Young's modulus of regenerated films prepared in  $\text{H}_2\text{SO}_4$  and NaOH/urea solvent systems were higher than those of the films obtained from LiCl/DMAc solvent. Cellulose chain entanglement and hydrogen bonds are generated during regeneration to stabilize the cellulose films, and both molecular weight and concentration of cellulose



barrier property. TGA and DTG curves are shown in Figure 4.6. The slight weight loss before 150 °C was due to the evaporation of moisture content in the films [31]. All the samples had the major loss of weight in the range of 265 °C to 370 °C, which corresponded to thermal decomposition and carbonization of cellulose [10]. The  $T_{max}$  of T-H, J-H, B-H, B-N, and B-D were 302.09 °C, 295.05 °C, 301.47 °C, 325.66 °C, and 287.51 °C, respectively. The regenerated films prepared in H<sub>2</sub>SO<sub>4</sub> aqueous solution showed similar decomposition curves, which might be due to the similar chemical pretreatment and fabric concentration in solutions. However, the sample B-N prepared with the longest acid hydrolysis exhibited the highest  $T_{max}$ , while the  $T_{max}$  value of B-D film without any pretreatment was lowest. It indicated that, if the fabrics were not excessively hydrolyzed, the concentration of cellulose in solution played a more important role in the thermal stability of regenerated cellulose films. These results were in accordance with their mechanical properties.

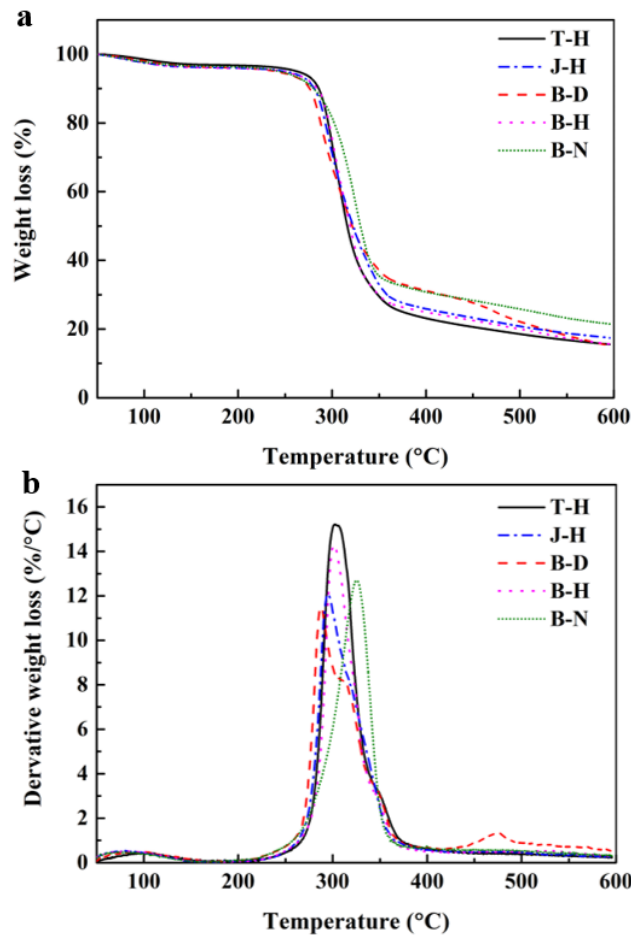


**Figure 4.6** TGA and DTG curves of regenerated cellulose films prepared in three solvent systems

WVP of regenerated cellulose films is shown in Figure 4.7. The film prepared from bed sheets in NaOH/urea aqueous solution exhibited the lowest WVP of  $0.81 \pm 0.10 \times 10^{-7} \text{ g m}^{-1} \text{ h}^{-1} \text{ Pa}^{-1}$ , while the other films displayed similar WVP values ( $p > 0.05$ ). It indicated that different cotton fabrics did not have a significant impact on water vapor diffusion. The increase of cellulose concentration in solution resulted in the formation of regenerated cellulose film with a denser structure, which increased the tortuosity and led to a slower water vapor diffusion process [32]. Although the concentration of B-D was lowest, the B-D and B-H samples had the similar WVP values. It might be due to the cellulose molecules without chemical pretreatment. The WVP values of regenerated films prepared from WCFs were much lower than those of bleached kraft pulp films, soybean protein isolate films, and sago starch films [5,33,34].

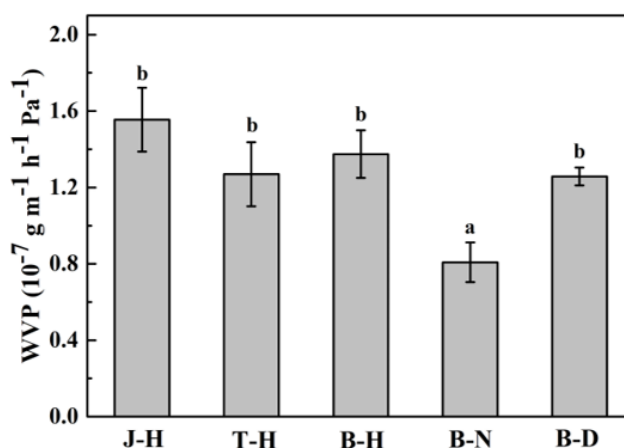


**Figure 4.7** WVP of regenerated cellulose films prepared in three solvent systems (different letters on the tops of columns represented the significant difference ( $p < 0.05$ ))

#### 4.5 Conclusion

T-shirts, bed sheets, and jeans could be directly dissolved in LiCl/DMAc solvent, but the dissolution required multiple activation steps, low cellulose concentration, high

dissolution temperature, and long dissolution time. After the appropriate chemical pretreatments, these cotton fabrics could be rapidly dissolved in H<sub>2</sub>SO<sub>4</sub> and NaOH/urea aqueous solutions, but cellulose was less stable in H<sub>2</sub>SO<sub>4</sub> and a fairly long acid hydrolysis was needed for the dissolution in NaOH/urea solvent. All the solutions were successfully regenerated into translucent cellulose films with smooth surface. The types of cotton fabrics did not have a significant impact on the mechanical, thermal and water vapor barrier properties of the resultant cellulose films, which would allow the recycle of mixed cotton fabrics through dissolution and regeneration. However, the increase of cellulose concentration in solution resulted in the films with denser structure and obviously improved properties. The films prepared from bed sheets in NaOH/urea solution exhibited the tensile strength of 76.21±8.26 MPa, maximum decomposition temperature of 325.66 °C, and water vapor permeability of 0.81±0.10×10<sup>-7</sup> g m<sup>-1</sup> h<sup>-1</sup> Pa<sup>-1</sup>, which were comparable to the samples from corn stalk pulp fines, spruce cellulose and oil palm biomass. Therefore, this study provides promising approaches to recycle waste cotton fabrics into biodegradable cellulose films, which have potential applications in food packaging and agriculture.

## 4.6 References

1. Dissanayake, D. G. K.; Weerasinghe, D. U.; Thebuwanage, L. M.; Bandara, U. A. A. N., An environmentally friendly sound insulation material from post-industrial textile waste and natural rubber. *Journal of Building Engineering* **2021**, *33*, 101606.
2. Ütebay, B.; Çelik, P.; Çay, A., Effects of cotton textile waste properties on recycled fibre quality. *Journal of Cleaner Production* **2019**, *222*, 29-35.
3. Çay, A.; Yanık, J.; Akduman, Ç.; Duman, G.; Ertaş, H., Application of textile waste derived biochars onto cotton fabric for improved performance and functional properties. *Journal of Cleaner Production* **2020**, *251*, 119664.
4. Yousef, S.; Tatariants, M.; Tichonovas, M.; Kliucininkas, L.; Lukošūtė, S.-I.; Yan, L., Sustainable green technology for recovery of cotton fibers and polyester from textile waste. *Journal of Cleaner Production* **2020**, *254*, 120078.
5. Huang, S.; Tao, R.; Ismail, A.; Wang, Y., Cellulose nanocrystals derived from textile waste through acid hydrolysis and oxidation as reinforcing agent of soy protein film. *Polymers* **2020**, *12* (4), 958.
6. Homem, N. C.; Amorim, M. T. P., Synthesis of cellulose acetate using as raw material textile wastes. *Materials Today: Proceedings* **2020**, *31*, S315-S317.
7. Peng, N.; Huang, D.; Gong, C.; Wang, Y.; Zhou, J.; Chang, C., Controlled arrangement of nanocellulose in polymeric matrix: From reinforcement to functionality. *ACS Nano* **2020**, *14* (12), 16169-16179.
8. Sandin, G.; Peters, G. M., Environmental impact of textile reuse and recycling – a review. *Journal of Cleaner Production* **2018**, *184*, 353-365.
9. Huang, W.; Wang, Y.; Zhang, L.; Chen, L., Rapid dissolution of spruce cellulose in H<sub>2</sub>SO<sub>4</sub> aqueous solution at low temperature. *Cellulose* **2016**, *23* (6), 3463-3473.
10. Han, Q.; Gao, X.; Zhang, H.; Chen, K.; Peng, L.; Jia, Q., Preparation and comparative assessment of regenerated cellulose films from corn (zea mays) stalk pulp fines in DMAc/LiCl solution. *Carbohydrate Polymers* **2019**, *218*, 315-323.

11. Zhang, Y.; Tian, Z.; Fu, Y.; Wang, Z.; Qin, M.; Yuan, Z., Responsive and patterned cellulose nanocrystal films modified by N-methylmorpholine-N-oxide. *Carbohydrate Polymers* **2020**, *228*, 115387.
12. Amalini, A. N.; Haida, M. K. N.; Imran, K.; Haafiz, M. K. M., Relationship between dissolution temperature and properties of oil palm biomass based-regenerated cellulose films prepared via ionic liquid. *Materials Chemistry and Physics* **2019**, *221*, 382-389.
13. Haq, M. A.; Habu, Y.; Yamamoto, K.; Takada, A.; Kadokawa, J., Ionic liquid induces flexibility and thermoplasticity in cellulose film. *Carbohydrate Polymers* **2019**, *223*, 6.
14. Cai, J.; Zhang, L., Rapid dissolution of cellulose in LiOH/urea and NaOH/urea aqueous solutions. *Macromolecular Bioscience* **2005**, *5* (6), 539-48.
15. Oliva, C.; Huang, W.; El Badri, S.; Lee, M. A. L.; Ronholm, J.; Chen, L.; Wang, Y., Concentrated sulfuric acid aqueous solution enables rapid recycling of cellulose from waste paper into antimicrobial packaging. *Carbohydrate Polymers* **2020**, *241*, 116256.
16. Zhao, G.; Lyu, X.; Lee, J.; Cui, X.; Chen, W.-N., Biodegradable and transparent cellulose film prepared eco-friendly from durian rind for packaging application. *Food Packaging and Shelf Life* **2019**, *21*, 100345.
17. Kiper, A. G.; Özyuguran, A.; Yaman, S., Electrospun cellulose nanofibers from toilet paper. *Journal of Material Cycles and Waste Management* **2020**, *22* (6), 1999-2011.
18. Li, R.; Wang, S.; Lu, A.; Zhang, L., Dissolution of cellulose from different sources in an NaOH/urea aqueous system at low temperature. *Cellulose* **2015**, *22* (1), 339-349.
19. Rebière, J. r. m.; Heuls, M. l.; Castignolles, P.; Gaborieau, M.; Rouilly, A.; Violleau, F. d. r.; Durrieu, V., Structural modifications of cellulose samples after dissolution into various solvent systems. *Analytical and Bioanalytical Chemistry* **2016**, *408* (29), 8403-8414.
20. Xia, Y.; Wang, Y.; Chen, L., Molecular structure, physicochemical characterization,

and in vitro degradation of barley protein films. *Journal of Agricultural Food Chemistry* **2011**, *59* (24), 13221-13229.

21. Agbor, V. B.; Cicek, N.; Sparling, R.; Berlin, A.; Levin, D. B., Biomass pretreatment: Fundamentals toward application. *Biotechnology Advances* **2011**, *29* (6), 675-685.

22. Gong, X.; Wang, Y.; Tian, Z.; Zheng, X.; Chen, L., Controlled production of spruce cellulose gels using an environmentally “green” system. *Cellulose* **2014**, *21* (3), 1667-1678.

23. Robert, T. O. C.; Elsie, F. D.; Donald, M., Applications of infrared absorption spectroscopy to investigations of cotton and modified cottons : Part I: Physical and crystalline modifications and oxidation. *Textile Research Journal* **1958**, *28* (5), 382-392.

24. Wei, Q.-Y.; Lin, H.; Yang, B.; Li, L.; Zhang, L.-Q.; Huang, H.-D.; Zhong, G.-J.; Xu, L.; Li, Z.-M., Structure and properties of all-cellulose composites prepared by controlling the dissolution temperature of a NaOH/urea solvent. *Industrial & Engineering Chemistry Research* **2020**, *59* (22), 10428-10435.

25. Mohamed, M. A.; Salleh, W. N. W.; Jaafar, J.; Asri, S. E. A. M.; Ismail, A. F., Physicochemical properties of “green” nanocrystalline cellulose isolated from recycled newspaper. *RSC Advances* **2015**, *5* (38), 29842-29849.

26. Sadeghifar, H.; Venditti, R.; Jur, J.; Gorga, R. E.; Pawlak, J. J., Cellulose-lignin biodegradable and flexible UV protection film. *ACS Sustainable Chemistry & Engineering* **2016**, *5* (1), 625-631.

27. Zhang, L.; Ruan, D.; Zhou, J., Structure and properties of regenerated cellulose films prepared from cotton linters in NaOH/urea aqueous solution. *Industrial & Engineering Chemistry Research* **2001**, *40* (25), 5923-5928.

28. Liu, S.; Zhang, L., Effects of polymer concentration and coagulation temperature on the properties of regenerated cellulose films prepared from LiOH/urea solution. *Cellulose* **2008**, *16* (2), 189-198.

29. Cotton, F. A., *Advanced inorganic chemistry*. 6th edition/ed.; Wiley: New York,

**1999.**

30. Bagde, P.; Nandanathangam, V., Mechanical, antibacterial and biodegradable properties of starch film containing bacteriocin immobilized crystalline nanocellulose. *Carbohydrate Polymers* **2019**, *222*, 115021.
31. Zhao, J.; He, X.; Wang, Y.; Zhang, W.; Zhang, X.; Zhang, X.; Deng, Y.; Lu, C., Reinforcement of all-cellulose nanocomposite films using native cellulose nanofibrils. *Carbohydrate Polymers* **2014**, *104*, 143-150.
32. Rafieian, F.; Shahedi, M.; Keramat, J.; Simonsen, J., Mechanical, thermal and barrier properties of nano-biocomposite based on gluten and carboxylated cellulose nanocrystals. *Industrial Crops and Products* **2014**, *53*, 282-288.
33. Bedane, A. H.; Eić, M.; Farmahini-Farahani, M.; Xiao, H., Water vapor transport properties of regenerated cellulose and nanofibrillated cellulose films. *Journal of Membrane Science* **2015**, *493*, 46-57.
34. Abrial, H.; Basri, A.; Muhammad, F.; Fernando, Y.; Hafizulhaq, F.; Mahardika, M.; Sugiarti, E.; Sapuan, S. M.; Ilyas, R. A.; Stephane, I., A simple method for improving the properties of the sago starch films prepared by using ultrasonication treatment. *Food Hydrocolloids* **2019**, *93*, 276-283.

### CONNECTING STATEMENT III

Three solvent systems: H<sub>2</sub>SO<sub>4</sub> aqueous solution, NaOH/urea aqueous solution, and LiCl/DMAc solution were applied to dissolve t-shirts, bed sheets, and jeans successfully. The dissolution behavior of WCFs in these solvent systems and properties of regenerated films were compared in **Chapter 4**. In **Chapter 5**, biodegradable antibacterial packaging films were prepared by loading different amounts of CNCs (3%, 5% and 10% of dry weight basis) onto the above prepared regenerated cellulose films. The structure, mechano-bactericidal activity and mechanical properties of all-cellulose films were investigated.

## CHAPTER 5. ALL-CELLULOSE FILMS WITH MECHANO-BACTERICIDAL ACTIVITY DERIVED FROM WASTE COTTON FABRICS

### 5.1 Abstract

Traditional approaches to eliminate the bacteria attachment rely on the incorporation of antibacterial agents in packaging materials, leading to increased antimicrobial resistance and potential undesired exposure to toxic compounds. In this work, a new strategy namely mechano-bactericidal effect inspired by the naturally occurring surfaces was applied to construct antibacterial films from waste cotton fabrics. Various amounts of CNCs were deposited on the surface of regenerated cellulose films. The results revealed that the all-cellulose films displayed an obvious and fast bactericidal activity against both Gram-negative (*E. coli*) and Gram-positive (*L. monocytogenes*) bacteria within 3 min contact. The increase of CNC contents from 3% to 10% slightly improved the bactericidal activity, but the extension of contacting time (up to 2 h) did not affect the log reduction of bacteria. In addition, the surface coating with CNCs significantly enhanced the tensile strength and Young's modulus of regenerated cellulose films from  $71.31\pm 6.10$  to  $131.44\pm 3.83$  MPa and from  $3051.39\pm 87.81$  to  $5704.33\pm 392.32$  MPa, respectively. Therefore, this work provides great prospects for the development of new generation of antibacterial packaging films.

**Keywords:** waste cotton fabrics, cellulose nanocrystals, regenerated cellulose films, mechano-bactericidal activity, foodborne bacteria

## 5.2 Introduction

The existence of pathogenic bacteria (e.g. *E. coli*, *L. monocytogenes*, and *S. aureus*) in food products can cause foodborne illness [1]. Traditional approaches to eliminate the presence of bacteria on the surfaces of food packaging are chemical-based, relying on the incorporation of antibacterial agents in the packaging materials [2]. However, the overuse of antibiotics and rapid evolution of resistant pathogens have led to increased antimicrobial resistance, resulting in significantly ineffective therapeutic efficacy [3]. Because of the uncontrolled and directionless diffusion, the released agents commonly do not achieve the desired effects even under a sufficient concentration [4]. In addition, those antibacterial agents may introduce potential exposure of undesired toxic compounds to food products [3].

A novel non-diffusive and non-toxic strategy to prevent bacteria adhesion on packaging materials by mechano-means has been explored. This mechano-bactericidal approach is based on the direct cell-surface contact. Bacterial cell membranes are physically damaged by nanopillars on the surface, leading to the final cell death [5]. Various naturally occurring surfaces such as insect wings and gecko skin have been reported to exhibit superior antibacterial activity [6-8]. For example, Truong et al. [9] found that damselfly wings showed bactericidal effects of 89.7% and 97.9% against *S. aureus* and *P. aeruginosa*, respectively. Inspired by these surfaces found in nature, synthetic surfaces with hierarchical nanostructures (e.g. pillars, hairs, and needles) have been developed, such as graphene and graphene-derived materials [10], titanium [11], black silicon [12], copper [13], and gold [14]. Compared with conventional chemical-based antibacterial agents, these bactericidal surfaces are sustainable and safe. Additionally, uneven nanotopography on the surfaces can either prevent the initial adhesion of bacteria or eliminate them once they contact the surfaces [3].

CNCs are rigid and possess a rod/needle-like shape with a diameter of 2-20 nm and a length of 100-500 nm [15]. This unusual morphology is similar to those nanostructured pillars; however, as far as we know, there is no report about the mechano-bactericidal effect of CNCs located on the surfaces of materials.

Cotton is one of the most consumed fibers in the textile industry, which consists over 90% of cellulose [16]. In our previous work, CNCs have been successfully extracted from WCFs [17], and WCFs could be dissolved and regenerated into biodegradable cellulose films. Thus, in this work, we aim to explore the possibility to fabricate all-cellulose films with mechano-bactericidal activity from WCFs. The structure of all-cellulose films was investigated by Fourier transform infrared spectroscopy and X-ray diffraction. Their bactericidal effect against Gram-negative (*E. Coli*) and Gram-positive (*L. monocytogenes*) foodborne bacteria were assessed by plate count method. In addition, the effect of CNCs on the mechanical properties of RC films was studied via tensile test.

### **5.3 Materials and methods**

#### **5.3.1 Materials**

WCFs were collected from the secondhand shop in Montreal, Canada. Sulfuric acid (95.0-98.0%) and sodium hydroxide were purchased from Sigma-Aldrich (MO, USA). Glutaraldehyde (50%) was purchased from Fisher Chemical (Ontario, Canada). Strains used in this study, *E. coli* K12 ATCC 25404 and *L. monocytogenes* LM 1870, were provided by the American Type Culture Collection (U.S.A.) and Health Canada (Canada), respectively. Prior to each experiment, the strains were propagated twice in TSB and incubated for 2.5 h at 37 °C to get fresh bacterial suspensions ( $\sim 10^7$  CFU/mL) of *E. coli* and *L. monocytogenes*.

### **5.3.2 Preparation of regenerated cellulose films**

WCFs were broken by a grinding machine (KRUPS, Ontario, Canada) and then soaked in 250 mL 20% (w/v) H<sub>2</sub>SO<sub>4</sub> for 72 h at 25 °C. After mechanical and chemistry pretreatments, the fabrics were washed thoroughly with distilled water and dried in the oven overnight. Pretreated fabrics (1 g) were added into 50 mL 64% (w/v) H<sub>2</sub>SO<sub>4</sub> aqueous solution that was pre-cooled to -20 °C, and then stirred at 750 rpm for 8 min in ice bath using IKA<sup>®</sup> Eurostar 60 digital mixer [18]. The obtained cellulosic solution was centrifuged at 6500 rpm for 5 min by Centrifuge 5430 (Eppendorf, USA) to remove bubbles. After centrifugation, the transparent and homogenous solution was immediately poured onto the glass plate and immersed in 10% (w/v) NaOH for 15 min. The RC film was washed with distilled water and finally dried in air at room temperature.

### **5.3.3 Extraction of CNCs**

The method of CNCs extraction from WCFs was described by Huang et al. [17]. The fabrics (5 g) were grinded and then mixed with 100 g of 60% (w/v) H<sub>2</sub>SO<sub>4</sub> aqueous solution. After stirring for 1 h at 25 °C, the suspension was diluted with cold water (1 L) to cease the hydrolysis. Then, CNCs were put in the dialysis bag for 48 h and washed with distilled water.

### **5.3.4 Fabrication of CNC/RC films**

CNCs coated RC films were fabricated by vacuum filtration method [19]. CNC suspensions (CNC contents: 3%, 5% and 10% of RC film dry weight; 1000 ppm) were gradually poured onto the RC films under vacuum. Because of the porous structure of RC films, only water could pass through and CNCs were deposited randomly on the surface of RC film. The obtained CNC/RC films were dried in air at room temperature (coded as 3%CNC/RC, 5%CNC/RC, and 10%CNC/RC).

### 5.3.5 Characterization

#### 5.3.5.1 Fourier transform infrared spectroscopy

The structures of CNCs, RC films, and CNC/RC films were studied by Nicolet 6700 spectrophotometer (Thermo Fisher Scientific Inc., MA, USA) equipped with an ATR accessory. The spectra were recorded as the average of 64 scans with the resolution of  $4\text{ cm}^{-1}$  from  $400\text{-}4000\text{ cm}^{-1}$  at  $25\text{ }^{\circ}\text{C}$ , using the empty accessory as blank [20].

#### 5.3.5.2 X-ray diffraction

XRD patterns of CNCs, RC films, and CNC/RC films were recorded by a Bruker D8 Discovery diffractometer (Bruker, Billerica, MA, USA), operating at 40 kV and 44 mA with the speed of  $2^{\circ}/\text{min}$ . The measurements were performed from  $4^{\circ}$  to  $45^{\circ}$ .

#### 5.3.5.3 Scanning electron microscopy

Bacterial suspension ( $100\text{ }\mu\text{L}$ ,  $\sim 10^7\text{ CFU/mL}$ ) was dropped on CNC/RC films ( $1\text{ cm} \times 1\text{ cm}$ ) and allowed to incubate for 3 min in a Petri dish. Then, 2% (w/v) glutaraldehyde in PBS was added on the films to fix bacteria. After 20 min, the films were gently washed by Milli-Q water and freeze-dried for SEM observation [6]. SEM images of surfaces were taken by a field-emission SEM (LEO ZEISS 1530 SEM, Germany) at 1 kV under  $5000\times$  magnification.

#### 5.3.5.4 Bactericidal activity

RC and CNC/RC films were cut into squares ( $1\text{ cm} \times 1\text{ cm}$ ) and laid in a Petri dish [7]. Bacterial suspensions ( $200\text{ }\mu\text{L}$ ,  $\sim 10^7\text{ CFU/mL}$ ) were added on the films and left for 3 min, 1 h, and 2 h, respectively. After the contact, bacterial suspensions were recovered, and the reduced CFU concentrations were determined by plate count which was done by serial dilutions of the recovered bacterial suspensions and spread plating on TSA for *E. coli* and BHI for *L. monocytogenes* suspensions. The plates were incubated at  $37\text{ }^{\circ}\text{C}$  for up to 24 h. A logarithmic reduction was calculated and expressed as  $\text{Log}_{10}\text{ CFU}$ . For

the CNC solution control, 200  $\mu$ L bacterial suspensions were added in 5 mL of CNC solution and incubated for 3 min, 1 h, and 2 h. Plate count was then applied to calculate the logarithmic reductions.

#### *5.3.5.5 Mechanical properties*

The tensile strength, Young's modulus and elongation at break of RC and CNC/RC films were tested by an Instron 5967 universal testing machine (Instron Corp., MA, USA) at the speed of 5 mm/min with the initial grip separation distance of 20 mm. Five strips were cut from each film with the dimension of 6 cm $\times$ 1 cm (length  $\times$  width). The thickness of each strip was detected by a digital micrometer (Fisherbrand, Fisher Scientific, Canada) with the precision of 1  $\mu$ m.

#### **5.3.6 Statistical analysis**

The experimental results were presented as the mean of three batches  $\pm$  SD. Statistical evaluation was carried out by ANOVA followed by multiple comparison tests by Duncan's multiple-range test with significant differences within samples at  $p < 0.05$ . All of analyses were performed through SPSS statistical software (IBM, New York, NY, USA)

### **5.4 Results and discussion**

#### **5.4.1 Structure of CNC/RC films**

FT-IR spectra were collected to study the structure of CNC/RC films. As shown in Figure 5.1, all samples exhibited similar characteristic absorption peaks. For example, the peak near 3336  $\text{cm}^{-1}$  was characteristic for the stretching vibration of hydroxyl groups and the inter-chain hydrogen bonds in cellulose [17]. The adsorption bands at 2890  $\text{cm}^{-1}$ , 1427  $\text{cm}^{-1}$ , 1371  $\text{cm}^{-1}$ , 1315  $\text{cm}^{-1}$  and 896  $\text{cm}^{-1}$  were attributed to the stretching and bending vibrations of C-H, the bending vibration of -CH<sub>2</sub> and -OH, and  $\beta$ -glycoside bonds of glucose ring, respectively [18,21]. Due to the incorporation of

CNCs, the absorption wavelength related to the stretching vibration of -OH peak of CNC/RC slightly shifted to a lower wavelength (from 3336  $\text{cm}^{-1}$  to 3329  $\text{cm}^{-1}$ ), indicating an increase in hydrogen bonds between hydroxyl groups of regenerated cellulose films and CNCs [22]. However, other differences introduced by the addition of CNCs were not obvious, as expected from the low CNC contents deposited on the surface of composite films. Figure 5.2 presents XRD patterns of CNC, RC and CNC/RC films. CNCs exhibited characteristic diffraction peaks at ca. 14.8° (11 $\bar{0}$ ), 16.4° (110), 22.5° (200), and 34° (040), which were typical for cellulose I crystals [23]. RC films showed a weak crystalline peak at about 20.6°, which suggested the transformation from cellulose I to cellulose II crystals after dissolution and regeneration [24]. Similar to RC films, CNC/RC films exhibited a broad and weak diffraction peak. No obvious differences were observed after the incorporation of CNCs because the CNC content was low (3-10% dry weight basis). Similar results have also been reported by Li et al. [25].

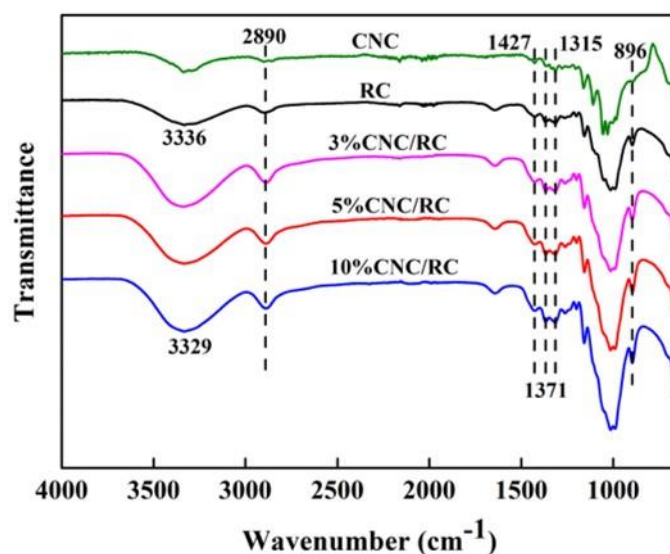


**Figure 5.1** FT-IR spectra of CNC, RC, and CNC/RC films

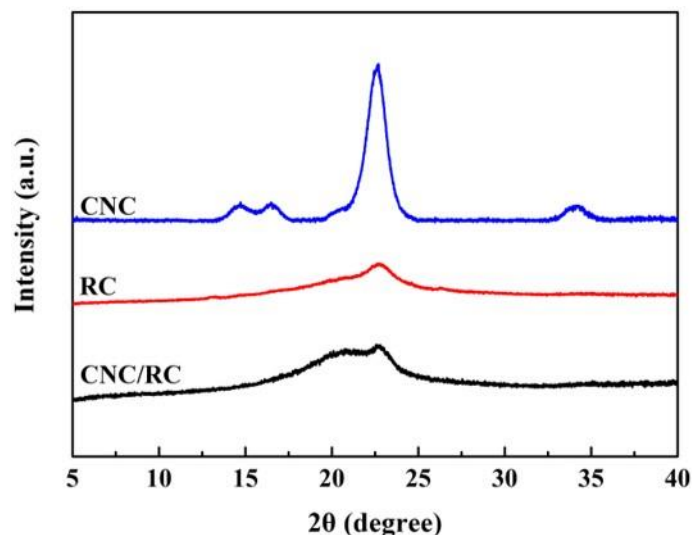


**Figure 5.2** XRD patterns of CNC, RC, and CNC/RC films

#### 5.4.2 Mechano-bactericidal activity of CNC/RC films

The mechano-bactericidal activity of CNC/RC films with different CNC contents was quantitatively assessed by contacting with foodborne bacteria for 3 min and using a standard plate count method. As shown in Figure 5.3, compared with the 0-0.1 log reduction efficiencies of control samples (regenerated cellulose films and free CNCs), all CNC/RC films exhibited superior bactericidal activity against *E. coli* and *L. monocytogenes*, indicating that the nanostructured surfaces exerted a promising effect on both Gram-positive and Gram-negative bacteria. Approximate 1 log CFU reduction of *E. coli* was observed while *L. monocytogenes* had a log reduction of about 0.8 CFU. It was because of that Gram-positive bacteria possess a thicker (20–80 nm) cell wall as outer shell of the cell than Gram-negative bacteria (<10 nm) and are more resistant to external stresses [26]. The increase in CNC contents from 3% to 10% slightly improved the bactericidal activities towards both bacteria. Based on the calculation, if 3% CNCs were uniformly dispersed, they could fully cover the surface of regenerated cellulose films. Further increase of CNC contents would not change the surface morphology too much, so the bactericidal activities were similar. It was worth noting that the bactericidal activities of CNC/RC films were comparable to those of gecko hairs (90-95% cell death of *S. mutans*) and GO nanosheets (80% cell death of *E. coli*) [8,19]. The

10%CNC/RC films were selected to study the effect of contact time on the bactericidal activity. As shown in Figure 5.4, the extension of contact times from 3 min to 2 h did not cause any significant change in log reduction of both bacteria, which indicated that bacteria were inhibited, injured and killed upon attaching the surface within a very short period. Ivanova et al. [27] also reported the quick response that the rupture point of the cells happened at around 3 min after the cell attachment. The morphologies of *E. coli* and *L. monocytogenes* attached on the surface of CNC/RC films were observed by SEM (as shown in Figure 5.5). CNCs were deposited on the surface and displayed a rough net structure. Bacteria were in close contact with CNCs and most of cells maintained their original shapes. Three models, the biophysical model, the analytical thermodynamic model, and the oxidative stress model, can be used to describe the mechanism of cell death on nano-patterned surfaces [4]. Since the first model is related to cell rupture, the observed bactericidal activity might be due to the large degree of bacterial membrane stretching and/or increased levels of reactive oxygen species and hydrogen peroxide.

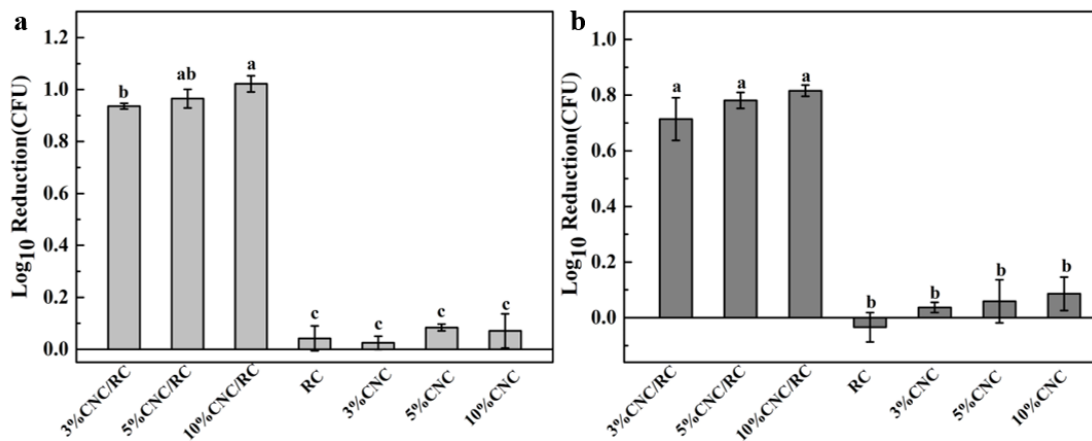


**Figure 5.3** Logarithmic reduction of (a) *E. coli* and (b) *L. monocytogenes* when incubated with CNC/RC films and controls for 3 min (different letters on the tops of columns represented the significant difference ( $p < 0.05$ ))

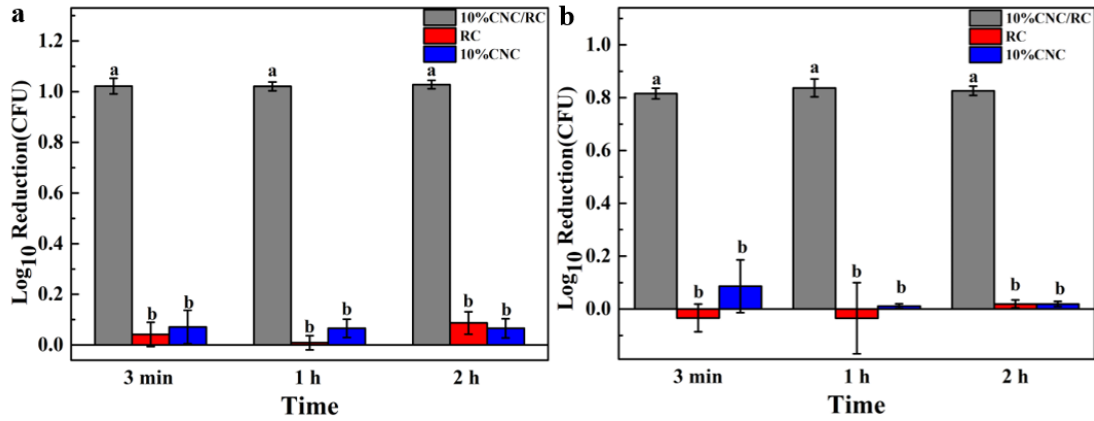


**Figure 5.4** Effect of various contact times on logarithmic reduction of (a) *E. coli* and (b) *L. monocytogenes* when incubated with 10% CNC/RC films and controls (different letters on the tops of columns represented the significant difference ( $p < 0.05$ ))

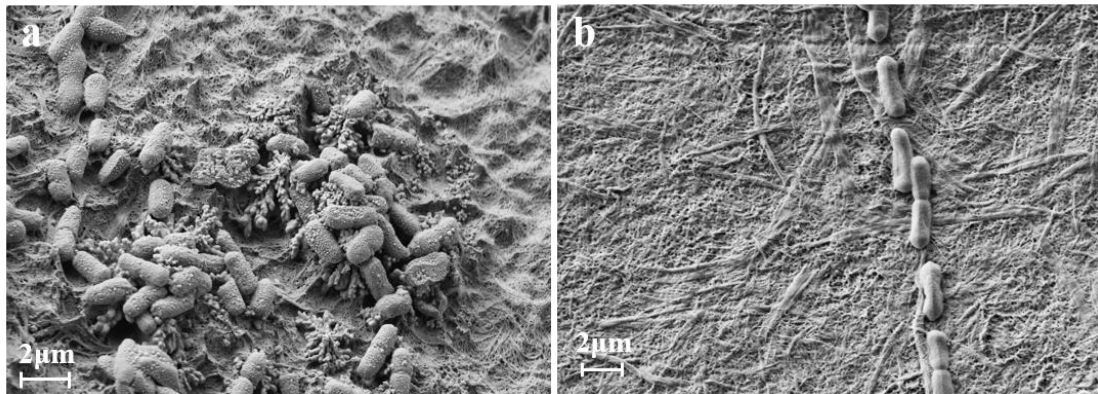


**Figure 5.5** (a) SEM micrograph showing morphology of *E. coli* on the CNC/RC film; and (b) SEM micrograph showing morphology of *L. monocytogenes* on the CNC/RC film

### 5.4.3 Mechanical properties of CNC/RC films

The mechanical properties of RC and CNC/RC films were tested to study the reinforcing effect of CNCs. As shown in Figure 5.6, CNCs had a profound effect on the mechanical properties. With the increase of CNC contents from 3% to 10%, the tensile strength and Young's modulus of RC films were significantly enhanced from  $87.70 \pm 2.96$  to  $131.44 \pm 3.83$  MPa and from  $3641.45 \pm 340.41$  to  $5704.33 \pm 392.32$  MPa, respectively. It was because of the favorable interactions (e.g. hydrogen bonds) between CNCs and regenerated cellulose films [28]. Additionally, the Eb values of CNC/RC

films were lower compared to that of RC film, since the reinforcement restricted the extension [29]. Similar phenomenon was also observed by Li et al. [25], where chitosan films displayed a great decrease in the Eb values from 20% to 6% when the content of cellulose whiskers increased from 0% to 30% (w/v). It was noted that different CNC contents resulted in significant increases in tensile strength and Young's modulus ( $p < 0.05$ ), but the difference of Eb was not obvious ( $p > 0.05$ ).

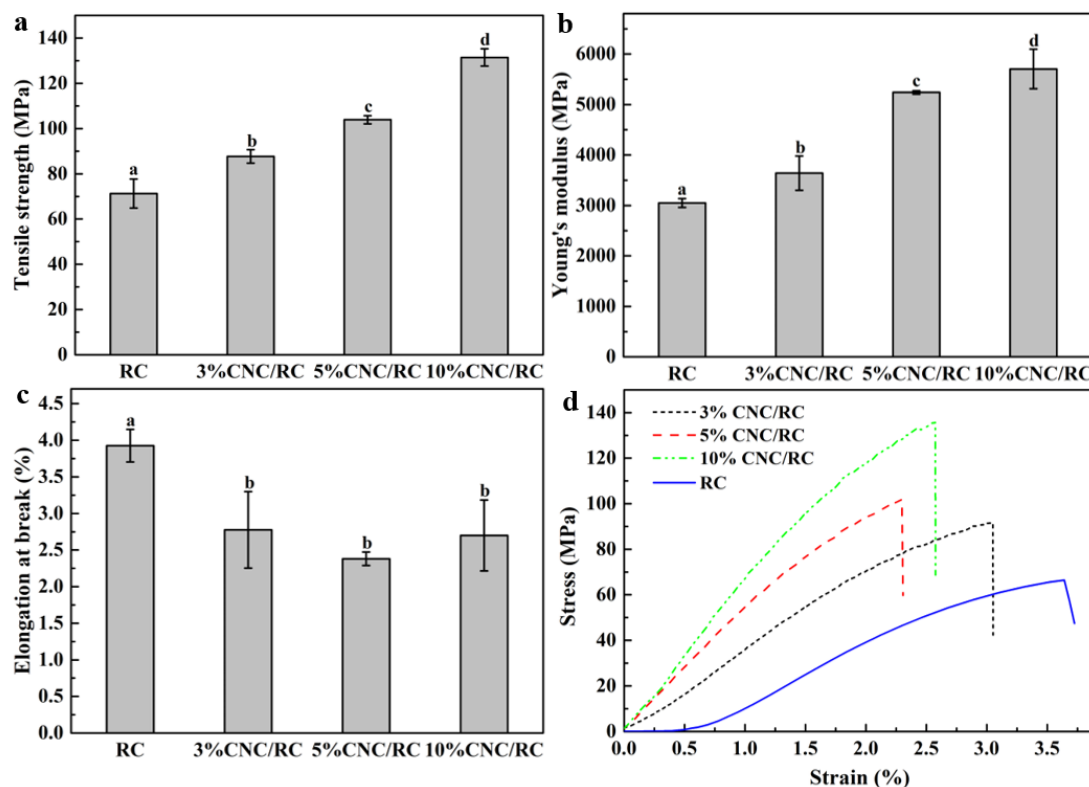


**Figure 5.6** Mechanical properties of RC and CNC/RC films (different letters on the tops of columns represented the significant difference ( $p < 0.05$ ))

## 5.5 Conclusion

CNC/RC films were successfully prepared from waste cotton fabrics by depositing CNCs on the surface of RC films. The 10% CNC/RC films exhibited notable mechano-bactericidal activity against *E. coli* (1.022 log reduction) and *L. monocytogenes* (0.8160 log reduction), which were comparable to those of natural occurring surfaces (e.g. gecko hairs) and bioinspired surfaces (e.g. GO nanostructure). Additionally, increasing

the cell-surface contact time (from 3 min to 2 h) did not significantly affect the bactericidal activity of CNC/RC films. The surface morphology of CNC/RC films confirmed the close contact between bacteria and the rough surface, which might result in the increased degree of bacterial membrane stretching and/or increased levels of reactive oxygen species and hydrogen peroxide. Moreover, the CNC layer deposited on the surface of RC films led to the improved tensile strength and Young's modulus (up to  $131.44 \pm 3.83$  MPa and  $5704.33 \pm 392.32$  MPa, respectively). Therefore, this work provides promising prospects on how nanostructured cellulose films can serve as effective antimicrobial materials, which can be potentially used in food-related applications.

## 5.6 References

1. Moye, Z. D.; Woolston, J.; Sulakvelidze, A., Bacteriophage applications for food production and processing. *Viruses* **2018**, *10* (4), 205.
2. Lin, N.; Berton, P.; Moraes, C.; Rogers, R. D.; Tufenkji, N., Nanodarts, nanoblades, and nanospikes: Mechano-bactericidal nanostructures and where to find them. *Advances in Colloid and Interface Science* **2018**, *252*, 55-68.
3. Elbourne, A.; Crawford, R. J.; Ivanova, E. P., Nano-structured antimicrobial surfaces: From nature to synthetic analogues. *Journal of Colloid and Interface Science* **2017**, *508*, 603-616.
4. Zhou, C.; Koshani, R.; O'Brien, B.; Ronholm, J.; Cao, X.; Wang, Y., Bio-inspired mechano-bactericidal nanostructures: A promising strategy for eliminating surface foodborne bacteria. *Current Opinion in Food Science* **2021**, *39*, 110-119.
5. Anselme, K.; Davidson, P.; Popa, A. M.; Giazson, M.; Liley, M.; Ploux, L., The interaction of cells and bacteria with surfaces structured at the nanometre scale. *Acta Biomaterialia* **2010**, *6* (10), 3824-3846.
6. Bandara, C. D.; Singh, S.; Afara, I. O.; Wolff, A.; Tesfamichael, T.; Ostrikov, K.; Oloyede, A., Bactericidal effects of natural nanotopography of dragonfly wing on *Escherichia Coli*. *ACS Applied Materials & Interfaces* **2017**, *9* (8), 6746-6760.
7. Pogodin, S.; Hasan, J.; Baulin, Vladimir A.; Webb, Hayden K.; Truong, Vi K.; Phong Nguyen, The H.; Boshkovikj, V.; Fluke, Christopher J.; Watson, Gregory S.; Watson, Jolanta A.; Crawford, Russell J.; Ivanova, Elena P., Biophysical model of bacterial cell interactions with nanopatterned cicada wing surfaces. *Biophysical Journal* **2013**, *104* (4), 835-840.
8. Li, X.; Cheung, G. S.; Watson, G. S.; Watson, J. A.; Lin, S.; Schwarzkopf, L.; Green, D. W., The nanotipped hairs of gecko skin and biotemplated replicas impair and/or kill pathogenic bacteria with high efficiency. *Nanoscale* **2016**, *8* (45), 18860-18869.
9. Truong, V. K.; Geeganagamage, N. M.; Baulin, V. A.; Vongsvivut, J.; Tobin, M. J.;

Luque, P.; Crawford, R. J.; Ivanova, E. P., The susceptibility of *Staphylococcus Aureus* CIP 65.8 and *Pseudomonas Aeruginosa* ATCC 9721 cells to the bactericidal action of nanostructured *Calopteryx haemorrhoidalis* damselfly wing surfaces. *Applied Microbiology and Biotechnology* **2017**, *101* (11), 4683-4690.

10. Sengupta, I.; Bhattacharya, P.; Talukdar, M.; Neogi, S.; Pal, S. K.; Chakraborty, S., Bactericidal effect of graphene oxide and reduced graphene oxide: Influence of shape of bacteria. *Colloid and Interface Science Communications* **2019**, *28*, 60-68.

11. Wandiyanto, J. V.; Al, K. M.; Truong, V. K.; Bazaka, O.; Crawford, R. J.; Ivanova, E. P.; Juodkazis, S.; Thissen, H.; Bazaka, K., The fate of osteoblast-like MG-63 cells on pre-infected bactericidal nanostructured titanium surfaces. *Materials* **2019**, *12* (10), 1575.

12. May, P. W.; Clegg, M.; Silva, T. A.; Zanin, H.; Fatibello-Filho, O.; Celorrio, V.; Fermin, D. J.; Welch, C. C.; Hazell, G.; Fisher, L.; Nobbs, A.; Su, B., Diamond-coated 'black silicon' as a promising material for high-surface-area electrochemical electrodes and antibacterial surfaces. *Journal of Materials Chemistry B* **2016**, *4* (34), 5737-5746.

13. Shalabayev, Z.; Balaz, M.; Daneu, N.; Dutkova, E.; Bujnakova, Z.; Kanuchova, M.; Dankova, Z.; Balazova, L.; Urakaev, F.; Tkacikova, L.; Burkitbayev, M., Sulfur-mediated mechanochemical synthesis of spherical and needle-like copper sulfide nanocrystals with antibacterial activity. *ACS Sustainable Chemistry & Engineering* **2019**, *7* (15), 12897-12909.

14. Wu, S.; Zuber, F.; Brugger, J.; Maniura-Weber, K.; Ren, Q., Antibacterial Au nanostructured surfaces. *Nanoscale* **2016**, *8* (5), 2620-2625.

15. Martelli-Tosi, M.; Esposito, B. S.; Cristina da Silva, N.; Tapia-Blácido, D. R.; Jafari, S. M., 14 - Reinforced nanocomposites for food packaging. In *Handbook of food nanotechnology*, Jafari, S. M., Ed. Academic Press: **2020**; pp 533-574.

16. Sandin, G.; Peters, G. M., Environmental impact of textile reuse and recycling – a review. *Journal of Cleaner Production* **2018**, *184*, 353-365.

17. Huang, S.; Tao, R.; Ismail, A.; Wang, Y., Cellulose nanocrystals derived from

textile waste through acid hydrolysis and oxidation as reinforcing agent of soy protein film. *Polymers* **2020**, *12* (4), 958.

18. Huang, W.; Wang, Y.; Zhang, L.; Chen, L., Rapid dissolution of spruce cellulose in H<sub>2</sub>SO<sub>4</sub> aqueous solution at low temperature. *Cellulose* **2016**, *23* (6), 3463-3473.

19. Zou, F.; Zhou, H.; Jeong, D. Y.; Kwon, J.; Eom, S. U.; Park, T. J.; Hong, S. W.; Lee, J., Wrinkled surface-mediated antibacterial activity of graphene oxide nanosheets. *ACS Applied Materials & Interfaces* **2017**, *9* (2), 1343-1351.

20. Oliva, C.; Huang, W.; El Badri, S.; Lee, M. A. L.; Ronholm, J.; Chen, L.; Wang, Y., Concentrated sulfuric acid aqueous solution enables rapid recycling of cellulose from waste paper into antimicrobial packaging. *Carbohydrate Polymers* **2020**, *241*, 116256.

21. Robert, T. O. C.; Elsie, F. D.; Donald, M., Applications of infrared absorption spectroscopy to investigations of cotton and modified cottons : Part I: Physical and crystalline modifications and oxidation. *Textile Research Journal* **1958**, *28* (5), 382-392.

22. Chen, Q.; Zong, Z.; Gao, X.; Zhao, Y.; Wang, J., Preparation and characterization of nanostarch-based green hard capsules reinforced by cellulose nanocrystals. *International Journal of Biological Macromolecules* **2021**, *167*, 1241-1247.

23. Mohamed, M. A.; Salleh, W. N. W.; Jaafar, J.; Asri, S. E. A. M.; Ismail, A. F., Physicochemical properties of “green” nanocrystalline cellulose isolated from recycled newspaper. *RSC Advances* **2015**, *5* (38), 29842-29849.

24. Sadeghifar, H.; Venditti, R.; Jur, J.; Gorga, R. E.; Pawlak, J. J., Cellulose-lignin biodegradable and flexible UV protection film. *ACS Sustainable Chemistry & Engineering* **2016**, *5* (1), 625-631.

25. Li, Q.; Zhou, J.; Zhang, L., Structure and properties of the nanocomposite films of chitosan reinforced with cellulose whiskers. *Journal of Polymer Science Part B: Polymer Physics* **2009**, *47* (11), 1069-1077.

26. Mai-Prochnow, A.; Clauson, M.; Hong, J.; Murphy, A. B., Gram positive and gram negative bacteria differ in their sensitivity to cold plasma. *Scientific Reports* **2016**, *6* (1), 3861.

27. Ivanova, E. P.; Hasan, J.; Webb, H. K.; Truong, V. K.; Watson, G. S.; Watson, J. A.; Baulin, V. A.; Pogodin, S.; Wang, J. Y.; Tobin, M. J.; Løbbe, C.; Crawford, R. J., Natural bactericidal surfaces: Mechanical rupture of *pseudomonas aeruginosa* cells by cicada wings. *Small* **2012**, *8* (16), 2489-2494.
28. Wang, Y.; Cao, X.; Zhang, L., Effects of cellulose whiskers on properties of soy protein thermoplastics. *Macromolecular Bioscience* **2006**, *6* (7), 524-531.
29. Khan, A.; Khan, R. A.; Salmieri, S.; Le Tien, C.; Riedl, B.; Bouchard, J.; Chauve, G.; Tan, V.; Kamal, M. R.; Lacroix, M., Mechanical and barrier properties of nanocrystalline cellulose reinforced chitosan based nanocomposite films. *Carbohydrate Polymers* **2012**, *90* (4), 1601-1608.

## CHAPTER 6 GENERAL SUMMARY AND CONCLUSION

### 6.1 General summary

The disposal, utilization and management issues of biomass wastes arise due to their increasing generation every year. In literature review 1, except from traditional methods such as incineration and landfill to treat biomass wastes, effective approaches have been explored by researchers to recycle them into value-added applications, including extraction of natural polymers (e.g. cellulose, lignin, gelatin and chitin), reuse of biomass wastes, and preparation of carbon-based materials as novel adsorbents, catalyst carriers, electrode materials and functional composites. Waste cotton fabrics, as a kind of biomass wastes, were successfully recycled into regenerated cellulose films through three solvent systems: H<sub>2</sub>SO<sub>4</sub> aqueous solution, NaOH/urea aqueous solution, and LiCl/DMAc solution. It was found that all three typical cotton fabrics: t-shirts, bed sheets and jeans could be dissolved in these solvent systems after appropriate mechanical and chemical pretreatments, but the dissolution in LiCl/DMAc solution needed multiple activation steps, low cellulose concentration (1%), high dissolution temperature (80 °C), and long dissolution time (~1 day). Although cotton fabrics dissolved rapidly in H<sub>2</sub>SO<sub>4</sub> and NaOH/urea aqueous solution (only 8 min) under a lower temperature, cellulose solution was less stable in H<sub>2</sub>SO<sub>4</sub> solvent, and a longer acid hydrolysis time (6-7 days) was required before the dissolution in NaOH/urea solvent. Compared to different types of cotton fabrics, these three solvent systems had significant effect on the mechanical, thermal and water vapor barrier properties of the translucent cellulose films. Results showed that films prepared from bed sheets in NaOH/urea solvent system displayed the highest tensile strength (76.21±8.26 MPa), thermal stability (maximum decomposition temperature 325.66 °C), and water vapor barrier property (0.81±0.10×10<sup>-7</sup> g m<sup>-1</sup> h<sup>-1</sup> Pa<sup>-1</sup>). It was because higher cellulose concentration in NaOH/urea solution resulted in the stronger cellulose chain

entanglement and hydrogen bonds, leading to the denser structure and improved properties of films.

Contamination of food by bacteria is a major food safety concern owing to the serious human illness that it can lead to. An effective bio-inspired mechano-bactericidal nanostructure has been studied to physically eliminate bacteria from outer surfaces of food products and minimize drug resistance. Based on the research reviewed in literature review 2, antimicrobial packaging films that did not rely on the release of active agents were fabricated by depositing CNCs on the surface of regenerated cellulose films to inhibit the growth of *E. coli* and *L. monocytogenes*. The results revealed that CNC-coated RC films could kill both Gram-positive and Gram-negative foodborne bacteria quickly (in 3 min); however, increasing the bacteria-surface contact time (up to 2 h) did not significantly affect the mechano-bactericidal activity. The film with 10% CNC exhibited the highest bactericidal activity against *E. coli* (1.022 log reduction) and *L. monocytogenes* (0.8160 log reduction), which was comparable to other natural and synthetic nanostructures (e.g. gecko hairs and graphene oxide nanosheet). The incorporation of CNCs also largely reinforced the mechanical properties of RC films, and the obtained all-cellulose films have potential to be used as biodegradable antibacterial packaging materials.

## **6.2 Suggestions for future work**

This work provides promising prospects on recycling waste cotton fabrics into regenerated cellulose films with superior bactericidal activity, which can be potentially used in food and biological applications. Based on the results obtained in this study, we conclude that the type of waste cotton fabrics is an insignificant factor for the properties of regenerated cellulose films, which allows the recycling of mixed cotton fabrics by dissolution and regeneration. It is also possible to use this method to recycle waste

fabrics containing cotton and other components (e.g. polycotton blends and wool/cotton blends), and further investigation in the future study is needed.

Although the mechano-bactericidal activity of all-cellulose films was quantitatively assessed, the mechanism of bactericidal activity has not been clearly explored. Further investigations, such as high-resolution SEM images for the observation of the interactions between bacteria and nanostructured surface, and oxidative stress measurement, are therefore necessary.

The safety issue of all-cellulose films should be investigated in the future. The toxicity of CNCs is still not confirmed, although most of current research works consider they are safe. The interactions between CNCs and regenerated cellulose films are physical, so the release of CNCs at different environmental conditions should be studied to evaluate the potential effect on food products and human health.

## REFERENCES

1. Tripathi, N.; Hills, C. D.; Singh, R. S.; Atkinson, C. J., Biomass waste utilisation in low-carbon products: Harnessing a major potential resource. *npj Climate and Atmospheric Science* **2019**, *2* (1), 35.
2. Hakeem, K. R.; Jawaid, M.; Alothman, O. Y., *Agricultural biomass based potential materials*. Springer: Cham, Switzerland, **2015**.
3. Dissanayake, D. G. K.; Weerasinghe, D. U.; Thebuwanage, L. M.; Bandara, U. A. A. N., An environmentally friendly sound insulation material from post-industrial textile waste and natural rubber. *Journal of Building Engineering* **2021**, *33*, 101606.
4. Çay, A.; Yanık, J.; Akduman, Ç.; Duman, G.; Ertaş, H., Application of textile waste derived biochars onto cotton fabric for improved performance and functional properties. *Journal of Cleaner Production* **2020**, *251*, 119664.
5. Ütebay, B.; Çelik, P.; Çay, A., Effects of cotton textile waste properties on recycled fibre quality. *Journal of Cleaner Production* **2019**, *222*, 29-35.
6. Sandin, G.; Peters, G. M., Environmental impact of textile reuse and recycling – a review. *Journal of Cleaner Production* **2018**, *184*, 353-365.
7. Cai, J.; Zhang, L., Rapid dissolution of cellulose in LiOH/urea and NaOH/urea aqueous solutions. *Macromolecular Bioscience* **2005**, *5* (6), 539-548.
8. Huang, S.; Tao, R.; Ismail, A.; Wang, Y., Cellulose nanocrystals derived from textile waste through acid hydrolysis and oxidation as reinforcing agent of soy protein film. *Polymers* **2020**, *12* (4), 958.
9. Xia, G.; Wan, J.; Zhang, J.; Zhang, X.; Xu, L.; Wu, J.; He, J.; Zhang, J., Cellulose-based films prepared directly from waste newspapers via an ionic liquid. *Carbohydrate Polymers* **2016**, *151*, 223-229.
10. Han, Q.; Gao, X.; Zhang, H.; Chen, K.; Peng, L.; Jia, Q., Preparation and comparative assessment of regenerated cellulose films from corn (zea mays) stalk pulp fines in DMAc/LiCl solution. *Carbohydrate Polymers* **2019**, *218*, 315-323.

11. Huang, W.; Wang, Y.; Zhang, L.; Chen, L., Rapid dissolution of spruce cellulose in H<sub>2</sub>SO<sub>4</sub> aqueous solution at low temperature. *Cellulose* **2016**, *23* (6), 3463-3473.
12. Moye, Z. D.; Woolston, J.; Sulakvelidze, A., Bacteriophage applications for food production and processing. *Viruses* **2018**, *10* (4), 205.
13. Zhou, C.; Koshani, R.; O'Brien, B.; Ronholm, J.; Cao, X.; Wang, Y., Bio-inspired mechano-bactericidal nanostructures: A promising strategy for eliminating surface foodborne bacteria. *Current Opinion in Food Science* **2021**, *39*, 110-119.
14. Watson, G. S.; Cribb, B. W.; Schwarzkopf, L.; Watson, J. A., Contaminant adhesion (aerial/ground biofouling) on the skin of a gecko. *Journal of The Royal Society Interface* **2015**, *12* (108), 20150318.
15. Sengupta, I.; Bhattacharya, P.; Talukdar, M.; Neogi, S.; Pal, S. K.; Chakraborty, S., Bactericidal effect of graphene oxide and reduced graphene oxide: Influence of shape of bacteria. *Colloid and Interface Science Communications* **2019**, *28*, 60-68.
- Wandiyanto, J. V.; Al, K. M.; Truong, V. K.; Bazaka, O.; Crawford, R. J.; Ivanova, E. P.; Juodkazis, S.; Thissen, H.; Bazaka, K., The fate of osteoblast-like MG-63 cells on pre-infected bactericidal nanostructured titanium surfaces. *Materials* **2019**, *12* (10), 1575.
17. Ivanova, E. P.; Hasan, J.; Webb, H. K.; Gervinskas, G.; Juodkazis, S.; Truong, V. K.; Wu, A. H. F.; Lamb, R. N.; Baulin, V. A.; Watson, G. S.; Watson, J. A.; Mainwaring, D. E.; Crawford, R. J., Bactericidal activity of black silicon. *Nature Communications* **2013**, *4* (1), 2838.
18. Pogodin, S.; Hasan, J.; Baulin, Vladimir A.; Webb, Hayden K.; Truong, Vi K.; Phong Nguyen, The H.; Boshkovikj, V.; Fluke, Christopher J.; Watson, Gregory S.; Watson, Jolanta A.; Crawford, Russell J.; Ivanova, Elena P., Biophysical model of bacterial cell interactions with nanopatterned cicada wing surfaces. *Biophysical Journal* **2013**, *104* (4), 835-840.
19. Martelli-Tosi, M.; Esposito, B. S.; Cristina da Silva, N.; Tapia-Blácido, D. R.; Jafari, S. M., 14 - Reinforced nanocomposites for food packaging. In *Handbook of food*

*nanotechnology*, Jafari, S. M., Ed. Academic Press: **2020**; pp 533-574.